FORECAST VERTICAL VELOCITY AND TEMPERATURE, HORIZONTAL WIND DIRECTION, AND WIND VELOCITY ERROR COUPLING WITHIN UPPER TROPOSPHERE MM5 AND WRF FORECASTING

A Dissertation

Presented to

the Faculty of the Department of Earth and Atmospheric Sciences

University of Houston

In Partial Fulfillment

of the Requirements for the Degree

Doctor of Philosophy

By

Kelly Michael Soich

December 2012

FORECAST VERTICAL VELOCITY AND TEMPERATURE, HORIZONTAL WIND DIRECTION, AND WIND VELOCITY ERROR COUPLING WITHIN UPPER TROPOSPHERE MM5 AND WRF FORECASTING

_____

Kelly Michael Soich

APPROVED:

_____

Dr. Bernhard Rappengueck, Chairman

_____

Dr. Xun Jiang

_____

Dr. Max Schauck

_____

Dr. Fong Ngan
Cooperative Institute for Climate and Satellites, University of Maryland

_____

Dr. Mark Smith, Dean, College of Natural Sciences and Mathematics

ACKNOWLEDGEMENTS

My special thanks to Dr. Bernhard Rappenglueck for guidance, support, and patience during this undertaking. His continual suggestions provided significant motivation to continue looking beyond the surface and consistently improve upon writing of this manuscript. Additional thanks to Dr. Xun Jiang, Dr. Fong Ngan, and Dr. Max Schauck for allowing me to pursue this topic and providing additional guidance when needed.

I would also like to thank the members of the 187th Airlift Squadron, Wyoming Air National Guard for allowing me to use the C-130 during this project. Their constant willingness to help is a cornerstone in completing this endeavor. Very special thanks to Oceaneering Space Systems and my teammates who have unquestionably supported my time away during this endeavor.

I would like to express my appreciation to the Joint Army and Air Force, Weather Network for model and forecasting access, Steven Rugg at the Air Force Weather Agency for model physics package information, the University of Wyoming for radiosonde database use, and the International Institute for Applied Systems Analysis of Laxenburg, Austria for use of the Harmonized World Soil Database

Finally, my sincere and deepest gratitude goes to my wife and daughter. Without their patience, understanding, support, and unwavering sacrifice this dream would have never become a reality nor ever been accomplished.

FORECAST VERTICAL VELOCITY AND TEMPERATURE, HORIZONTAL WIND DIRECTION, AND WIND VELOCITY ERROR COUPLING WITHIN UPPER TROPOSPHERE MM5 AND WRF FORECASTING

An Abstract of a Dissertation
Presented to
the Faculty of the Department of Earth and Atmospheric Sciences
University of Houston

In Partial Fulfillment
of the Requirements for the Degree
Doctor of Philosophy

By
Kelly Michael Soich

December 2012

ABSTRACT

The Pennsylvania State University (PSU) Fifth Generation Mesoscale Model (MM5) and Weather Research and Forecasting (WRF) models have predicted temperature, horizontal wind direction, and velocity for aviation purposes. In situ observations have not been utilized to assess MM5 and WRF upper troposphere temperature, horizontal wind direction, and velocity prediction. Regression analysis of MM5 and WRF forecast and aircraft observed data from seven flights in February and April 2009 over North America, Europe, and Southwest Asia between 6000-7600 meters above sea level indicated temperature, horizontal wind direction, and velocity errors were coupled to forecast vertical velocities less than 100 kilometers laterally of the modeled flight tracks between 39-59 degrees north latitude.

Temperature error and forecast vertical velocity coupling occurred over land, surface elevations of 0-499 meters above sea level, different vegetative, and urban surface type in MM5 and WRF forecasts. Horizontal wind direction and forecast vertical velocity coupling was indicated in WRF forecasts over land, water, and surface elevations of 400-499 meters above sea level. Horizontal wind velocity and forecast vertical velocity coupling was found over land, inversely over water, surface elevations of 100-199 meters above sea level, and non-urban surface type in MM5 and WRF forecasts between 0-99, 400-499, and 700-999 meters above sea level.

Temperature and forecast vertical velocity coupling in MM5 and WRF forecasts may stem from erroneous long wave radiation upwelling parameterization, evapotranspiration errors in the land surface model, and entrainment in the cumulus parameterization schemes. Incorrect model parameterization schemes may be affecting temperature

differentials across frontal zones erroneously forecasting vertical velocity causing horizontal wind direction and velocity coupling to forecast vertical velocity in MM5 and WRF forecasts.

TABLE OF CONTENTS

LIST OF FIGURES

1.6. Difference in upper troposphere MM5 and WRF horizontal wind direction forecasts (°*T*) and aircraft observed horizontal wind velocities (°*T*) compared to forecast vertical velocity (mb s^{-1}) within 100 kilometers (km) lateral distance deviation from MM5 and WRF modeled flight tracks ($R = 0.1$).

1.7. MM5 and WRF forecasted horizontal wind velocity (ms^{-1}) in the upper troposphere with aircraft horizontal wind velocity observations (ms^{-1}) taken while ascending and descending between 39-59 degrees (°) north latitude (*N*) en route from North America to Southwest Asia in February 2009 and returning to North America in April 2009.

1.8. Difference in upper troposphere combined MM5 and WRF horizontal wind velocity forecasts and aircraft observed temperatures compared to lateral distance deviation from MM5 and WRF model tracks (R=0.0).

1.9. Difference in upper troposphere combined MM5 and WRF horizontal wind velocity forecasts and aircraft observed horizontal wind velocity (ms^{-1}) compared to forecast vertical velocity (mb s^{-1}) within 100 kilometers (km) lateral distance deviation from MM5 and WRF modeled flight tracks ($R = -0.1$).

2.1. WRF upper troposphere vertical cross-section forecast on 14 Feb 2009 for the planned route of flight between England and Romania. Model grid spacing defaulted to 45 kilometers (km), temperature in degrees Celsius (°*C*) (dotted horizontal line), wind direction in degrees (north at top of page) (barbs), wind velocity in knots (KT) (barb flags), cloud prediction (dark solid line) and vertical velocity (microbar sec^{-1}) (vertical dotted lines). Forecast initiation was England (*a*) and terminating in Romania (*c*) with the midpoint in the Czech Republic (*b*) as depicted by the map inset (top right) with latitude (*N*) and longitude (*W* and *E*) displayed at bottom, altitude in millibars (mb) (scale left) and pressure altitude in flight levels (FL) equating to thousands of feet (160 = 16000 feet) (scale right).

2.2. Radiosonde station locations, type of surface type and surface elevation profile in meters above sea level for MM5 and WRF modeled flight tracks and actual aircraft observation flight tracks during February and April 2009. Chart adapted from the Harmonized World Soil Database (HWSD) (Fischer et al. 2011).

3.1. Upper troposphere aircraft temperature observations (T_{Ob}) and WRF temperature forecasts (T_F) over land compared to temperature error (T_E) and forecast vertical velocity (VV_F) coupling ($R^2 = 0.2$).

3.2. Upper troposphere aircraft temperature observations (T_{Ob}) and WRF temperature forecasts (T_F) over water compared to temperature error (T_E) and forecast vertical velocity (VV_F) coupling ($R^2 = 0.0$).

3.13. WRF upper troposphere combined horizontal wind velocity error (WV_E) (ms^{-1}) and forecast vertical velocity (VV_F) (mb s^{-1}) comparison between 0-399 meters (m) surface elevation above sea level (CI=0) between 39-59 degrees (°) north latitude (*N*) ($R^2 = 0.1$).

3.14. Surface analysis (right) and 500 hectopascals (hPa) temperature and pressure (upper left) charts compared to MM5 multi-leg vertical cross section (lower left) forecast on 12 February 2009. Dashed lines indicate convective and frontal zone crossing during aircraft flight (Colorado State University 2012, United Kingdom Meteorological Office 2012).

3.15. Surface analysis (right) and 500 hectopascals (hPa) temperature and pressure (upper left) charts compared to MM5 multi-leg vertical cross section (lower left) forecast on 4 April 2009. Dashed lines indicate convective and frontal zone crossing during aircraft flight (Colorado State University 2012, United Kingdom Meteorological Office 2012).

LIST OF TABLES

Chapter 1

Introduction

1.1 Background

Atmospheric temperature prediction has improved escalating atmospheric modeling skill and providing high degrees of success in regional climate modeling. Prior to computer modeling, weather prediction methods utilized manual calculations to solve lengthy mathematical formulas deriving atmospheric temperature, horizontal wind direction, and velocity in which to base operational decisions (i.e. optimal aircraft cruise altitude) (Zhu et al. 2002). Advancements in computer technology allow atmospheric models to quickly calculate atmospheric temperature, horizontal wind direction, and velocity, and include rapid assimilation of sounding data improving the skill of meteorological predictions (Ali 2004). Computer technology improvements in atmospheric model computations (i.e. processor speed) require continued test and validation to ensure atmospheric temperature, horizontal wind direction, and velocity modeling skill is not degraded (Cheng and Steenburgh 2005, Knutti et al. 2010). Therefore, atmospheric temperature, horizontal wind direction, and velocity forecasting requires comparison to in situ temperature measurements and other modeled physical parameters (i.e. forecast vertical velocity) determining if temperature, horizontal wind direction, and velocity errors are exhibited in model prediction (Manning and Davis 1997).

Weather observations assist forecast model evaluation indicating potential biasing of temperature, horizontal wind direction, and velocity using radio soundings and aircraft observations. One forecast model using aircraft observations and radio sounding data for

verification is the Pennsylvania State University (PSU) Fifth Generation Mesoscale Model (MM5) discussed by Grell et al. (1994). Chandrasekar et al. (2002) compared rawinsonde temperature observations to MM5 forecasts indicating MM5 temperature error ranged between 0.5-3.6 degrees (°) Celsius (*C*) in the atmospheric column between altitudes of 850-250 hectopascals (hPa) over Philadelphia, PA. MM5 horizontal wind velocity forecasts were compared to rawinsonde observations, indicating MM5 forecast error ranged between 0.8-3.6 meters per second (ms^{-1}).

MM5 forecasts were evaluated against historical radiosonde temperature and horizontal wind direction and velocity observations over Antarctica up to 700 hPa (Guo et al. 2003). Radiosonde launches occurred from surface elevations up to 3400 meters (*m*) above sea level ranging from costal to middle continent launch sites. Comparison of 700 hPa MM5 forecast and observed temperatures indicated differences < 2.0°*C.* Weather station observation comparisons to MM5 700 hPa horizontal wind velocity forecasts produced a bias range of -2.2 to 0.1 ms^{-1} and a root mean square error (RMSE) between 3.3-4.4 ms^{-1}. MM5 700 hPa forecast and observed horizontal wind direction bias was found to range from 5.8-9.7° (RMSE=16.7-17.6°) (Guo et al. 2003).

MM5 forecasts were compared to aircraft and automated weather station observations while studying Greenland's katabatic layer by Bromwich et al. (2001). MM5 forecasted horizontal wind velocity bias was 0.3°*C* (RMSE=4.6 ms^{-1}) at altitudes ≤ 400 *m* above ground level. MM5 forecasted horizontal wind direction remained close to predicted values ≤ 400 *m* but deviated from model forecast (± 17°) with increasing height. MM5 potential temperature forecast also indicated a bias of 1.2°*C* (RMSE=2.2°*C*) ≤ 400 *m* above ground level. Comparison of graphical information displaying MM5

temperature, horizontal wind direction, and velocity against aircraft observations ≤ 400 *m* above ground level, indicated MM5 forecast accuracy decreased with height.

Using aircraft and ground station observations to understand accuracy of MM5 temperature, horizontal wind direction, and velocity prediction paved the way for new forecast models. The Weather Research and Forecasting model (WRF) described by Skamarock et al. (2008) and discussed by Zhang et al. (2009) was implemented to improve accuracy of computer weather forecasting (Hines and Bromwich 2008). WRF was developed through National Center for Atmospheric Research (NCAR), U.S. Air Force Weather Agency (AFWA), Forecast Systems Laboratory (FSL), National Center for Environmental Prediction (NCEP), Naval Research Laboratory, University of Oklahoma and National Oceanic and Atmospheric Association (NOAA) collaboration incorporating improved physics packages over MM5 optimizing performance (Cheng and Steenburgh 2005). WRF provides numerical weather prediction incorporating real time data assimilation leading to improvement in skill over MM5 (Pattanayak and Mohanty 2008). Studies by Sauter and Henmi (2004) and Coniglio et al. (2010) described below are examples of ongoing skill assessment of WRF temperature, horizontal wind direction and velocity forecasts.

Surface observations were compared to WRF and MM5 temperature and horizontal wind velocity forecasts over complex surface terrain in central Utah (Sauter and Henmi, 2004). MM5 outperformed WRF in temperature forecasts by a delta (Δ) RMSE=0.6°*C* during winter months and exhibited similar temperature forecast skill during summer months (Δ RMSE=0.1°*C*). WRF outperformed MM5 in horizontal wind velocity forecasts during summer months (Δ RMSE=0.4 ms^{-1}) while WRF and MM5 forecast

performance indicated the same skill during winter months (Δ RMSE=0.0 ms^{-1}). WRF outperformed MM5 in horizontal wind direction forecasts during summer months (Δ RMSE=0.7°) and WRF and MM5 forecasts indicated the same skill during winter months (Δ RMSE=0.0°). Analysis of temperature, horizontal wind direction, and velocity forecasts indicated WRF skill was better than MM5 in most cases but still less than desirable and further work to improve skill was suggested.

WRF temperature forecasts were evaluated comparing cumulus parameterization schemes near storm environments at 2 *m* above ground level and 850 hPa over the United States (Coniglio et al. 2010). WRF temperature forecasts during thunderstorms indicated a bias of -1.3 to 0.5°*C* (Δ RMSE=0.8°*C*) at 2 *m* above ground level. However, at 850 hPa the bias of WRF temperature forecasts during thunderstorms decreased to a range of -0.2 to 0.0°*C* (Δ RMSE=0.3°*C*). MM5 and WRF forecast assessments generally occurred near the surface (≤ 400 *m*), at lower troposphere levels (≤ 700 hPa) and in the stratosphere (250 hPa) indicating varied bias and RMSE at these heights. To date MM5 forecast verification using in situ measurements still has not knowingly been accomplished at upper troposphere levels (500-400 hPa) over data sparse regions. WRF verification of troposphere forecasts has used in situ measurements through the lower troposphere and upper troposphere via observation networks over populated regions (Wilson et al. 2011; Wilson et al. 2012). Therefore it is unknown how MM5 and WRF temperature, horizontal wind direction and velocity forecasts perform in the upper troposphere over sparsely populated and data void regions.

MM5 and WRF forecast validation has been accomplished in the lower troposphere and further understanding of performance in the upper troposphere is needed, especially

where assimilation data is scarce. A complete understanding of MM5 and WRF forecast skill cannot be replicated using model to model comparison (Pattanayak and Mohanty 2008) or radio sounding and statistical analysis studies alone. For this reason, long range in situ measurements are needed in the upper troposphere. Aircraft observations have been used for temperature, horizontal wind direction, and velocity validation in the lower troposphere and aircraft are capable of providing abundant precision data over data sparse regions in the upper troposphere. Use of aircraft replaces the need for numerous radiosondes over long distances reducing statistical uncertainty with the potential to enhance MM5 and WRF prediction of mesoscale motion within the upper troposphere.

1.2 Motivation

In order to use MM5 and WRF forecasts with confidence, the capability to predict temperature, horizontal wind direction, and velocity within the upper troposphere requires thorough validation encompassing regions without radiosonde capability or frequent aircraft travel. MM5 and WRF are applied heavily in areas where temperature, horizontal wind direction, and velocity biasing might place upper troposphere forecast users (i.e. aircraft flight planners) in a vulnerable position such as improper selection of aircraft cruise altitudes. Vulnerabilities to the upper troposphere temperature forecast user may include erroneous areas of turbulence and incorrect cloud moisture prediction resulting in unexpected ice accumulation on aircraft control surfaces, reducing safety to flight crew and passengers. Increased cost to operations as a result of erroneous horizontal wind direction forecasts may result in less favorable flight routes chosen.

Additionally risk of economic loss may be increased as a result of incorrect conclusions regarding storm movement (Pattanayak and Mohanty 2008) and volcanic ash transport (Lin et al. 2011; Stohl et al. 2011), resulting in damage to aircraft structure or engines (Zhu et al. 2002).

Another model application which may be affected by erroneous MM5 and WRF horizontal wind velocity forecasting is fuel consumption planning during flight by air transportation companies, which may result in a shortage of available fuel in-flight (Mass 2006). Unintended use of in-flight fuel reserves may stem from aircraft holding delays due to unforeseen landing conditions at destinations owing to incorrect forecasting of storm or volcanic ash arrival (Coniglio et al. 2010; Lin et al. 2011; Stohl et al. 2011). Misuse of fuel reserves as a result of poor MM5 and WRF forecast skill reduces safety needlessly exposing users of aircraft to increased risk (Zhu et al. 2002). Scenarios similar to these must be reduced in order for upper troposphere prediction users to safely alleviate unnecessary aircraft operating expenses and eliminate the potential for aircraft loss (Mass 2006). To assist in reduction of risk and aid in understanding upper troposphere MM5 and WRF model anomalies, an evaluation for the presence of temperature, horizontal wind direction and velocity error, and forecast vertical velocity coupling was conducted.

This study began with operational testing of MM5 and WRF upper troposphere forecasts for worldwide use by aircraft identifying any temperature, horizontal wind direction, and velocity forecast anomalies which may exist. Operational testing was accomplished on six successive transcontinental flights and one transoceanic flight within the upper troposphere using pre-designated flight routes between 39-59 degrees (°)

north latitude (*N*). Upper troposphere temperature, horizontal wind direction, and velocity observations were taken over North America, the North Atlantic Ocean, Europe, and Southwest Asia using aircraft navigation system displays. Aircraft observations occurred during cruise flight between 6000-7600 *m* above sea level. Upper troposphere observations were compared to MM5 and WRF upper troposphere multi-leg vertical cross section temperature, horizontal wind direction, and velocity forecasts for analysis.

1.2.1 Temperature

MM5 and WRF temperature errors (i.e. differences between upper troposphere forecasts and aircraft observations) were determined and an RMSE=1.8°*C* computed (Fig. 1.1). An RMSE=1.8°*C* was initially thought to have been due to lateral distance deviation of the aircraft from MM5 and WRF modeled flight tracks as a result of required course deviations by air traffic control or hazardous weather avoidance. A correlation test was accomplished between the upper troposphere combined MM5 and WRF temperature error and lateral distance deviations up to 100 kilometers (km) from the model flight tracks producing a correlation coefficient (*R*) of 0.1, suggesting lateral distance deviations were not the prime contributor to RMSE, and indicating another cause (Fig. 1.2). MM5 and WRF upper troposphere temperature errors were plotted in time series, producing a similar signature as MM5 and WRF upper troposphere forecasted vertical velocity (Fig. 1.3).

MM5 and WRF upper troposphere forecast and observed wind direction were compared in a time series plot indicating differences between forecast and observed horizontal wind direction resulting in a RMSE=71.3 degrees true (°*T*) (compass degrees

uncompensated for magnetic declination) (Fig. 1.4). Off course maneuvering from the modeled flight tracks occurred during observation flights complying with air traffic control direction or hazardous weather avoidance, suggesting a potential cause for horizontal wind velocity errors. Combined MM5 and WRF horizontal wind direction errors were plotted against lateral distance deviations up to 100 km from modeled flight tracks and a correlation test completed indicating lateral distance deviation from model flight tracks was a partial cause of horizontal wind direction error (R=0.4), but suggesting an additional contributing factor (R<1.0) (Fig. 1.5).

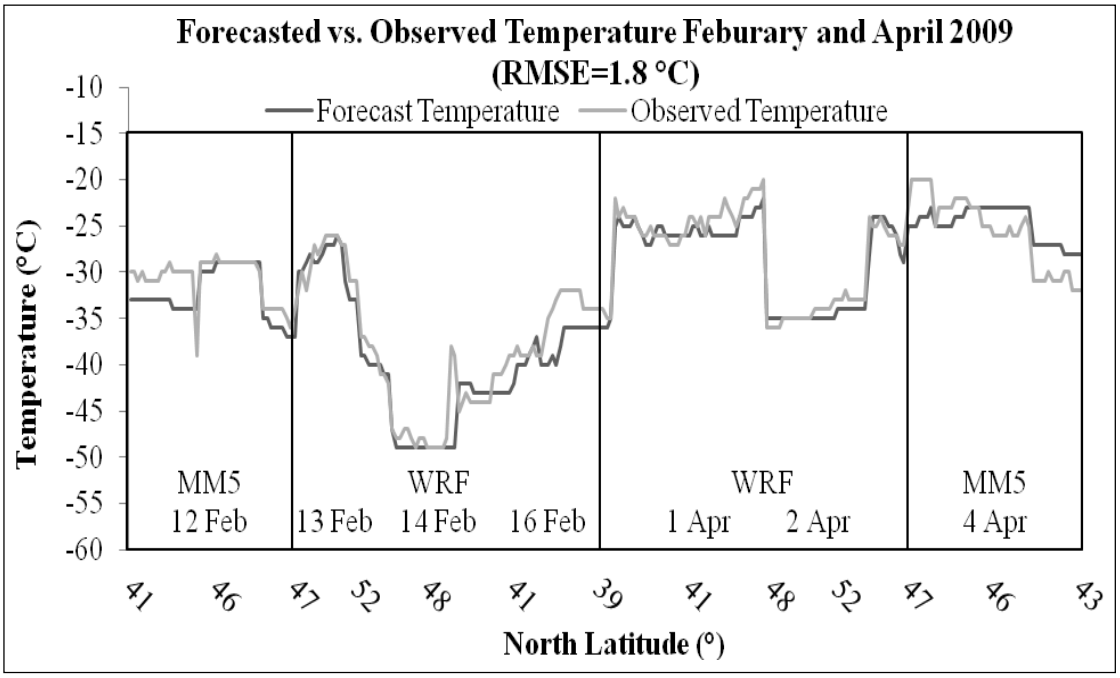

FIG. 1.1. MM5 and WRF forecasted temperatures (°*C*) in the upper troposphere with aircraft temperature observations (°*C*) taken while ascending and descending between 39-59 degrees (°) north latitude (*N*) en route from North America to Southwest Asia in February 2009 and returning to North America in April 2009.

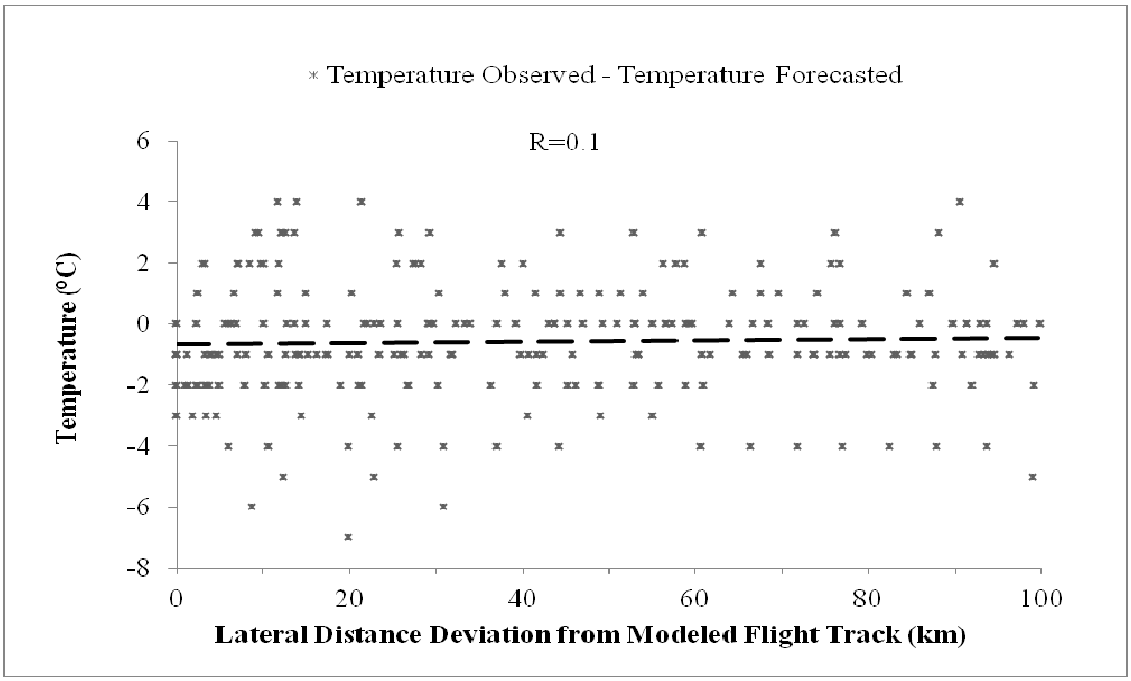

FIG. 1.2. Difference in upper troposphere combined MM5 and WRF temperature forecasts and aircraft observed temperatures compared to lateral distance deviation from MM5 and WRF model tracks (R=0.1).

1.2.2 Horizontal Wind Direction

Soich and Rappenglueck (2012) suggested forecast vertical velocity and temperature error in the upper troposphere were linked, providing rationale attempting to link forecast vertical velocity to horizontal wind direction errors in MM5 and WRF upper troposphere forecasts. MM5 and WRF upper troposphere horizontal wind direction errors were plotted in time series against forecast vertical velocity and a correlation test was accomplished indicating a subtle link (R=0.1) (Fig. 1.6).

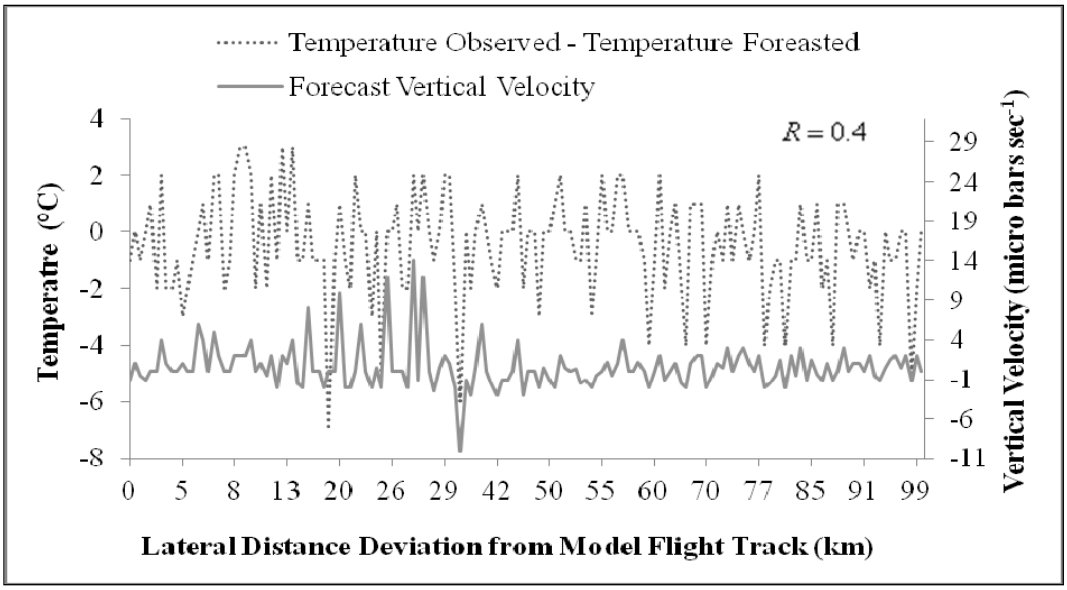

FIG. 1.3. Difference in upper troposphere combined MM5 and WRF temperature forecasts and aircraft observed temperatures compared to forecast vertical velocity within 100 kilometers (km) lateral distance deviation from MM5 and WRF modeled flight tracks ($R = 0.4$).

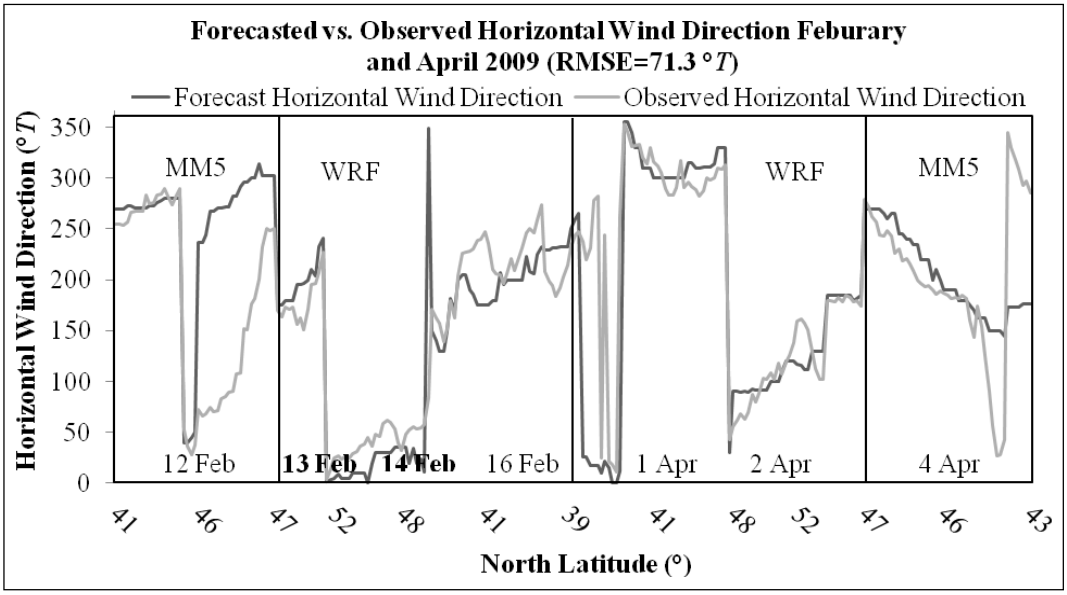

FIG. 1.4. MM5 and WRF forecasted horizontal wind direction (°*T*) (compass degrees uncompensated for magnetic declination) in the upper troposphere with aircraft horizontal wind direction observations (°*T*) taken while ascending and descending between 30-59 degrees (°) north latitude (*N*) en route from North America to Southwest Asia in February 2009 and returning to North America in April 2009.

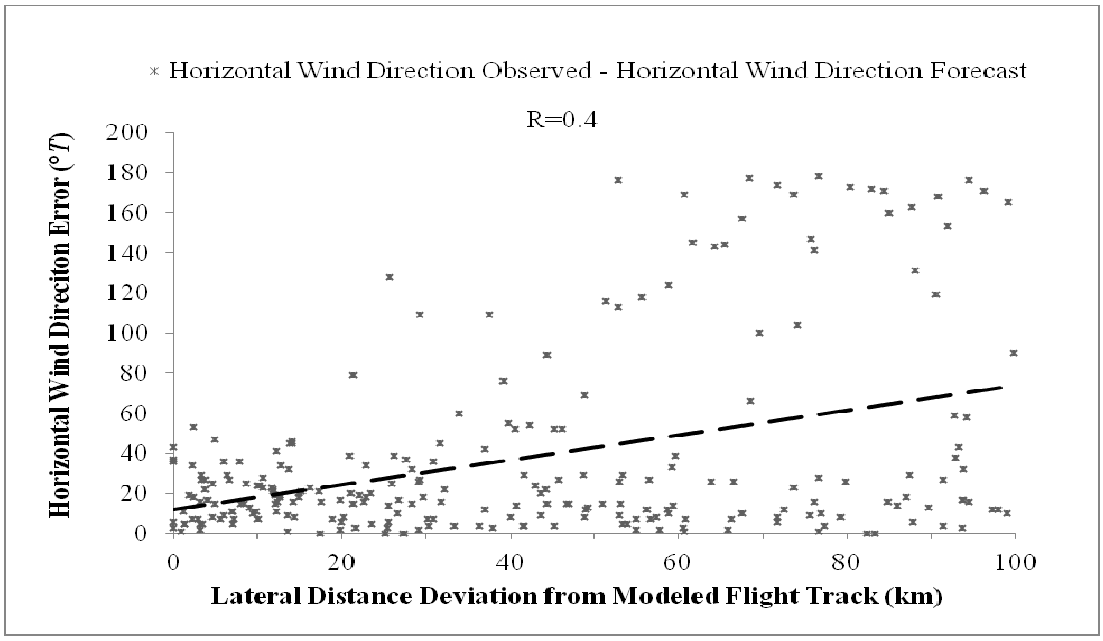

FIG. 1.5. Difference in upper troposphere combined MM5 and WRF horizontal wind direction forecasts (°*T*) and aircraft observed horizontal wind direction (°*T*) compared to lateral distance deviation from MM5 and WRF model tracks (*R*=0.4).

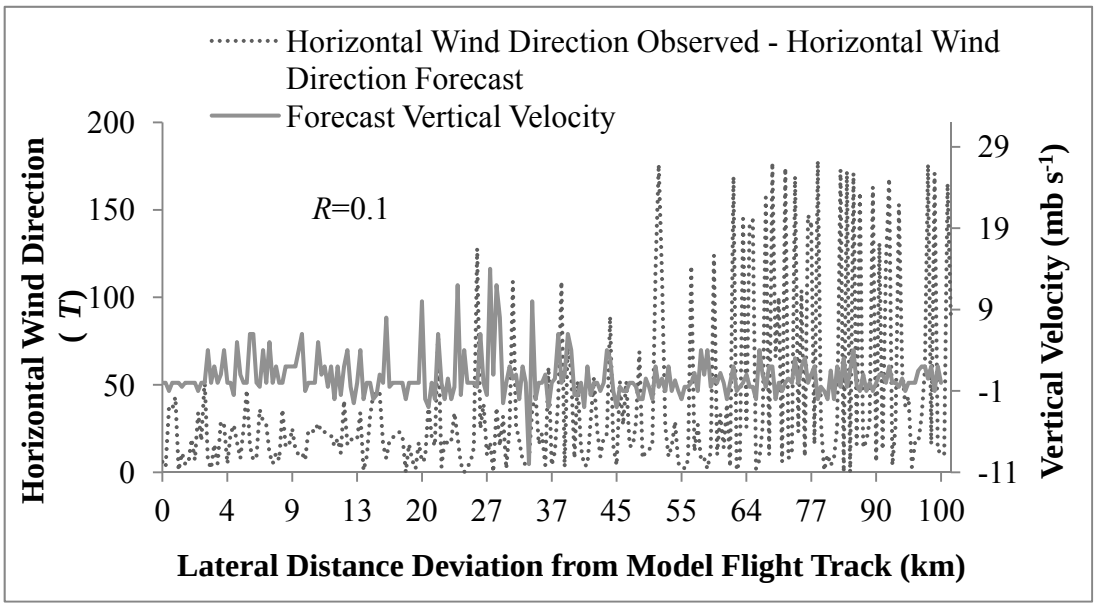

FIG. 1.6. Difference in upper troposphere MM5 and WRF horizontal wind direction forecasts (°*T*) and aircraft observed horizontal wind velocities (°*T*) compared to forecast vertical velocity (mb s^{-1}) within 100 kilometers (km) lateral distance deviation from MM5 and WRF modeled flight tracks (*R*=0.1).

1.2.3 Horizontal Wind Velocity

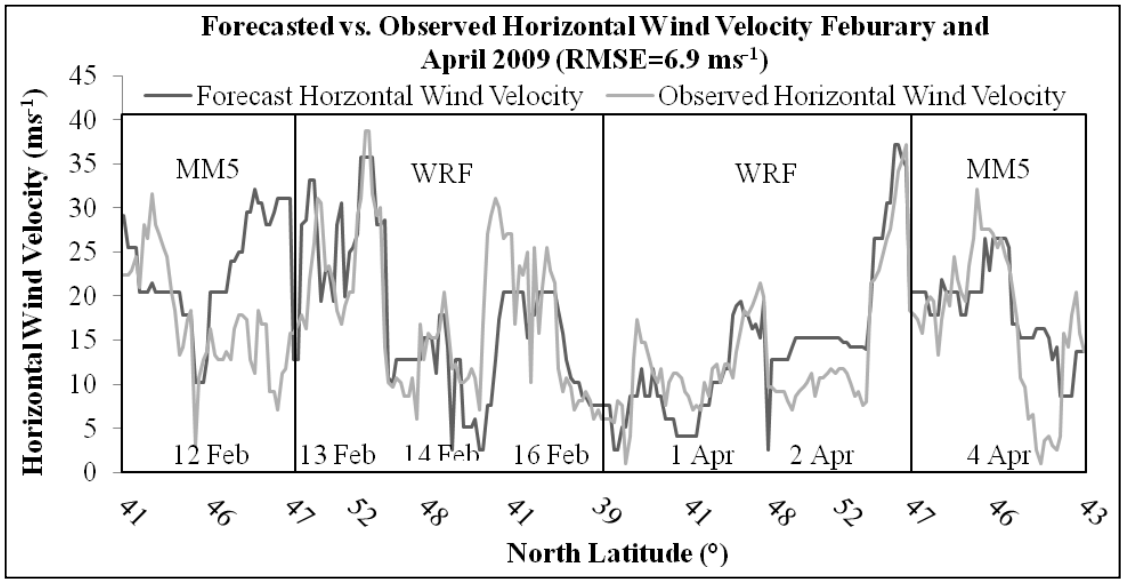

FIG. 1.7. MM5 and WRF forecasted horizontal wind velocity (ms^{-1}) in the upper troposphere with aircraft horizontal wind velocity observations (ms^{-1}) taken while ascending and descending between 39-59 degrees (°) north latitude (*N*) en route from North America to Southwest Asia in February 2009 and returning to North America in April 2009.

Combined MM5 and WRF horizontal wind velocity errors were calculated indicating positive and negative biases, and were thought to be a product of lateral distance deviation from modeled flight tracks as a result of off-course maneuvering required for hazardous weather avoidance or by air traffic control (Fig. 1.7). A correlation test was accomplished where R=0.0, indicating lateral distance deviations from modeled flight tracks were not a primary contributor and another cause for horizontal wind velocity error exists (Fig. 1.8). Coupling of temperature error and forecast vertical velocity has been indicated in upper troposphere forecasts, suggesting the possibility that forecast

vertical velocity may be a cause for horizontal wind velocity errors in upper troposphere MM5 and WRF forecasts (Soich and Rappenglueck 2012).

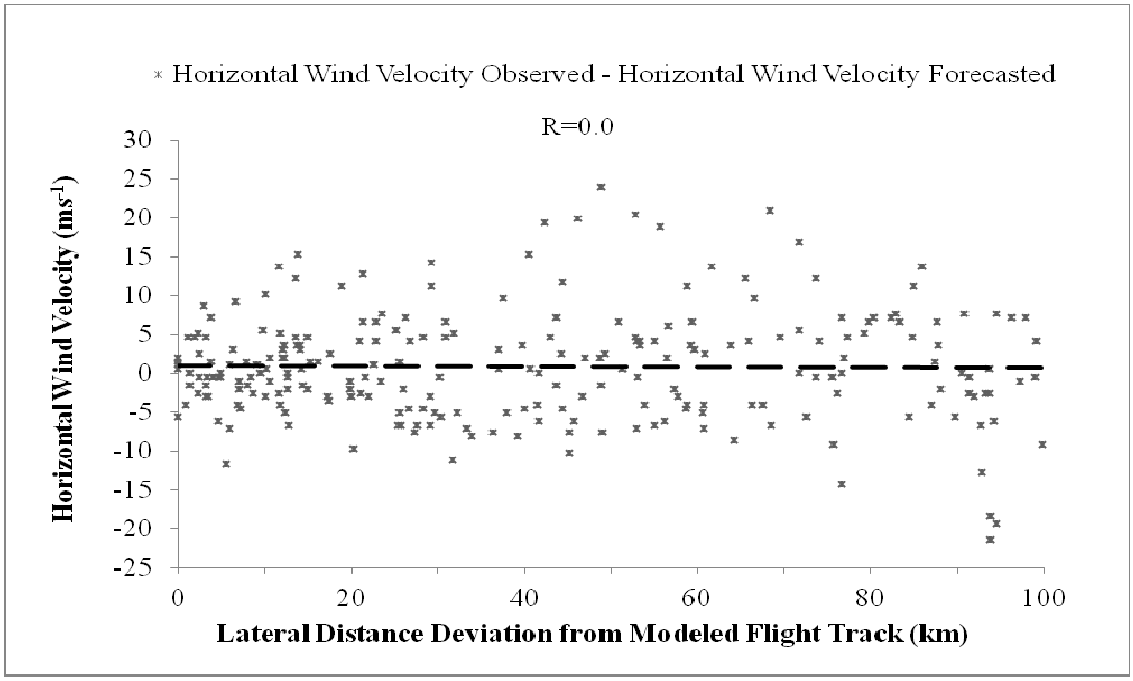

FIG. 1.8. Difference in upper troposphere combined MM5 and WRF horizontal wind velocity forecasts and aircraft observed temperatures compared to lateral distance deviation from MM5 and WRF model tracks (R=0.0).

Horizontal wind velocity data within 100 km lateral distance deviation from modeled flight tracks were assembled looking for correlations signifying coupling of MM5 and WRF forecast vertical velocity and horizontal wind velocity in the upper troposphere (Fig. 1.9). Correlation testing indicated an inverse relationship where R=-0.1 suggesting horizontal wind velocity error may be inversely coupled to forecast vertical velocity. Figure 1.9 indicates increases in MM5 and WRF horizontal wind velocity error near 50 km lateral distance deviation from modeled flight tracks are complimented by decreases in forecast vertical velocity.

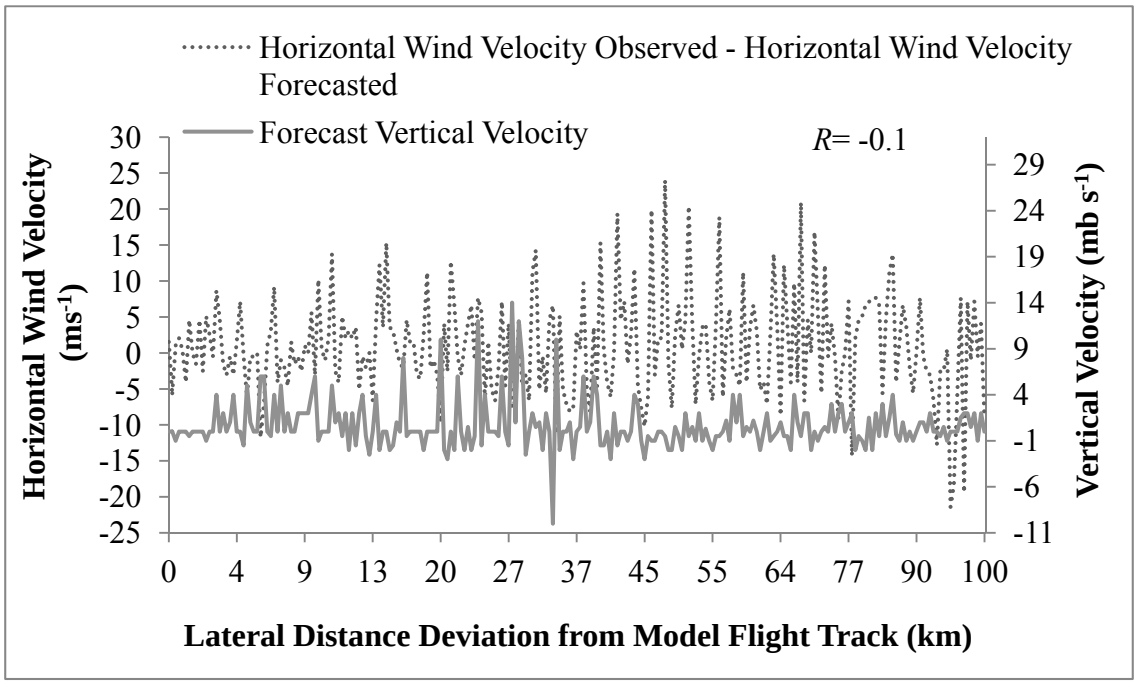

FIG. 1.9. Difference in upper troposphere combined MM5 and WRF horizontal wind velocity forecasts and aircraft observed horizontal wind velocity (ms^{-1}) compared to forecast vertical velocity (mb s^{-1}) within 100 kilometers (km) lateral distance deviation from MM5 and WRF modeled flight tracks (R=-0.1).

1.3 Questions

The similarity in signature between MM5 and WRF upper troposphere temperature (R=0.4), horizontal wind direction (R=0.1), and velocity (R=-0.1) error and forecasted vertical velocity prompted correlation testing providing the motivation for this study attempting to answer the following question:

1) Is temperature, horizontal wind direction, and velocity error and forecast vertical velocity coupling an anomaly in MM5 and WRF upper troposphere temperature forecasts?

Further examination of Figures 1.3, 1.6, and 1.9 suggested variation of temperature, horizontal wind direction, and velocity error in MM5 and WRF upper troposphere

forecasts within 100 km of lateral distance deviation from modeled flight tracks between 39-59°*N* lead to the question:

2) Is there a lateral distance deviation from upper troposphere MM5 or WRF modeled tracks where temperature, horizontal wind direction, and velocity error and forecast vertical velocity coupling diminishes?

Research into land and atmospheric changes by Evans and Geerken (2004), Giorgi (2006), Sheffield and Wood (2008), Pitman et al. (2009), Myoung et al. (2012), de Noblet-Ducoudré et al. (2012), and Boisier et al. (2012) led to another question:

3) Is temperature, horizontal wind direction, and velocity error and forecast vertical velocity coupling in MM5 and WRF upper troposphere forecast related to or enhanced by geographical traits such as a change in surface elevation above sea level or surface type such as land, water, urban influences, or different vegetation types?

RMSE and regression analysis was performed on MM5 and WRF upper troposphere temperature, horizontal wind direction, and velocity error data, indicating an association with forecast vertical velocity over different surface elevations above sea level and surface type such as land, water, urban, or vegetation (Jolliffe 2007). Evaluation of these parameters at upper troposphere levels provided insight into a MM5 and WRF model anomaly, shedding light into MM5 and WRF upper troposphere temperature, horizontal wind direction, and velocity forecast performance (Cocke et al. 2006).

1.4 Dissertation Overview

Chapter 2 discusses methodology and analysis methods used to collect upper troposphere temperature, horizontal wind direction, and velocity observations. Chapter 2 also discusses the source of model data and vertical velocity, temperature, horizontal wind direction, and velocity value extraction methods from model outputs. RMSE and regression analysis coupling temperature, horizontal wind direction, and velocity errors to forecast vertical velocity within 100 km lateral distance deviation of model flight tracks, different surface elevations above sea level, and different surface cover is presented in Chapter 3. Chapter 3 also discusses potential causes of temperature, horizontal wind direction, and velocity error and forecast vertical velocity coupling in MM5 and WRF upper troposphere forecasts. Conclusions of this study are presented in Chapter 4 along with recommendations for future work.

Chapter 2

Experimental Design

2.1 Overview

MM5 and WRF upper troposphere vertical velocity, temperature, horizontal wind direction, and velocity forecasts were provided by AFWA and upper troposphere observations taken using aircraft navigation systems while established in long range cruise flight. Aircraft navigation system displayed temperature, horizontal wind direction, and velocity were recorded by flight crews and compared to MM5 and WRF forecast temperature, horizontal wind direction, and velocity determining forecast error. Aircraft observation and radiosonde sounding temperature, horizontal wind direction, and velocity were compared when available ensuring anomalies were not present in aircraft systems corrupting model testing. Data sets were stratified and tested utilizing RMSE and regression analysis, identifying statistically significant temperature, horizontal wind direction, and velocity error and forecast vertical velocity coupling relationships. Statistically significant data were tested to a 95% confidence interval confirming temperature, horizontal wind direction, and velocity error and forecast vertical velocity coupling relationships in MM5 and WRF upper troposphere forecasts.

2.1.1 Aircraft Selection

Aircraft type selection was critical to best accomplish upper troposphere temperature, horizontal wind direction, and velocity observation (Cardinali et al. 2004, Wroblewski et al. 2010). Larger jet aircraft were unfavorable due to cruise altitudes above upper troposphere levels, while smaller aircraft were unable to operate at distances required for

long range observations (Moninger et al. 2003). Aircraft availability was considered requiring upper troposphere temperature, horizontal wind direction, and velocity observations to be accomplished concurrent to an already designated flight easing the selection process. The aircraft of choice was the C-130 Hercules which met all requirements of cruise altitude, observation recording feasibility, distance capability, and availability. The aircraft was provided through Wyoming Air National Guard cooperation and supported by 187th Airlift Squadron flight crews.

2.1.2 Temperature Observation Collection

Atmospheric temperature was provided by a single Goodrich 102A external probe mounted on the aircraft fuselage feeding data to the aircraft air data computer (ADC) and total air temperature gauge (T_G) (Goodrich 2002a). The probe integrates protection against inlet blockage from dust, insects, or bird strikes and provides thermal protection to prevent inlet blockage from ice formation without degrading accuracy (Goodrich 2002b). Total air temperature compressibility correction factors were applied to C-130 temperature gauge observations per aircraft operating procedures in agreement to findings by Khelif et al. (1999). Once aircraft capability was identified and found to be satisfactory, a spread sheet for manual in-flight data recording was developed using Microsoft Excel®. Upper troposphere temperature data collection was accomplished on pre-designated flights, while established at cruise altitude reducing ADC and navigation solution errors which may be caused by aircraft climb or descent (Cole and Jardin 2000).

Upper troposphere temperature observations took place on one transoceanic and three transcontinental flights in February 2009 and three transcontinental flights in April

2009 between 39-59°*N*, totaling seven separate observation data sets. Upper troposphere temperature observations were manually recorded in-flight from aircraft navigation system displays and T_G readings between 6000-7600 *m* above sea level every five minutes resulting in 25 km intervals. Data recording included universal coordinated time (UTC), observation geographical coordinates, aircraft altimeter, T_G, and aircraft navigation system displayed ambient air temperature. Compressibility at the temperature probe intake required a correction factor of -10°*C* (Eq. 2.1) (U.S. Air Force 2006) to all T_G readings deriving observed upper troposphere ambient air temperature (T_{Ob}) and found to be equivalent when compared to ADC air temperature calculations (Goodrich 2002a).

$$T_{\mathrm{Ob}} = T_G - 10°C \qquad (2.1)$$

Aircraft geographical position and altitude were plotted on printed MM5 and WRF forecasts and corresponding MM5 or WRF upper troposphere temperature values were manually recorded into data logs.

2.1.3 Horizontal Wind Direction and Velocity Observation Collection

The Wyoming Air National Guard C-130 aircraft was equipped with either Rosemount 0856NM1 or 0856NM2 pitot-static probes in addition to the single 102A temperature probe (Goodrich 2002a). The four pitot-static probes were mounted on the forward fuselage and aerodynamically compensated for local static errors due to position placement with continuous access to opposing airflow. The pitot-static probes were heated preventing port blockage similar to the temperature probe. Pitot-static probes

located on the forward fuselage are interchangeable without recalibration providing a Δ in static pressure (P_s) repeatability to $\Delta P_s = \pm 0.002 q_c$ where q_c represents impact pressure (Goodrich 2002a). Since the probes are calibrated to a $\Delta P_s = \pm 0.002 q_c$ and interchangeable without recalibration additional correction factors as discussed by Khelif et al. (1999) were not needed.

Aircraft horizontal wind direction and velocity is derived as a product of opposed airflow collection through the four pitot-static ports and single air temperature probe as the aircraft passes through an opposing air stream. Pressure is routed through pneumatic tubing where the ADC measures static pressure for altitude determination (Goodrich 2002b). Differences between opposed airflow entering the pitot probe opening (P_t) and P_s result in q_c used by the ADC for speed calculations (Eq. 2.2a).

$$q_c = P_t - P_s \tag{2.2a}$$

Once q_c has been determined, aircraft speed is computed as a Mach number (*M*) by the ADC:

$$M = \sqrt{5\left(\frac{q_c}{P_s} + 1\right)^{2/7} - 1} \tag{2.2b}$$

M is used with the temperature reading from the air temperature probe (T_t) by the ADC resolving the aircraft's true airspeed (TAS) through the air by

$$\mathrm{TAS} = Md\sqrt{\frac{T_t - 10}{1 + 0.2M^2}} \tag{2.3c}$$

in which

$$d = \left(\sqrt{\rho R}\right)(1.94261 \text{ kts}) = 38.96695 \text{ kts} \quad (2.2d)$$

where d is the speed of sound constant through air derived from the specific gas constant (R) and specific heat (ρ) of air adjusted for speed in knots (kts) (Eq. 2.2d) (Goodrich 2002b). The ADC incorporates TAS as a coordinate in the geodetic system combining aircraft heading inputs from aircraft inertial navigation units (INU) and desired course line (van den Kroonenberg et al. 2008).

The three remaining geodetic coordinates used in the horizontal wind direction (WD) calculation are derived from aircraft true heading (TH), aircraft true course (TC), and aircraft speed over the ground. The aircraft ground speed (GS) is determined by

$$\text{GS} = \frac{D}{\Psi} \quad (2.3a)$$

where D is the distance between geographical points and Ψ the time measured to cover distance D. The difference in compass heading in °T (HD) must be computed and is the angular difference between TH and TC:

$$\text{HD}=\text{TH}-\text{TC} \quad (2.3b)$$

in which TH represents compass headings in °T measured by the INU and TC the desired flight track in °T over the Earth's surface applied by the ADC to solve for WD (Eq. 2.3c) (Khelif et al. 1999).

$$\text{WD}=\text{TC}+\text{atan2}\{[\text{TAS}(\sin \text{HD})][\text{TAS}(\cos \text{HD})]-\text{GS}\} \quad (2.3c)$$

Results from Equation 2.3c are displayed in °T by the navigation system providing the horizontal wind direction observation (WD_{Ob}). The ADC uses TAS, GS, TH, and TC to derive horizontal wind velocity using Equation 2.4a (Khelif et al. 1999). Horizontal wind

velocity is displayed by the aircraft navigation system in knots (WV_{kts}) and manually converted to a horizontal wind velocity observation (WV_{Ob}) in ms^{-1} using Equation 2.4b.

$$WV=\sqrt{TAS\text{-}GS^2+\left\{\left(4\times TAS\times GS\right)\times\left[\sin\left(\frac{TH\text{-}TC}{2}\right)\right]^2\right\}} \qquad (2.4a)$$

$$WV_{Ob}=WV_{kts}\times 0.51 \qquad (2.4b)$$

WD_{Ob} and WV_{Ob} were manually recorded in Microsoft Excel® concurrent with T_{Ob} as discussed above during non-maneuvering flight eliminating potential ADC solution errors which can be induced during aircraft climb or descent causing erroneous output (Cole and Jardin 2000).

2.1.4 Observation and Aircraft Instrument System Verification

Upper troposphere radiosonde temperature (T_R), horizontal wind direction (WD_R), and velocity (WV_R) records were retrieved post flight near actual aircraft flight tracks when available using the University of Wyoming Upper Air Sounding Database (University of Wyoming 2012) and exhibited in Tables 2.1-2.3. 0000 UTC and 1200 UTC soundings were used enveloping the time of aircraft passage near the sounding station. Aircraft temperature, horizontal wind direction, and velocity observation altitudes were not shown on radiosonde data requiring interpolation of T_R , WD_R , and WV_R rounded to the whole number corresponding to aircraft navigation system display format. T_R was corrected for atmospheric heating or cooling as a result of time (T_{RC}) through interpolation of T_R . T_{Ob} was compared to T_{RC} by

$$T_{\Delta} = T_{\mathrm{RC}} - T_{\mathrm{Ob}} \qquad (2.5a)$$

yielding a temperature delta (T_{Δ}) range of 2.0°C (12 February) to -3.0°C (4 April). T_{Δ} remained warmer during most flights in February 2009 while decreasing to a cooling trend for flights in April 2009 over varying lateral distance deviations (km) between sounding locations and T_{Ob} at aircraft observation heights.

Radiosonde horizontal wind direction (WD_{R}) in °T was corrected ($\mathrm{WD}_{\mathrm{RC}}$) for changes in horizontal wind direction as result of changes in air mass or pressure over time. $\mathrm{WD}_{\mathrm{Ob}}$ were compared to $\mathrm{WD}_{\mathrm{RC}}$ identifying calculation errors by the ADC which may hinder model testing. An absolute horizontal wind direction delta (WD_{Δ}) was computed by

$$\left|\mathrm{WD}_{\Delta}\right| = \left|\mathrm{WD}_{\mathrm{RC}} - \mathrm{WD}_{\mathrm{Ob}}\right| \qquad (2.5b)$$

A $\left|\mathrm{WD}_{\Delta}\right|$ range of 1.0-44.0°T was exhibited where seven $\left|\mathrm{WD}_{\Delta}\right|$ were < 10.0°T and four $\left|\mathrm{WD}_{\Delta}\right|$ > 22.0°T. Sounding corrections ($\mathrm{WV}_{\mathrm{RC}}$) were also applied to radiosonde horizontal wind velocity (WV_{R}) using interpolation to compensate for changes over time in horizontal wind velocity conditions (air mass and pressure) during aircraft passage overhead of the sounding stations.

The absolute difference of horizontal wind velocity (WV_{Δ}) between $\mathrm{WV}_{\mathrm{RC}}$ and $\mathrm{WV}_{\mathrm{Ob}}$ was computed using Equation 2.5c checking aircraft instrumentation for computation errors which may affect model testing.

$$\left|\mathrm{WV}_{\Delta}\right| = \mathrm{WV}_{\mathrm{RC}} - \mathrm{WV}_{\mathrm{Ob}} \qquad (2.5c)$$

Calculations from Equation 2.5c yielded $|WV_{\Delta}| < 10.0$ ms^{-1} for all observation flight comparisons displayed in Table 2.3. Each flight posted at least one $|WV_{\Delta}| \leq 6.0$ ms^{-1} with the exception of 4 April 2009 resulting in a $|WV_{\Delta}| \leq 10.0$ ms^{-1}. Of the eleven $|WV_{\Delta}|$ computed seven were < 5.0 ms^{-1}. Although interpolation can introduce some uncertainty into the analysis averaged T_{Δ}, $|WD_{\Delta}|$ and $|WV_{\Delta}|$ of the seven sounding stations within 100 km of the aircraft indicated small Δ values (Tables 2.1 through 2.3). T_{Δ} indicated an average value of -1.0°C and a standard deviation (σ) of 1.2°C suggesting no visible shift in T_G measurements which may be due to indicator malfunction or probe inlet blockage. Navigation system errors which would affect WD_{Ob} and WV_{Ob} attributed to pitot/static inlet blockage or drift of the INU causing aircraft geographical position errors in concert with TAS and/or GS errors calculated by the ADC.

$|WD_{\Delta}|$ indicated an average value of 6.4°T (σ=8.4°T) and $|WV_{\Delta}|$ indicated an average value of 4.1 ms^{-1} (σ=3.3 ms^{-1}) indicating no malfunction in the aircraft navigation systems suggesting no observable aircraft instrumentation shift. Therefore, comparison of aircraft observations to radiosonde measurements promoted reasonable confidence in data purity similar to Moniger et al. (2003) and Benjamin et al. (2010).

TABLE 2.1. Comparison of upper troposphere radiosonde temperature soundings (T_{RC}) to aircraft observed temperature (T_{Ob}) near actual observation aircraft flight tracks (University of Wyoming 2012).

Sortie Date (2009)	Station (UTC)	Aircraft (UTC)	Station	Dist[2] (km)	Height (m)	T_R	T_{RC}	T_{Ob}	T_Δ
12 February	1200 0000[1]	1910	Caribou Canada	142	7013	-31 -29	-30	-29	+1
14 February	1200 0000[1]	1605	De Bilt Netherlands	107	7013	-38 -39	-38	-37	+1
	1200 0000[1]	1645	Meiningen Germany	96	7013	-43 -43	-43	-42	+1
	1200 0000[1]	1815	Budapest Hungary	170	7623	-48 -51	-50	-48	+2
16 February	0000 1200	0440	Samsun Turkey	26	7013	-44 -41	-43	-44	-1
	0000 1200	0505	Erzurum Turkey	85	7013	-39 -40	-39	-40	-1
1 April	0000 1200	0800	Erzurum Turkey	93	6098	-21[3] -21	-21	-21	0
2 April	0000 1200	0820	Bucharest Romania	35	6708	-22 -29	-27	-29	-2
	0000 1200	0925	Budapest Hungary	4	7318	-34 -34	-34	-36	-2
	0000 1200	1050	Meiningen Germany	52	7318	-35 -32	-32	-34	-2
4 April	1200	1235	Caribou Canada	142	6708	-23	-23	-26	-3

No reporting stations available for 13 February due to transoceanic flight.

[1] Radiosonde launch occurred on UTC day after aircraft passage.

[2] Lateral distance delta of the radiosonde geographic position from aircraft geographic position at aircraft observation altitude without regard to time of observations. Accuracy ±20 km (Seidel et al. 2011).

[3] Samsun, Turkey 0000 UTC sounding used in place of Erzurum, Turkey 0000 UTC sounding due to unavailable data.

TABLE 2.2. Comparison of upper troposphere radiosonde horizontal wind direction soundings (WD_{RC}) to aircraft observed horizontal wind direction (WD_{Ob}) near actual observation aircraft flight track.

Sortie Date (2009)	Aircraft (UTC)	Station	Dist[2] (km)	Height (m)	WD_R	WD_{RC}	WD_{Ob}	$\lvert WD_\Delta \rvert$
12 February	1910	Caribou Canada	142	7013	066 029	051	029	22
14 February	1605	De Bilt, Netherlands	107	7013	027 001	010	005	5
	1645	Meiningen, Germany	96	7013	039 020	028	034	6
	1815	Budapest, Hungary	170	7623	053 001	027	051	24
16 February	0440	Samsun, Turkey	26	7013	204 204	204	208	4
	0505	Erzurum, Turkey	85	7013	239 224	230	205	25
1 April	0800	Erzurum, Turkey	93	6098	310[3] 301	307	306	1
2 April	0820	Bucharest, Romania	35	6708	304 313	310	305	5
	0925	Budapest, Hungary	4	7318	036 090	077	080	3
	1050	Meiningen, Germany	52	7318	108 115	114	115	1
4 April	1235	Caribou Canada	142	6708	182	182	180	2

No reporting stations available for 13 February due to transoceanic flight.

[1] Radiosonde launch occurred on UTC day after aircraft passage.

[2] Lateral distance delta of the radiosonde geographic position from aircraft geographic position at aircraft observation altitude without regard to time of observations. Accuracy ±20 km (Seidel et al. 2011).

[3] Samsun, Turkey 0000 UTC sounding used in place of Erzurum, Turkey 0000 UTC sounding due to unavailable data.

TABLE 2.3. Comparison of upper troposphere radiosonde horizontal wind velocity soundings (WV_{RC}) to aircraft observed horizontal wind velocity (WV_{Ob}) near actual observation aircraft flight track (University of Wyoming 2012).

Sortie Date (2009)	Station (UTC)	Aircraft (UTC)	Station	Dist[2] (km)	Height (m)	WV_R	WV_{RC}	WV_{Ob}	$\lvert WV_\Delta \rvert$
12 February	1200 0000[1]	1910	Caribou Canada	142	7013	17 7	13	17	4
14 February	1200 0000[1]	1605	De Bilt, Netherlands	107	7013	36 20	31	33	2
	1200 0000[1]	1645	Meiningen, Germany	96	7013	5 38	14	5	9
	1200 0000[1]	1815	Budapest, Hungary	170	7623	17 9	13	19	6
16 February	0000 1200	0440	Samsun, Turkey	26	7013	11 28	18	11	7
	0000 1200	0505	Erzurum, Turkey	85	7013	27 23	25	27	2
1 April	0000 1200	0800	Erzurum, Turkey	93	6098	14[3] 23	20	14	6
2 April	0000 1200	0820	Bucharest, Romania	35	6708	15 7	10	14	4
	0000 1200	0925	Budapest, Hungary	4	7318	8 11	12	11	1
	0000 1200	1050	Meiningen, Germany	52	7318	11 14	14	14	0
4 April	1200	1235	Caribou Canada	142	6708	27	27	17	10

No reporting stations available for 13 February due to transoceanic flight.

[1] Radiosonde launch occurred on UTC day after aircraft passage.

[2] Lateral distance delta of the radiosonde geographic position from aircraft geographic position at aircraft observation altitude without regard to time of observations. Accuracy ±20 km (Seidel et al. 2011).

[3] Samsun, Turkey 0000 UTC sounding used in place of Erzurum, Turkey 0000 UTC sounding due to unavailable data.

2.1.5 Source of Model Data

Determining temperature, horizontal wind direction, and velocity error and forecast vertical velocity coupling for MM5 and WRF forecasts within the upper troposphere required employment of model forecasts in a similar manner as a potential user (i.e. aviation flight planning). To simulate forecast user employment, access was obtained to use the AFWA Joint Air Force and Army Weather Information Network (JAAWIN) Interactive Grid Analysis Display System (IGrADS) to run MM5 and WRF upper troposphere forecasts in which T_{Ob}, $\mathrm{WD}_{\mathrm{Ob}}$, and $\mathrm{WV}_{\mathrm{Ob}}$ were compared (Telfeyan et al. 2005). At the time of study initiation, JAAWIN's authorized computer model coverage was the MM5 for North America and version 3.0.1.1 of the WRF-Var (variational data assimilation) for the Atlantic Ocean, Europe and Southwest Asia. The IGrADS user interface allowed forecast users to select certain forecast physical parameters such as isotherms, horizontal wind direction, and velocity barbs, lower and upper height boundaries, model route start and stop locations, a model route segment midpoint, and forecast start and stop times for the model route segments. MM5 and WRF physics packages and domain settings were configuration controlled by JAAWIN with no ability for modification by the IGrADS user serving as a limitation preventing physics package modification for testing.

JAAWIN's forecast domains covered the landmasses of North America (MM5), Europe and Asia (WRF). JAAWIN controlled parent domains for MM5 and WRF were set at 45 km with 15 km nesting encompassing all modeled flight tracks. MM5 and WRF utilized the Rapid Radiative Transfer Model Long Wave Radiation (RRTM) and Simple

Short Wave Radiation schemes and employed the Noah land surface model. The Medium Range Forecast Planetary Boundary Layer (MRF PBL) and Kain-Fritsch cumulus parameterization schemes were selected by JAAWIN for MM5 using fixed sigma vertical layering and Multivariate Optimum Interpolation (MVOI) assimilation. MM5 utilized the upper radiative boundary conditions which were standard on the MM5 model while JAAWIN employed Vertical-Velocity and traditional Rayleigh dampening for WRF upper boundary conditions. JAAWIN's approved WRF physics packages consisted of the Yonsei University Planetary Boundary Layer (YSU PBL), New Kain-Fritsch cumulus parameterization and WRF Single Moment Five (WSM 5) schemes employing floating sigma vertical layering and Three-dimensional Variational Data Assimilation (3DVAR). The vertical boundaries of the MM5 and WRF model runs were set to begin at the surface and terminate at a height of 9100 *m.* In between 500-400 hPa the models have five layers, each of them between 500-540 *m* thick.

Upper troposphere temperature, horizontal wind direction, and velocity observation time periods were identified during February and April 2009 based on aircraft availability of flights over sparsely traveled or radiosonde deficient regions within the upper troposphere. Once flight routes were designated and flight planning completed the MM5 and WRF multi-leg route forecast parameters were entered into JAAWIN's online IGrADS user interface three hours prior to flight departure and completed within five minutes of model route parameter entry. Although observation flight routes used great circle routing, JAAWIN's IGrADS user interface system operated in straight line courses requiring desired flight altitudes, initial starting point, midpoint, and termination point. The take off time at the start point, estimated time over the midpoint, and

estimated landing time at the termination point were entered into the IGrADS user interface producing time accurate forecasts across the flight route requiring no additional time correction needed between aircraft observed and forecasted temperature, horizontal wind direction, and velocity data.

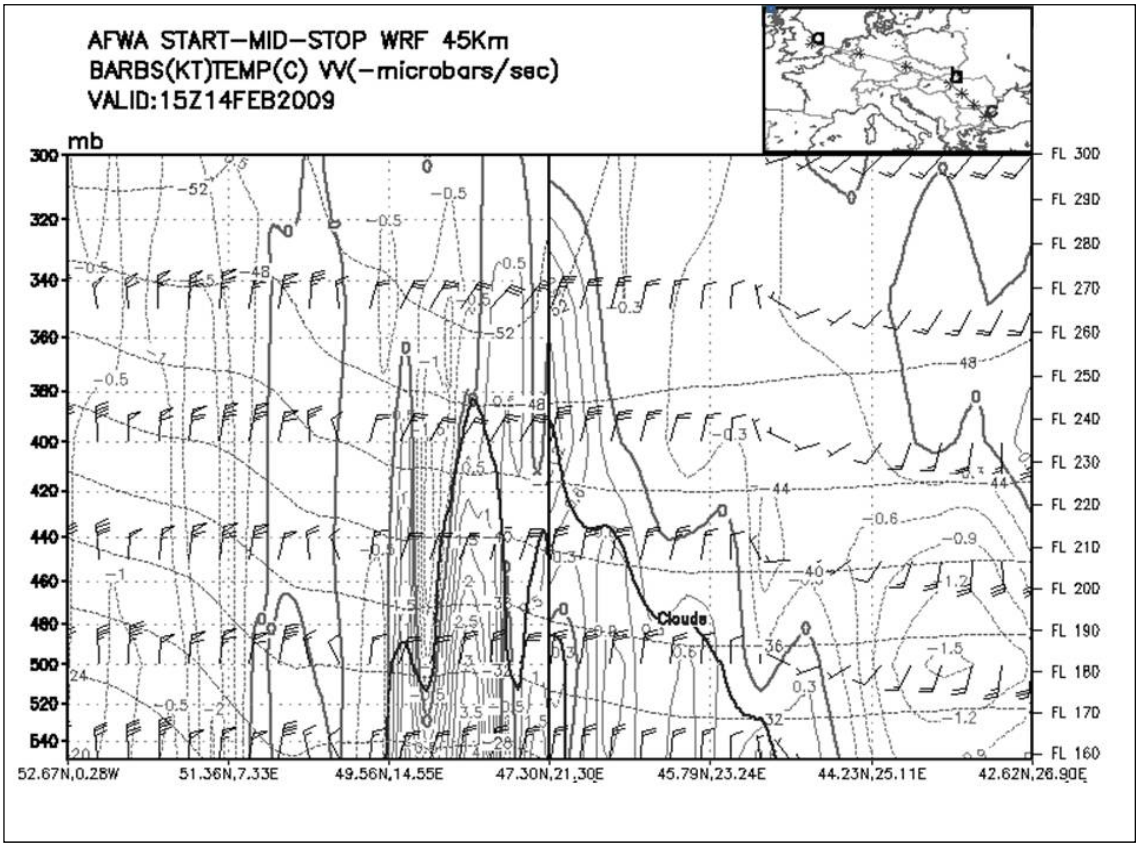

FIG. 2.1. WRF upper troposphere vertical cross-section forecast on 14 Feb 2009 for the planned route of flight between England and Romania. Model grid spacing defaulted to 45 kilometers (km), temperature in degrees Celsius (°*C*) (dotted horizontal line), wind direction in degrees (north at top of page) (barbs), wind velocity in knots (KT) (barb flags), cloud prediction (dark solid line) and vertical velocity (microbars sec^{-1}) (vertical dotted lines). Forecast initiation was England (*a*) and terminating in Romania (*c*) with the midpoint in the Czech Republic (*b*) as depicted by the map inset (top right) with latitude (*N*) and longitude (*W* and *E*) displayed at bottom, altitude in millibars (mb) (scale left) and pressure altitude in flight levels (FL) equating to thousands of feet (160 = 16000 feet) (scale right).

MM5 and WRF forecast outputs were printed for T_{Ob}, WD_{Ob}, and WV_{Ob} comparison with isotherms in °*C*, forecast wind direction depicted by wind barbs in °*T*, horizontal wind velocity in knots, forecast vertical velocity in microbars sec^{-1} (mb s^{-1}) cloud formation profiles, altitude in thousands of feet, and latitude and longitude in degrees (Fig. 2.1).

Upper troposphere forecast (denoted by subscript *F*) vertical velocity (VV_F), temperature (T_F), horizontal wind direction (WD_F) and velocity (WV_F) were extracted from the MM5 and WRF printed outputs. A grid was included on each printed MM5 and WRF output and used to plot aircraft position (latitude and longitude) on the x-axis and aircraft altitude in thousands of feet on the y-axis. Isotherms on the MM5 and WRF forecast outputs were in 4°*C* increments and isotherms were not always depicted at the intersection of aircraft position and altitude so T_F was interpolated by

$$T_F = \frac{\left(A_{\text{Ob}} - A_L\right)\left(T_U - T_L\right)}{A_U - A_L} + T_L \qquad (2.6a)$$

where A_{Ob} is the aircraft observation altitude, A_L the matching isotherm altitude height below A_{Ob}, A_U the matching isotherm height above A_{Ob}, T_L the modeled isotherm corresponding to A_L, and T_U the modeled isotherm corresponding to A_U resulting in a computed T_F rounded to the whole number corresponding to aircraft navigation system temperature format. MM5 and WRF upper troposphere WD_F were manually interpolated when aircraft position (latitude/longitude) and altitude grid plots did not intersect a forecast wind barb by

$$\mathrm{WD}_F = \frac{\left(A_{\mathrm{Ob}} - A_L\right)\left(\mathrm{WD}_U - \mathrm{WD}_L\right)}{A_U - A_L} + \mathrm{WD}_L \qquad (2.6b)$$

where WD_L is the modeled horizontal wind direction barb value for A_L and WD_U the modeled horizontal wind direction barb value for A_U resulting in a calculated WD_F rounded to the whole number matching aircraft navigation horizontal wind direction display format.

Interpolation of upper troposphere WV_F was used when horizontal wind velocity barbs did not intersect the aircraft altitude and latitude and longitude grid on the model output using Equation 2.6c.

$$\mathrm{WV}_F = \frac{\left(A_{\mathrm{Ob}} - A_L\right)\left(\mathrm{WV}_U - \mathrm{WV}_L\right)}{A_U - A_L} + \mathrm{WV}_L \qquad (2.6c)$$

In Equation 2.6c, WD_L is the modeled horizontal wind velocity related to A_L, and WD_U is the modeled horizontal wind velocity barb related to A_U, resulting in a calculated WV_F rounded to the whole number equivalent to aircraft navigation system horizontal wind velocity format. VV_F microbar gradients varied on the MM5 and WRF forecast outputs and microbars were not always depicted at the aircraft position and altitude intersection therefore interpolation was accomplished by

$$\mathrm{VV}_F = \frac{\left(\mathrm{LL}_{\mathrm{Ob}} - \mathrm{LL}_L\right)\left(\mathrm{VV}_R - \mathrm{VV}_L\right)}{\mathrm{LL}_R - \mathrm{LL}_L} + \mathrm{VV}_L \qquad (2.6d)$$

where $\mathrm{LL}_{\mathrm{Ob}}$ represents the latitude and longitude of the observation, LL_L the latitude and longitude of the model depicted microbar intercept left of $\mathrm{LL}_{\mathrm{Ob}}$ on the x-axis, LL_R

the model depicted microbar intercept on the x-axis to the right of $\mathrm{LL}_{\mathrm{Ob}}$, VV_{L} the corresponding microbar value of LL_{L}, and VV_{R} the corresponding microbar value of LL_{R}. Differences between the latitude and longitude points ($\mathrm{LL}_{\mathrm{Ob}}, \mathrm{LL}_{L}, \mathrm{LL}_{R}$) in Equation 2.6d represent distances in km and were computed using Global Positioning System (GPS) software. Manual extraction of model values occurred three times with navigational plotting equipment capable of measuring in 1.0° angles and divide spatial areas down to 1.5 centimeters. Interpolation presents a potential error for the analysis and was mitigated to the maximum extent possible by using the average of the three interpolated values suggesting the estimated error to be less than 0.5°*C*, 2.0°*T*, 1.9 ms^{-1} and 0.5 mb s^{-1} based on the resolution of the model values.

2.1.6 Post-flight Processing

Lateral distance deviation from MM5 and WRF modeled flight tracks were noted as insignificant (T_{Ob} *R*=0.1 and $\mathrm{WV}_{\mathrm{Ob}}$ *R*=0.1) and $\mathrm{WD}_{\mathrm{Ob}}$ computational resolutions of 2.0°*T* indicating lateral corrections of T_{Ob}, $\mathrm{WD}_{\mathrm{Ob}}$, and $\mathrm{WV}_{\mathrm{Ob}}$ to match MM5 and WRF modeled flight tracks were deemed unnecessary. T_{Ob}, $\mathrm{WD}_{\mathrm{Ob}}$, and $\mathrm{WV}_{\mathrm{Ob}}$ were arranged by smallest to largest lateral distance deviation from the model flight tracks and T_{Ob}, $\mathrm{WD}_{\mathrm{Ob}}$, and $\mathrm{WV}_{\mathrm{Ob}}$ within 100 km of lateral deviation were used providing representative data nearest the modeled flight tracks for analysis. Data were classified into 0-50 km and 51-100 km data sets to determine a point where temperature, horizontal wind direction and velocity error and VV_{F} coupling may no longer exist. Surface

elevation above sea level was derived through charted GPS elevation data and classified into sets of 100 *m* increments ascending in height from 0-699 *m* above sea level. For > 699 *m* in surface elevation above sea level, data points were combined into varying categories due to diminishing T_{Ob} data populations.

Upper troposphere T_{Ob}, WD_{Ob}, and WV_{Ob} were classified referencing the Harmonized World Soil Database (HWSD) depicted in Figure 2.2, determining if upper troposphere temperature, horizontal wind direction, and velocity error and VV_F coupling favor a surface type (Fischer et al. 2011). The HWSD map is a compilation of six separate supplementary databases allowing surface type classification by land, water, grass/scrub brush, crops, forest, no vegetation, and urban development. The database map allowed category definition up to > 75% vegetation type, however interference by blending of the 50-75% and > 75% map categories caused difficulty declaring > 75% coverage for all T_{Ob}, WD_{Ob}, and WV_{Ob}. Therefore the surface type category was declared using > 50% for vegetation and > 10% urban surface type. Snow cover was indicated by archived data over forest surface type on both MM5 flights over northeast Canada (Quebec to Caribou; *n*=7) and on both WRF flights between Regensburg, Germany and the Czech Republic border (*n*=4). All other surface types did not indicate snow cover (Montreal Weather Center 2012; National Weather Service 2012).

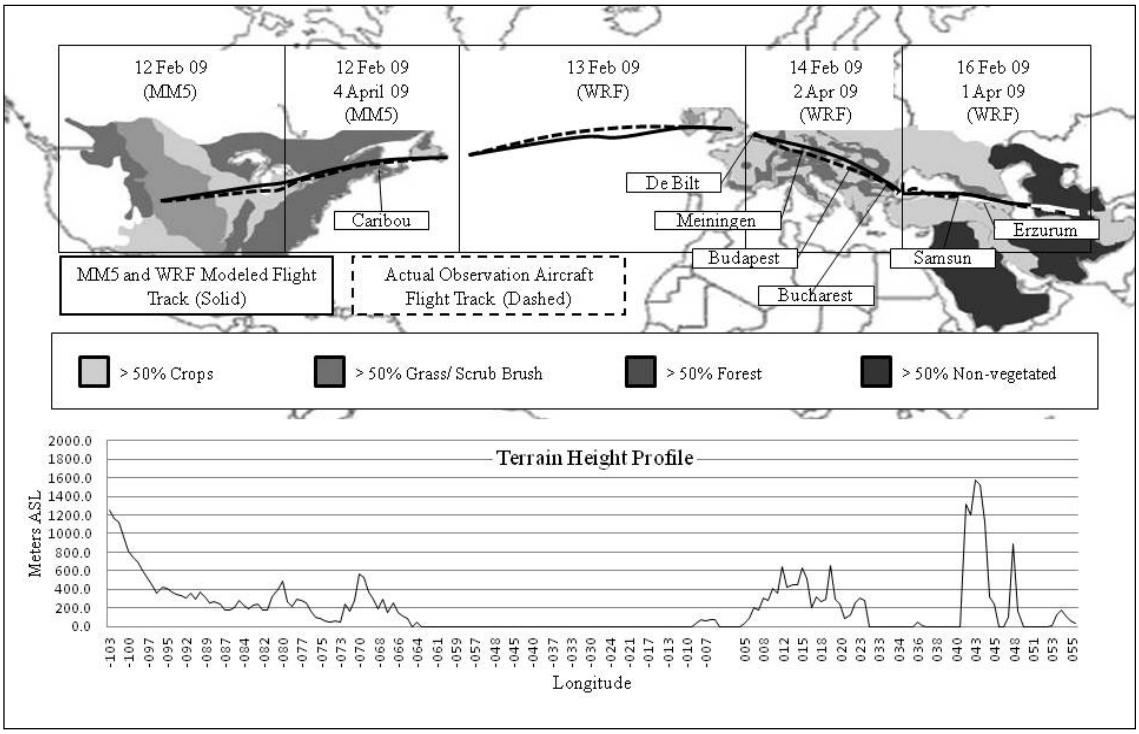

FIG. 2.2. Radiosonde station locations, type of surface type and surface elevation profile in meters above sea level for MM5 and WRF modeled flight tracks and actual aircraft observation flight tracks during February and April 2009. Chart adapted from the Harmonized World Soil Database (HWSD) (Fischer et al. 2011).

2.1.7 Analysis

RMSE was determined for each data set measuring skill as a potential marker to highlight the presence of temperature, horizontal wind direction, and velocity error and VV_F coupling. The initial step was to determine the upper troposphere temperature error (T_E) between T_{Ob} and T_F defined as

$$T_E = T_{\mathrm{Ob}} - T_F \qquad (2.7a)$$

the horizontal wind direction error (WD_E) defined by the absolute difference of $\mathrm{WD}_{\mathrm{Ob}}$ and WD_F by

$$\left|\mathrm{WD}_E\right| = \mathrm{WD}_{\mathrm{Ob}} - \mathrm{WD}_F \tag{2.7b}$$

and the horizontal wind velocity error (WV_E) defined as the difference between $\mathrm{WV}_{\mathrm{Ob}}$ and WV_F derived from

$$\mathrm{WV}_E = \mathrm{WV}_{\mathrm{Ob}} - \mathrm{WV}_F \tag{2.7c}$$

A correction factor was applied to WD_E derived in Equation 2.7b by eliminating coterminal direction headings ($\mathrm{WD}_{\mathrm{EC}}$) when WD_E exceeded 180°*T*, as discussed by Zill and Dewar (2010) and represented as

$$\left|\mathrm{WD}_{\mathrm{EC}}\right| = \left|\mathrm{WD}_E - 180^\circ\right| \tag{2.7d}$$

RMSE was then computed for data sets by

$$\mathrm{RMSE} = \sqrt{\frac{1}{n}\sum_{j=1}^{n}\left(X_{\mathrm{Ej}}\right)^2} \tag{2.8}$$

where X_E represents the tested parameter error (T_E , WD_E , WV_E) and *n* the number of observations (Stull 2000). A regression analysis was performed on each data set to establish a coupling relationship of T_E , WD_E , and WV_E to VV_F using a simple linear model detailed by Riggs (1985) and defined as

$$X_E = a(\mathrm{VV}_F) + b \tag{2.9a}$$

where the slope of the linear equation (*a*) is computed by

$$a = \frac{n\sum_{j=1}^{n}\left(\mathrm{VV}_{\mathrm{F\,j}} X_{\mathrm{E\,j}}\right) \sum_{j=1}^{n}\mathrm{VV}_{\mathrm{F\,j}} \sum_{j=1}^{n} X_{\mathrm{E\,j}}}{n\sum_{j=1}^{n}\mathrm{VV}_{\mathrm{F\,j}}^2 - \left(\sum_{j=1}^{n}\mathrm{VV}_{\mathrm{F\,j}}\right)^2} \tag{2.9b}$$

and the intercept of the linear equation (*b*) derived from

$$b = \frac{\sum_{j=1}^{n} X_{\mathrm{E\,j}} - a\sum_{j=1}^{n} \mathrm{VV}_{\mathrm{F\,j}}}{n} \qquad (2.9c)$$

The coefficient of determination (R^2) was used as a primary discriminator assessing the performance of the linear data fit calculated by

$$R^2 = \frac{\mathrm{SS}_R}{\mathrm{SS}_T} \qquad (2.10a)$$

with SS_R representing the sum squares of deviation of X_E from the experimental average error ($X_{\mathrm{E\,avg}}$) for each observation point j ($1 \leq j \leq n$):

$$\mathrm{SS}_R = \sum_{j=1}^{n} \left(X_{\mathrm{E\,j}} - X_{\mathrm{E\,avg}} \right)^2 \qquad (2.10b)$$

and SS_T signified by the totals of sum square error and regression error depicted as

$$\mathrm{SS}_T = \mathrm{SS}_E + \mathrm{SS}_R \qquad (2.10c)$$

in which SS_E represents the sum square error of the X_E residuals (γ) of j (Riggs 1985):

$$\mathrm{SS}_E = \sum_{j=1}^{n} \left(r_j - r_{\mathrm{avg}} \right)^2 \qquad (2.10d)$$

A standard error of regression (SE_R) was computed to further substantiate fit of regression through assessment of data set accuracy (Riggs 1985). SE_R depicted the experimental accuracy related to X_E along the regression line expressed as

$$\mathrm{SE}_R = \sqrt{\frac{\mathrm{SS}_R}{n-2}} \qquad (2.11)$$

The lower (denoted by subscript *L*) ($\mathrm{VV_{FL}}$) and upper (denoted by subscript *U*) ($\mathrm{VV_{FU}}$) bounded confidence interval (CI) of 0.95 were computed using Equation 2.12a.

$$(\mathrm{CI}=0.95) = \mathrm{VV_{F\,j}} - \mathrm{SE} \times t_{(1-\mathrm{P\,j})} \qquad (2.12a)$$

In this definition, *t* corresponds to the t-number resultant from the t-statistic, the p-value (P j) from the statistical significance test of VV_F , and SE the standard error of VV_F :

$$\mathrm{SE}=\sqrt{\frac{\mathrm{SS}_E\left(\frac{1}{n-(i+1)}\right)}{\sum_{j=1}^{n}\mathrm{VV}_{\mathrm{F\,j}}^2}} \qquad (2.12b)$$

where *i* is the number of independent variables (Riggs 1985).

Identification of T_E , WD_E , and WV_E coupling to VV_F was accomplished using $R^2 \geq 0.1$, rounded to one decimal place where $R^2 = 1.0$ demonstrates a perfect fit (Knutti et al. 2010). After R^2 was determined CI was tested by

$$\mathrm{VV_{FL}}(\mathrm{CI}=0.95) < 0 > \mathrm{VV_{FU}}(\mathrm{CI}=0.95) \qquad (2.13)$$

where inclusion of zero (CI=0) signifies rejection of T_E , WD_E , and WV_E coupling to VV_F qualifying determinations made by $R^2 = 0.0$.

Chapter 3

Results and Discussion

3.1 Temperature

3.1.1 MM5 and WRF Upper Troposphere Forecast Temperature RMSE Evaluation

RMSE scores were computed for all upper troposphere MM5 and WRF T_E data subcategories listed in Tables 3.1-3.3b and tested as markers to help identify T_E and VV_F coupling prior to regression analysis. RMSE analysis indicated WRF exhibited good (T_E RMSE$\leq 2.0°C$) T_E skill (WRF 0-50 km land T_E RMSE=1.8°*C*; WRF 51-100 km land T_E RMSE=1.1°*C*), while MM5 displayed moderate T_E skill (T_E RMSE=2.1-5.0°*C*) (MM5 0-50 km land T_E RMSE=2.2°*C*; MM5 51-100 km land T_E RMSE=2.4°*C*) in upper troposphere forecasts over land between 0-50 km and 51-100 km lateral distance deviation from modeled flight tracks (Table 3.1). MM5 and WRF exhibited good T_E skill in upper troposphere forecasts over water between 0-50 km lateral distance deviation from modeled flight tracks (MM5 and WRF 0-50 km water T_E RMSE=2.0°*C*) and improvement in T_E skill by MM5 (MM5 51-100 km water T_E RMSE=1.5°*C*) and WRF (WRF 51-100 km water T_E RMSE=1.0°*C*) upper troposphere forecasts over water between 51-100 km lateral distance deviation from modeled flight tracks.

MM5 indicated good T_E skill in upper troposphere forecasts over surface elevations $\leq$ 299 *m* above sea level differing by a T_E RMSE=0.2°*C* (Table 3.2a). MM5 exhibited

moderate T_E skill over surface elevations between 300-399 *m* (MM5 300-399 *m* T_E RMSE=3.4°*C*) and 400-499 *m* above sea level (MM5 400-499 *m* T_E RMSE=3.7°*C*) (Table 3.2a). WRF indicated moderate T_E skill over surface elevations between 100-199 *m* above sea level (WRF 100-199 *m* T_E RMSE=2.8°*C*), improving in T_E skill between 0-99 *m* (WRF 0-99 *m* T_E RMSE=1.3°*C*), 200-299 *m* (WRF 200-299 *m* T_E RMSE=0.8°*C*), 300-399 *m* (WRF 300-399 *m* T_E RMSE=1.2°*C*) and 400-499 *m* (WRF 400-499 *m* T_E RMSE=1.5°*C*) surface elevation above sea level. MM5 was not utilized over surface elevations > 499 *m* above sea level (Europe and Southwest Asia) but WRF was used for upper troposphere forecasts, producing T_E RMSE scores ranging between 0.7°*C* (good) and 2.9°*C* (moderate) over surface elevations > 499 *m* above sea level, indicating varied T_E skill with increased surface elevation (Table 3.2b).

MM5 (MM5 grass/scrub brush T_E RMSE=2.3°*C*) and WRF (WRF grass/scrub brush T_E RMSE=2.4°*C*) upper troposphere forecast exhibited moderate T_E skill over grass/scrub brush. WRF forecasts indicated good T_E skill over crops (WRF crops T_E RMSE=0.9°*C*), while MM5 forecast T_E skill remained moderate (MM5 crops T_E RMSE=4.1°*C*) (Table 3.3a). MM5 and WRF upper troposphere forecasts exhibited good T_E skill over forest regions (MM5 forest T_E RMSE=0.8°*C*; WRF forest T_E RMSE=1.8°*C*) and urban areas (MM5 urban T_E RMSE=0.9°*C*; WRF T_E urban RMSE=1.5°*C*) (Table 3.3b).

TABLE 3.1. RMSE (°C) and regression analysis results for temperature error (T_E) (°C) and forecast vertical velocity (mb s^{-1}) (VV_F) coupling for lateral distance deviation from MM5 and WRF modeled flight track.

Bold figures indicate: $R^2 \geq 0.1; CI \neq 0$ *Indicates CI=0		0-50 km		51-100 km	
		Land	Water	**Land**	Water
RMSE	MM5	2.2	2.0	2.4	1.5
	WRF	1.8	2.0	1.1	1.0
R^2	MM5	**0.6**	0.0	**0.6**	0.0
	WRF	**0.3**	0.0	**0.3**	0.0
SE_R	MM5	1.4	1.0	1.2	0.8
	WRF	1.4	1.9	1.0	0.9
a	MM5	0.5	0.0	1.1	0.7
	WRF	0.2	0.0	0.4	0.2
b	MM5	0.1	-2.1	-1.8	-1.0
	WRF	-0.9	-0.8	-0.2	-0.5
n	MM5	30	4	29	7
	WRF	61	40	43	13
CI=0.95					
MM5	VV_{FU}	**0.4**	-8.2*	**0.7**	-3.9*
	VV_{FL}	**0.7**	4.2	**1.4**	5.2
WRF	VV_{FU}	**0.1**	-1.4*	**0.2**	-0.1*
	VV_{FL}	**0.3**	0.2	**0.6**	0.1

TABLE 3.2a. RMSE (°C) and regression analysis results for upper troposphere temperature error (T_E) (°C) and forecast vertical velocity (mb s^{-1}) (VV_F) coupling over surface elevations ≤ 499 meters (m) above sea level.

Bold figures indicate: $R^2 \geq 0.1; CI \neq 0$ *Indicates CI=0		**0-99 *m***	100-199 *m*	200-299 *m*	**300-399 *m***	400-499 *m*
RMSE	MM5	1.7	1.5	1.3	3.4	3.7
	WRF	1.3	2.8	0.8	1.2	1.5
R^2	MM5	0.0	0.1	0.1	**0.8**	0.0
	WRF	**0.3**	0.1	0.0	**0.4**	0.1
SE_R	MM5	1.6	1.5	1.4	1.5	0.7
	WRF	1.1	2.3	0.8	1.0	1.5
a	MM5	0.2	0.2	0.8	1.3	0.0
	WRF	0.4	0.8	0.1	0.2	0.4
b	MM5	0.4	0.2	-0.9	-1.6	-3.6
	WRF	-0.3	-1.5	-0.2	-0.1	-0.7
n	MM5	11	14	7	12	3
	WRF	23	12	13	11	11
CI=0.95						
MM5	VV_{FU}	-0.4*	-0.3*	-1.5*	**0.9**	-5.1*
	VV_{FL}	1.7	0.7	3.1	**1.8**	2.2
WRF	VV_{FU}	**0.1**	-3.2*	-0.7*	**0.1**	-1.8*
	VV_{FL}	**0.6**	0.2	0.3	**0.4**	0.4

TABLE 3.2b. RMSE (°*C*) and regression analysis results for upper troposphere temperature error (T_E) (°*C*) and forecast vertical velocity (mb s^{-1}) (VV_F) coupling over surface elevations > 500 meters (*m*) above sea level.

Bold figures indicate: $R^2 \geq 0.1; \text{CI} \neq 0$ *Indicates CI=0		500-599 *m*	**600-699 *m***	**700-999 *m***	1000-1299 *m*	1300 *m*<
RMSE	MM5	-	-	-	-	-
	WRF	1.1	1.2	2.9	-	0.7
R^2	MM5	-	-	-	-	-
	WRF	0.6	**0.9**	**1.0**	-	0.4
SE_R	MM5	-	-	-	-	-
	WRF	0.3	0.9	0.9	-	0.2
a	MM5	-	-	-	-	-
	WRF	0.3	0.8	0.9	-	0.3
b	MM5	-	-	-	-	-
	WRF	-0.2	-0.7	-0.2	-	0.4
n	MM5	-	-	-	-	-
	WRF	6	5	8	-	11
CI=0.95						
MM5	VV_{FU}	-	-	-	-	-
	VV_{FL}					
WRF	VV_{FU}	-0.7*	**0.5**	**0.8**	-	-0.1*
	VV_{FL}	2.1	**2.1**	**0.4**		0.3

TABLE 3.3a. RMSE (°C) and regression analysis results for upper troposphere temperature error (T_E) (°C) and forecast vertical velocity (mb s^{-1}) (VV_F) coupling over land, water, crops and grass/scrub brush surface type.

Bold figures indicate: $R^2 \geq 0.1; CI \neq 0$ *Indicates CI=0		**Land**	Water	**Grass/ scrub brush**	**Crops**
RMSE	MM5	2.3	1.7	2.3	4.1
	WRF	1.5	1.8	2.4	0.9
R^2	MM5	**0.5**	0.1	0.0	**0.2**
	WRF	**0.2**	0.0	**0.4**	**0.3**
SE_R	MM5	0.5	0.8	0.7	0.3
	WRF	1.3	1.6	1.8	0.6
a	MM5	0.7	0.7	-0.3	0.3
	WRF	0.2	0.0	0.3	0.5
b	MM5	-0.9	-1.1	-2.9	-4.7
	WRF	-0.6	-0.7	-1.3	-0.4
n	MM5	59	11	10	8
	WRF	104	53	26	49
CI=0.95					
MM5	VV_{FU}	**0.5**	-0.1*	-1.3*	**-3.6**
	VV_{FL}	**0.9**	0.4	0.8	**-5.6**
WRF	VV_{FU}	**0.2**	-0.2*	**0.1**	**0.3**
	VV_{FL}	**0.3**	-0.4	**0.4**	**0.7**

TABLE 3.3b. RMSE (°C) and regression analysis results for upper troposphere temperature error (T_E) (°C) and forecast vertical velocity (mb s^{-1}) (VV_F) coupling over forest, no vegetation, urban and non-urban surface type.

Bold figures indicate: $R^2 \geq 0.1; CI \neq 0$ *Indicates CI=0		Forest	No Vegetation	**Urban**	**Non-Urban**
RMSE	MM5	1.8	-	0.9	2.4
	WRF	0.8	1.6	1.5	1.3
R^2	MM5	0.1	-	0.3	**0.4**
	WRF	0.1	0.0	**0.3**	0.1
SE_R	MM5	1.4	-	0.5	1.6
	WRF	0.8	1.6	0.3	1.3
a	MM5	0.3	-	0.3	0.7
	WRF	0.3	0.2	0.2	0.3
b	MM5	0.3	-	0.5	-1.0
	WRF	0.1	-0.9	-0.3	-0.1
n	MM5	41	-	4	55
	WRF	11	18	69	35
CI=0.95					
MM5	VV_{FU}	0.0*	-	-0.8*	**-1.1**
	VV_{FL}	0.6		1.3	**-2.1**
WRF	VV_{FU}	-0.3*	-0.4*	**-0.6**	0.4*
	VV_{FL}	0.8	0.8	**-1.2**	-0.6

MM5 showed moderate T_E skill over non-urban areas (MM5 non-urban T_E RMSE=2.4°C) and was not used over non-vegetated areas, so a T_E RMSE score was not computed. WRF was utilized over non-vegetated areas indicating good T_E skill (WRF no vegetation T_E RMSE=1.6°C), similar to upper troposphere forecasts over areas of non-urban development (WRF non-urban T_E RMSE=1.3°C).

3.1.2 Lateral Distance Deviation from MM5 and WRF Modeled Flight Track

MM5 and WRF upper troposphere T_E data within 100 km laterally of MM5 and WRF forecast modeled flight tracks were tested and results detailed in Table 3.1. Strong (R^2=0.6-0.9) T_E and VV_F coupling was indicated in MM5 upper troposphere forecasts over land between 0-50 and 51-100 km lateral distance deviation from modeled flight tracks, where MM5 0-50 km land and MM5 51-100 km land $R^2 = 0.6$ and confidence intervals were exclusive of zero ($CI \neq 0$). T_E and VV_F coupling was rejected between 0-50 and 51-100 km lateral distance deviation from modeled flight tracks in MM5 upper troposphere forecasts over water where MM5 0-50 km and MM5 51-100 km water $R^2 = 0.0$. WRF upper troposphere forecasts exhibited moderate ($R^2 = 0.3$-0.5) T_E and VV_F coupling over land between 0-50 km lateral distance deviation from modeled flight tracks where WRF 0-50 km land $R^2 = 0.3$ ($CI \neq 0$) and no T_E and VV_F coupling exhibited over water between 0-50 km lateral distance deviation from modeled flight tracks in WRF (WRF 0-50 km water $R^2 = 0.0$) upper troposphere forecasts. Between 51-100 km lateral distance deviation from modeled flight tracks WRF upper troposphere forecasts continued to indicate moderate (WRF 51-100 km land $R^2 = 0.3$; $CI \neq 0$) T_E and VV_F coupling over land with no indication of T_E and VV_F coupling in WRF upper troposphere forecasts over water (WRF 51-100 km water $R^2 = 0.0$).

3.1.3 Changes in Surface Elevation above Sea Level

MM5 and WRF T_E surface elevation data sets were tested determining if T_E and VV_F coupling in MM5 and WRF upper troposphere forecasts is specific to surface elevation above sea level. Strong to moderate T_E and VV_F coupling was exhibited by MM5 (MM5 300-399 m, $R^2 = 0.8$) and WRF (WRF 300-399 m $R^2 = 0.4$) upper troposphere forecasts over surface elevations between 300-399 *m* above sea level exhibited by MM5 and WRF 300-399 m $CI \neq 0$ (Table 3.2a). No indication of T_E and VV_F coupling was indicated in MM5 upper troposphere forecasts over surface elevations between 0-99 *m* above sea level where MM5 0-99 m $R^2 = 0.0$. MM5 and WRF upper troposphere forecasts over surface elevations between 100-299 *m* and 400-499 *m* above sea level indicated no T_E and VV_F coupling and MM5 and WRF 100-299 *m* and 400-499 *m* CI=0. Surface elevation data sets > 499 *m* above sea level contained no MM5 upper troposphere T_E data; however WRF upper troposphere forecasts exhibited strong T_E and VV_F coupling over surface elevations between 600-699 *m* (WRF 600-699 m $R^2 = 0.9$; $CI \neq 0$) and 700-999 *m* (WRF 700-999 m, $R^2 = 1.0$; $CI \neq 0$) above sea level with $n \leq 8$ (Table 3.2b).

3.1.4 Surface Type

Upper troposphere temperature error data were classified by surface type isolating T_E and VV_F coupling in MM5 and WRF over land, water, vegetation, and urban

surface type with findings displayed in Tables 3.3a and 3.3b. Weak ($R^2 = 0.1$ or 0.2) T_E and VV_F coupling was indicated in MM5 (MM5 land $R^2 = 0.5$; $CI \neq 0$) and WRF (WRF land $R^2 = 0.2$; $CI \neq 0$) upper troposphere forecasts over land, while T_E and VV_F coupling was not present in MM5 and WRF upper troposphere forecasts over water with MM5 and WRF water CI=0. T_E and VV_F coupling in MM5 upper troposphere forecasts over grass/scrub brush was not indicated; however WRF upper troposphere forecasts did indicate moderate T_E and VV_F coupling over grass/scrub brush (WRF grass/scrub brush $R^2 = 0.4$; $CI \neq 0$). Weak to moderate T_E and VV_F coupling was indicated in MM5 (MM5 crops $R^2 = 0.2$; $CI \neq 0$) and WRF (WRF crops $R^2 = 0.3$; $CI \neq 0$) upper troposphere forecasts over crops (Table 3.3a). T_E and VV_F coupling was not detected in MM5 and WRF upper troposphere forecasts over forest covered surfaces with CI=0 and no indication of T_E and VV_F coupling in WRF upper troposphere forecasts over non-vegetated areas (WRF no vegetation $R^2 = 0.0$). MM5 and WRF upper troposphere forecasts indicated T_E and VV_F coupling differently over urban influences where MM5 upper troposphere forecasts (MM5 non-urban $R^2 = 0.4$; $CI \neq 0$) indicated T_E and VV_F coupling over non-urban influences and WRF upper troposphere forecasts (WRF urban $R^2 = 0.3$; $CI \neq 0$) indicated T_E and VV_F coupling over urban influences (Table 3.3b).

3.1.5 Discussion

Regression analysis indicated significant statistical evidence supporting T_E and VV_F coupling in MM5 and WRF upper troposphere forecasts within 100 km lateral distance deviation from modeled flight tracks, over different surface type and surface elevations above sea level. An attempt was made to correlate RMSE with T_E and VV_F coupling which posted an $R = 0.0$ indicating RMSE is not a good indicator of T_E and VV_F coupling presence in MM5 and WRF upper troposphere forecasts.

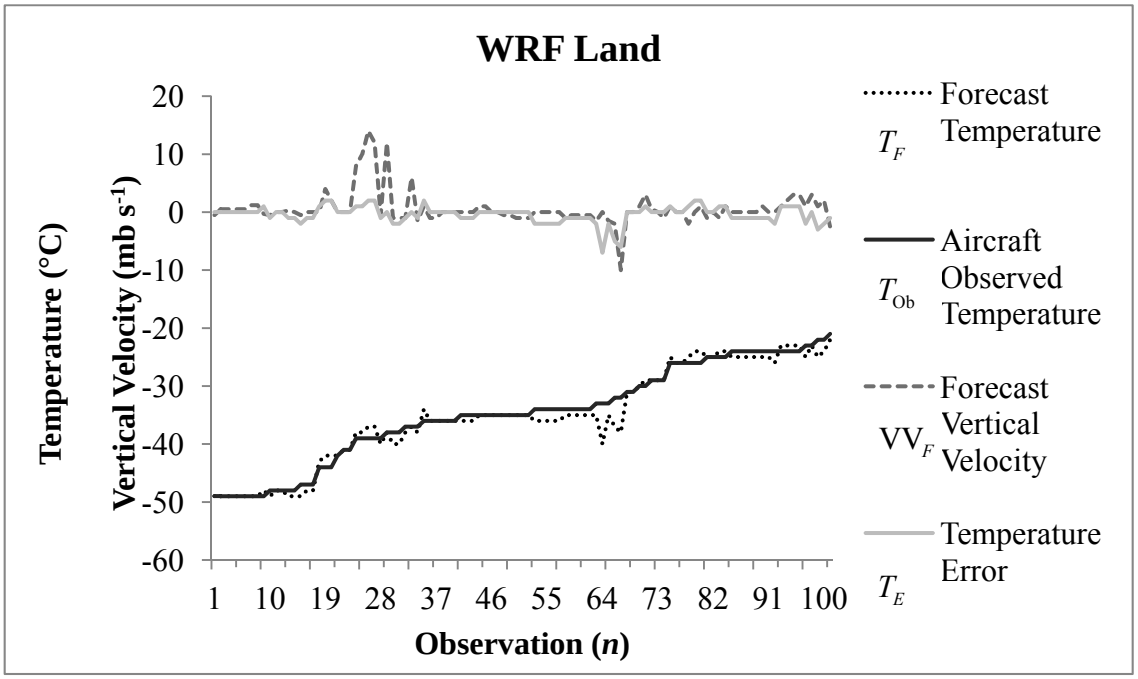

FIG. 3.1. Upper troposphere aircraft temperature observations (T_{Ob}) and WRF temperature forecasts (T_F) over land compared to temperature error (T_E) and forecast vertical velocity (VV_F) coupling ($R^2 = 0.2$).

Rejection of RMSE as a T_E and VV_F coupling indicator in MM5 and WRF upper troposphere forecasts is a result of similar RMSE values where T_E and VV_F coupling exists (i.e. WRF land RMSE=1.5°C and $R^2 = 0.2$) and where T_E and VV_F coupling is not present (i.e. WRF water RMSE=1.8°C and $R^2 = 0.0$) (Table 3.3a). Examination of Figure 3.1 indicated positive and negative temperature biases which tend to mirror VV_F and initially pointed toward T_E and VV_F coupling in MM5 and WRF upper troposphere forecasts. When T_{Ob} were arranged in the order of coldest to warmest a visual depiction of T_E and VV_F coupling was displayed corresponding to noticeable fluctuations in T_E (Fig. 3.1).

Figure 3.1 displays WRF T_E and T_{Ob} data over land illustrating T_E and VV_F coupling where T_{Ob} were arranged from coldest to warmest. Figure 3.1 also is characteristic of MM5 and WRF upper troposphere forecasts where T_E and VV_F coupling is present ($R^2 \geq 0.1$; $\mathrm{CI} \neq 0$). Figure 3.1 suggests when $T_E \geq 2.0\,°C$ a corresponding increase in VV_F magnitude is observed as exhibited by *n*=25, *n*=65 and *n*=81. Figure 3.2 displays WRF T_F and T_{Ob} data over water where T_{Ob} were arranged from coldest to warmest and no T_E and VV_F coupling present ($R^2 = 0.0$ or CI=0) which is representative for MM5 and WRF upper troposphere forecasts which did not indicate T_E and VV_F coupling ($R^2 = 0.0$ or CI=0). The increases in magnitude of VV_F displayed in Figure 3.1 corresponding to $T_E \geq 2.0\,°C$ were not displayed in Figure 3.2 where changes in VV_F magnitude were independent of T_E in MM5 and WRF upper

troposphere forecasts over water (*n*=10, *n*=36 and *n*=44). Therefore T_E appears to be the driver in erronous VV_F events over land in MM5 and WRF upper troposphere forecasts which may result in erroneous cloud formation prediction causing incorrect forcasting of precipitation and turbulence.

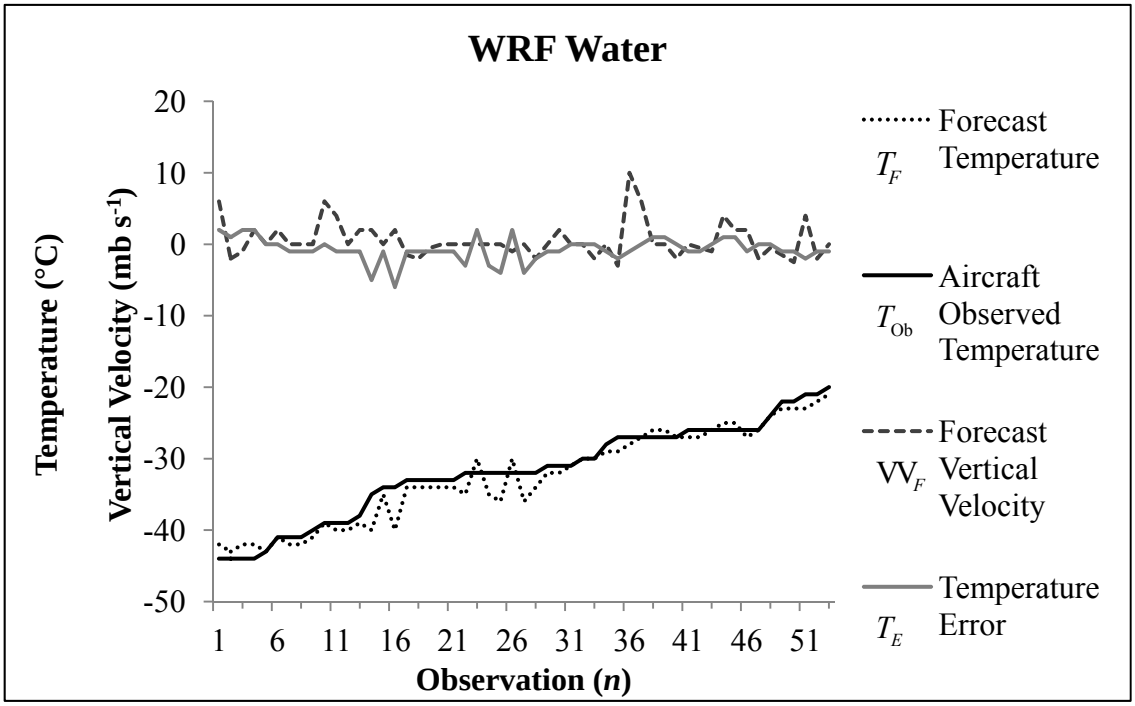

FIG. 3.2. Upper troposphere aircraft temperature observations (T_{Ob}) and WRF temperature forecasts (T_F) over water compared to temperature error (T_E) and forecast vertical velocity (VV_F) coupling ($R^2 = 0.0$).

Since T_E and VV_F coupling in MM5 (MM5 land $R^2 = 0.5$; $CI \neq 0$) and WRF (WRF land $R^2 = 0.2$; $CI \neq 0$) upper troposphere forecasts occurs over land rather than over water (WRF and MM5 water $R^2 = 0.0$ or CI=0) the possibility exists that differential heating and/or humidity may be a cause for MM5 and WRF upper

troposphere T_E (Table 3.3a). Where MM5 and WRF upper troposphere forecasts are biased cold, entrainment of air into areas of VV_F may actually be dryer and warmer than predicted causing increased T_E and over predicting VV_F creating incorrect turbulence intensity (Fig. 3.1; *n*=29, *n*=69, *n*=97). Under forecasting of temperature in MM5 and WRF upper troposphere forecasts may be tied to upwelling long wave radiation incorrectly parameterized over land in RRTM due to changes in upwelling long wave radiation angle and azimuth resulting from changes in slope at different surface elevations above sea level (Yang et al. 2012). MM5 and WRF upper troposphere T_E may possibly be forcing incorrect VV_F through changes in radiative flux as a result of land-surface changes between urban and urban free regions analogous to large cities surrounded by expanses of rolling hills and vegetation. T_E and VV_F coupling is not observed in MM5 and WRF upper troposphere forecasts over water where water bodies do not experience land-surface changes allowing for homogeneous radiative flux and decreases in occurrence of T_E as depicted in Figure 3.2.

A second mechanism for MM5 and WRF upper troposphere T_E instigating incorrect VV_F may be entrainment of more water vapor than predicted in areas of VV_F releasing latent heat and warming the area surrounding VV_F creating a larger T_E propagating an incorrect increase in VV_F. One possible cause for increased humidity is the disturbance of water runoff patterns causing soil to remain saturated creating a source for increased humidity not captured in MM5 and WRF calculations. Evapotranspiration rates from croplands and urban vegetation irrigation may be greater than estimated over grass/scrub

brush and non-urban regions releasing more moisture than predicted increasing humidity that is unaccounted for in MM5 and WRF. Snow cover was observed over a small subset of forest surface type (MM5 *n*=7, WRF *n*=4) but was not considered a factor since T_E and VV_F coupling was not exhibited in general over forest surface type (Table 3.3b). Incorrect evapotranspiration rates could be a result of deforestation and replacement with broad leaf vegetation such as aspen, corn or grasses which have higher evapotranspiration rates than traditional forest vegetation such as pine and/or leaf loss due to seasonal changes. This may explain why T_E and VV_F coupling is observed in MM5 and WRF upper troposphere forecasts over crop and grass/scrub brush regions while T_E and VV_F coupling is not exhibited in MM5 and WRF upper troposphere forecasts over forested areas.

Addressing the corrective factors within the physics packages used by AFWA for JAAWIN applications is beyond the scope of this study, but similarities in the physics packages used by MM5 and WRF may provide a starting point to address T_E and VV_F coupling within the MM5 and WRF models. As detailed in section three (Tables 3.1-3.3b), MM5 (MM5 land $R^2 = 0.5$; $\mathrm{CI} \neq 0$) and WRF (WRF land $R^2 = 0.2$; $\mathrm{CI} \neq 0$) upper troposphere forecasts have indicated susceptibility to T_E and VV_F coupling over land suggesting the possibility this anomaly may exist in one or more shared physics packages. JAAWIN MM5 and WRF forecasts utilized the Noah land surface model governing physical processes in MM5 and WRF such as soil and vegetation mediums, evapotranspiration rates and soil saturation properties which may not be parameterized

correctly (Chen and Dudhia 2001a; Chen and Dudhia 2001b; Hogue et al. 2005; Lemone et al. 2008; Wei et al. 2012). The New Kain-Fritsch cumulus parameterization scheme (Table 3.3a; WRF land $R^2 = 0.2$; $\mathrm{CI} \neq 0$) saw reduced T_E and VV_F coupling over the Kain-Fritsch cumulus parameterization scheme (Table 3.3a; MM5 land $R^2 = 0.5$; $\mathrm{CI} \neq 0$) but still may be inducing incorrect VV_F . This may be caused by the dry air minimum entrainment rate incorrectly applied if model humidity levels are biased low resulting in latent heat flux in the cumulus parameterization schemes (Kain and Fritsch 1990; Siebesma and Holtslag 1996; Derbyshire et al. 2004; Kain 2004; Jonker 2005; de Rooy and Siebesma 2008).

If anomalies in the physics packages remain unaddressed, forecasting of vertical velocity may affect cloud and turbulence prediction decreasing the use of MM5 and WRF in upper troposphere applications such as aircraft flight planning over sparsely populated regions (i.e. western Asia, Atlantic Ocean and likely others). If erroneous VV_F areas and intensities are allowed to be forecasted along a route of flight an unnecessary lateral deviation to a less desired pre-planned flight track may occur resulting in increased time and fuel expenditures. For example if aircraft operating costs are $5000 per flight hour, an unnecessary deviation of 100 km to avoid areas of incorrectly forecasted turbulence may result in a 300 km increase in travel distance and an additional expenditure of $2500 at a cruise speed of 556 kilometers per hour (kph). Working towards improving WRF and MM5 upper troposphere temperature forecasts and eliminating forecast vertical velocity anomalies will help improve air transport

operations by reducing unnecessary aircraft deviations resulting in possible economic savings and conservation of resources.

3.2 Horizontal Wind Direction

3.2.1 MM5 and WRF Upper Troposphere Forecast Horizontal Wind Direction RMSE Evaluation

WRF upper troposphere forecasts indicated moderate (WRF WD_E RMSE=15-30°*T*) WD_E skill (WRF 0-50 km land WD_E RMSE=28.4°*T*) and MM5 indicated poor (WD_E RMSE>30°*T*) WD_E skill (MM5 0-50 km land WD_E RMSE=45.1°*T*) over land increasing to moderate WD_E skill (MM5 0-50 km water WD_E RMSE=26.6°*T*; WRF 0-50 km water WD_E RMSE=23.9°*T*) in forecasts over water between 0-50 km lateral distance deviation from modeled flight tracks (Table 3.4). MM5 and WRF upper troposphere forecasts indicated poor WD_E skill over land (MM5 51-100 km land WD_E RMSE=121.2°*T*; WRF 51-100 km land WD_E RMSE=58.5°*T*) and water (MM5 51-100 km water WD_E RMSE=144.1°*T*; WRF 51-100 km water WD_E RMSE=34.7°*T*) between 51-100 km lateral distance deviation from modeled flight tracks.

TABLE 3.4. RMSE (°T) and regression analysis results for upper troposphere horizontal wind direction error (°T) (WD_E) and forecast vertical velocity (mb s^{-1}) (VV_F) coupling for lateral distance deviation from MM5 and WRF modeled flight tracks.

Bold figures indicate: $R^2 \geq 0.1; CI \neq 0$ *Indicates CI=0		0-50 km		51-100 km	
		Land	**Water**	**Land**	Water
RMSE	MM5	45.1	26.6	121.2	144.1
	WRF	28.4	23.9	58.5	34.7
R^2	MM5	0.0	-0.2	0.3	0.3
	WRF	**-0.1**	**0.2**	**0.2**	0.0
SE_R	MM5	35.7	18.9	52.1	23.1
	WRF	14.4	11.9	42.0	19.5
a	MM5	2.1	-4.2	39.5	64.8
	WRF	-1.5	2.1	17.3	-1.8
b	MM5	25.5	20.3	77.6	174.0
	WRF	25.5	17.7	31.4	32.4
n	MM5	30	22	29	7
	WRF	61	40	43	13
CI=0.95					
MM5	VV_{FU}	-2.6*	-8.6*	-26.4*	-75.8*
	VV_{FL}	6.8	0.2	52.6	205.4
WRF	VV_{FU}	**-2.5**	**0.7**	**7.3**	-7.7*
	VV_{FL}	**-0.5**	**3.4**	**27.2**	4.1

TABLE 3.5a. RMSE (°*T*) and regression analysis results for upper troposphere horizontal wind direction error (°*T*) (WD_E) and forecast vertical velocity (mb s^{-1}) (VV_F) coupling over surface elevations ≤ 499 meters (*m*) above sea level.

Bold figures indicate: $R^2 \geq 0.1; CI \neq 0$ *Indicates CI=0		0-99 *m*	100-199 *m*	200-299 *m*	300-399 *m*	**400-499 *m***
RMSE	MM5	113.1	131.4	106.7	35.7	12.5
	WRF	11.0	26.0	34.0	21	49.4
R^2	MM5	-0.3	0.0	0.0	0.0	0.1
	WRF	0.2	0.0	-0.1	0.0	**0.9**
SE_R	MM5	65.5	65.9	91.4	35.7	10.4
	WRF	43.3	15.4	23.8	12.4	17.2
a	MM5	-18.3	-6.6	11.5	0.6	1.2
	WRF	11.0	-0.2	-2.0	-0.4	47.9
b	MM5	124.7	126.8	47.4	17.9	8.7
	WRF	51.6	22.7	29.1	14.4	35.7
n	MM5	11	14	7	12	3
	WRF	23	12	13	11	11
CI=0.95						
MM5	VV_{FU}	-41.8*	-31.2*	-159.3*	-2.7*	-4.2*
	VV_{FL}	5.3	18.1	180.0	3.0	6.7
WRF	VV_{FU}	0.0*	-17.8*	-7.4*	-2.7*	**32.2**
	VV_{FL}	22.1	17.4	3.5	2.0	**63.6**

TABLE 3.5b. RMSE (°*T*) and regression analysis results for upper troposphere horizontal wind direction error (°*T*) (WD_E) and forecast vertical velocity (mb s^{-1}) (VV_F) coupling over surface elevations > 500 meters (*m*) above sea level.

Bold figures indicate: $R^2 \geq 0.1; CI \neq 0$ *Indicates CI=0		500-599 *m*	600-699 *m*	700-999 *m*	1000-1299 *m*	1300 *m*<
RMSE	MM5	-	-	-	-	-
	WRF	7.0	14.6	24.8	-	19.7
R^2	MM5	-	-	-	-	-
	WRF	0.5	0.5	-0.3	-	-0.2
SE_R	MM5	-	-	-	-	-
	WRF	3.4	6.9	13.2	-	10.7
a	MM5	-	-	-	-	-
	WRF	4.9	7.2	-1.6	-	-1.2
b	MM5	-	-	-	-	-
	WRF	7.1	10.4	19.0	-	17.4
n	MM5	-	-	-	-	-
	WRF	6	5	8	-	11
CI=0.95						
MM5	VV_{FU}	-	-	-	-	-
	VV_{FL}					
WRF	VV_{FU}	-4.4*	-6.6*	-8.4*	-	-2.7*
	VV_{FL}	14.3	21.0	5.1		0.8

MM5 forecasts displayed poor WD_E skill over surface elevations between 0-99 *m* (MM5 0-99 *m* WD_E RMSE=113.1°*T*) improving to good (WD_E RMSE $\leq$ 14.9°*T*) WD_E skill with increased surface elevation above sea level (MM5 400-499 *m* WD_E RMSE=12.5°*T*) (Table 3.5a). WRF upper troposphere forecast WD_E skill varied between good (WRF 0-99 *m* WD_E RMSE=11.0°*T*) and moderate (WRF 400-499 *m* WD_E RMSE=49.4°*T*) over surface elevations of ≤ 499 *m* above sea level.

TABLE 3.6a. RMSE (°T) and regression analysis results for upper troposphere horizontal wind direction error (°T) (WD_E) and forecast vertical velocity (mb s^{-1}) (VV_F) coupling over land, water, crops and grass/scrub brush surface type.

Bold figures indicate: $R^2 \geq 0.1; CI \neq 0$ *Indicates CI=0		Land	Water	Grass/ scrub brush	Crops
RMSE	MM5	83.0	74.5	26.8	34.7
	WRF	49.5	27.4	39.9	38.1
R^2	MM5	0.1	-0.1	0.1	0.3
	WRF	0.0	0.1	0.0	0.1
SE_R	MM5	62.9	56.4	22.3	26.5
	WRF	38.9	15.4	34.9	26.5
a	MM5	6.9	-11.6	3.2	10.5
	WRF	0.4	1.5	-1.2	7.4
b	MM5	49.0	52.5	21.1	25.7
	WRF	31.1	20.8	24.0	30.3
n	MM5	59	11	10	8
	WRF	104	53	26	49
		CI=0.95			
MM5	VV_{FU}	-0.4*	-24.1*	-3.5*	-0.8*
	VV_{FL}	14.3	1.0	9.9	21.9
WRF	VV_{FU}	-2.2*	-0.1*	-3.9*	-1.8*
	VV_{FL}	2.9	3.1	1.6	16.7

TABLE 3.6b. RMSE (°*T*) and regression analysis results for upper troposphere horizontal wind direction error (°*T*) (WD_E) and forecast vertical velocity (mb s^{-1}) (VV_F) coupling over forest, no vegetation, urban and non-urban surface type.

Bold figures indicate: $R^2 \geq 0.1; CI \neq 0$ *Indicates CI=0		Forest	**No Vegetation**	Urban	**Non-Urban**
RMSE	MM5	107.4	-	39.2	93.4
	WRF	45.2	79.7	35.2	62.4
R^2	MM5	0.0	-	0.0	0.1
	WRF	0.0	**0.4**	0.0	**0.2**
SE_R	MM5	73.8	-	30.0	67.4
	WRF	38.6	41.2	22.6	46.0
a	MM5	-1.1	-	1.3	9.4
	WRF	3.5	23.5	-1.0	15.1
b	MM5	84.3	-	21.9	58.2
	WRF	26.4	41.8	23.0	36.4
n	MM5	41	-	4	55
	WRF	11	18	69	35
CI=0.95					
MM5	VV_{FU}	-14.4*	-	-5.3*	-0.4*
	VV_{FL}	12.2		7.9	19.2
WRF	VV_{FU}	-11.0*	**8.6**	-2.6*	**5.2**
	VV_{FL}	17.9	**38.3**	0.6	**25.0**

MM5 upper troposphere forecasts were not used over surface elevations > 499 *m* above sea level (Europe and Southwest Asia), however WRF forecasts were used and good (WRF 500-599 *m* WD_E RMSE=7.0°*T*; *n*=6) to moderate (WRF 1300 *m* < WD_E RMSE=19.7°*T* ; *n*=11) WD_E skill was displayed (Table 3.5b).

According to Table 3.6a MM5 and WRF upper troposphere forecasts indicated poor WD_E skill over land (MM5 land WD_E RMSE=49.5°*T*; WRF land WD_E RMSE=83.0°*T*), poor WD_E skill by MM5 (MM5 water WD_E RMSE=74.5°*T*) and moderate WD_E skill by WRF forecasts over water (WRF water WD_E RMSE=27.4°*T*). MM5 upper troposphere forecasts indicated moderate WD_E skill over grass/scrub brush (MM5 grass/scrub brush WD_E RMSE=26.8°*T*) while WRF forecasts indicated poor WD_E skill (WRF grass/scrub brush WD_E RMSE=39.9°*T*). MM5 and WRF forecasts exhibited poor WD_E skill over crops (MM5 crops WD_E RMSE=34.7°*T*; WRF crops WD_E RMSE=38.1°*T*) and forest surface type (MM5 forest WD_E RMSE=107.4°*T*; WRF forest WD_E RMSE=45.2°*T*) (Table 3.6b). MM5 and WRF upper troposphere forecasts also displayed poor WD_E skill over urban surface cover (MM5 urban WD_E RMSE=39.2°*T*; WRF urban WD_E RMSE=35.2°*T*) and worsened over non-urban areas (MM5 non-urban WD_E RMSE=93.4°*T*; WRF non-urban WD_E RMSE=62.4°*T*). MM5 upper troposphere forecasts were not used over non-vegetation areas; therefore WD_E skill was not assessed but WRF forecasts were utilized indicating poor WD_E skill (WRF no vegetation WD_E RMSE=79.7°*T*).

3.2.2 Lateral Distance Deviation from MM5 and WRF Modeled Flight Track

WRF upper troposphere forecasts exhibited weak inverse WD_E and VV_F coupling over land (Table 3.4; WRF 0-50 km land $R^2 = -0.1$; $CI \neq 0$) and weak WD_E and VV_F coupling over water (Table 3.4; WRF 0-50 km water $R^2 = 0.2$; $CI \neq 0$) between 0-50 km lateral distance deviation from modeled flight tracks. No presence of WD_E and VV_F coupling was exhibited in MM5 upper troposphere forecasts over land or water within 100 km lateral distance deviation from modeled flight tracks where the MM5 0-50 land $R^2 = 0.0$ and the MM5 0-50 water CI=0. Over land between 51-100 km lateral distance deviation from modeled flight tracks weak WD_E and VV_F coupling was indicated in WRF (WRF land 51-100 km $R^2 = 0.2$; $CI \neq 0$) upper troposphere forecasts and no WD_E and VV_F coupling was present in MM5 forecasts (MM5 51-100 km land CI=0). No indication of WD_E and VV_F coupling was exhibited by MM5 (MM5 51-100 km water CI=0) or WRF (WRF 51-100 km water $R^2 = 0.0$) upper troposphere forecasts over water between 51-100 km lateral distance deviation from modeled flight tracks (Table 3.4). These findings suggest WD_E and VV_F coupling occurred only in WRF upper troposphere forecasts and is sensitive to lateral distance deviation from modeled flight tracks.

3.2.3 Changes in Surface Elevation above Sea Level and Surface Type

WD_E and VV_F coupling was not detected in MM5 upper troposphere forecasts ≤ 499 *m* in surface elevation above sea level where MM5 surface elevation categories

posted an $R^2 = 0.0$ or CI=0 (Table 3a). No WD_E and VV_F coupling was noted in WRF upper troposphere forecasts over surface elevations $\leq$ 399 *m* (CI=0) above sea level but was displayed strongly in WRF forecasts over surface elevations between 400-499 *m* (WRF 400-499 *m* $R^2 = 0.9$; $CI \neq 0$) above sea level (Table 3.5a). MM5 upper troposphere forecasts were not utilized over surface elevations > 499 *m* above sea level and WD_E and VV_F coupling was rejected in WRF forecasts over surface elevations > 499 *m* above sea level with all CI=0 (Table 3.5b). WD_E and VV_F coupling was not present in MM5 and WRF upper troposphere forecasts over land (MM5 and WRF land CI=0), water (MM5 and WRF water CI=0), grass/scrub brush (MM5 and WRF grass/scrub brush CI=0) and crops (MM5 and WRF crops CI=0) (Table 3.6a). MM5 upper troposphere forecasts did not exhibit WD_E and VV_F coupling over forest (MM5 forest $R^2 = 0.0$), urban (MM5 urban $R^2 = 0.0$) and non-urban surface type (MM5 non-urban $CI \neq 0$), and was not used over non-vegetated regions (Table 3.6b). WD_E and VV_F coupling was exhibited in WRF upper troposphere forecasts over non-vegetated (WRF no vegetation $R^2 = 0.2$; $CI \neq 0$) and non-urban surface type (WRF non-urban $R^2 = 0.2$; $CI \neq 0$), suggesting WD_E and VV_F coupling is only specific to WRF forecasts relative to changes in surface elevation above sea level and certain surface type (Table 3.6b).

3.2.4 Discussion

WD_E RMSE was tested as an indicator for WD_E and VV_F coupling, and was considered a weak indicator of WD_E and VV_F coupling between 0-50 km lateral distance deviation from model flight tracks in WRF upper troposphere forecasts, but should be avoided due to low correlation (R=0.1) (Table 3.4). WD_E RMSE was assessed as an indicator of WD_E and VV_F coupling between 51-100 km lateral distance deviation from model flight tracks where R=0.0 indicating WD_E RMSE and is not a suitable indicator of WD_E and VV_F coupling in WRF upper troposphere forecasts. In WRF upper troposphere forecast over surface elevations $\leq$ 499 *m* above sea level WD_E RMSE was found to be a strong indicator of WD_E and VV_F coupling (R=0.8). However, use of WD_E RMSE as an indicator for WD_E and VV_F coupling should only be considered when WD_E RMSE $\geq 49.4\,°T$, since this was the only WD_E RMSE associated with WD_E and VV_F coupling in WRF forecasts (WRF 400-499 m $R^2 = 0.9$; $CI \neq 0$) (Table 3.5a). WD_E RMSE was considered to be of use as a WD_E and VV_F coupling indicator in WRF forecasts over different surface types where R=0.9 and should be considered valid when WD_E RMSE $\geq 62.4\,°T$ which was the lowest displayed WD_E RMSE associated with WD_E and VV_F coupling (WRF non-urban $R^2 = 0.2$; $CI \neq 0$) (Table 3.6b).

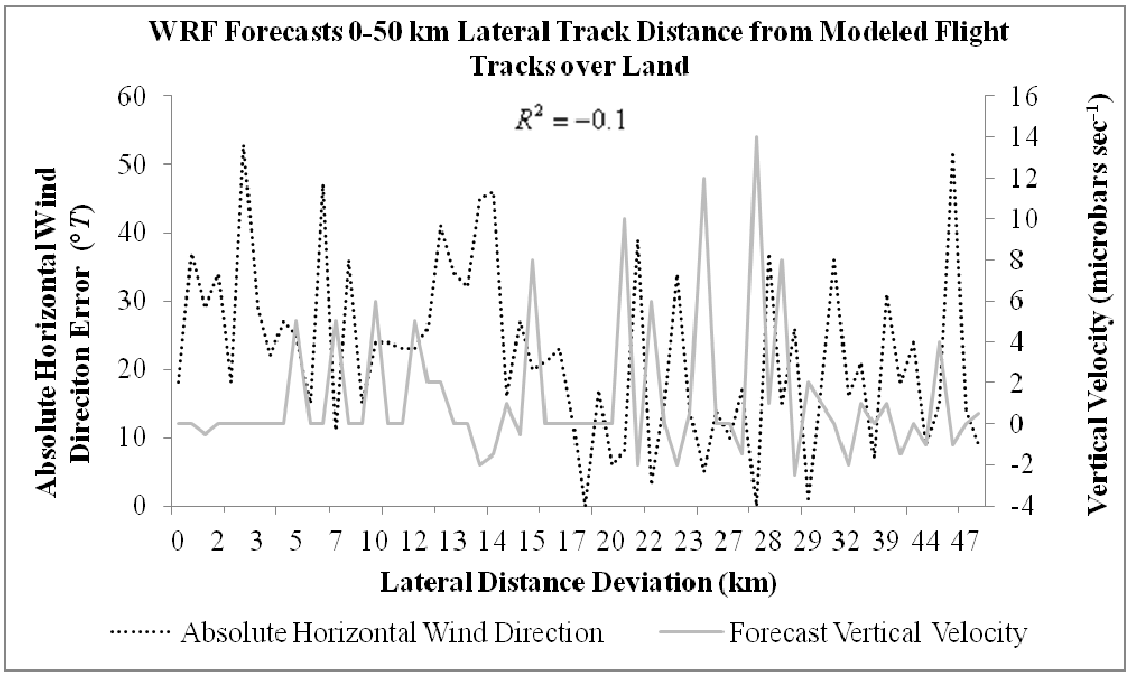

FIG. 3.3. Upper troposphere WRF horizontal wind direction forecast error (°*T*) and forecast vertical velocity (mb s^{-1}) within 0-50 kilometers (km) lateral distance deviation from MM5 and WRF modeled flight track over land ($R^2 = -0.1$).

WD_E and VV_F coupling was found in WRF upper troposphere forecasts over land (Table 3.4; WRF 0-50 km land $R^2 = -0.1$; $CI \neq 0$) and water (Table 3.4; WRF 0-50 km water $R^2 = 0.2$; $CI \neq 0$) between 0-50 km lateral distance deviation from model flight tracks and exhibited in Figures 3.3 and 3.4. Figure 3.3 displays inverse WD_E and VV_F coupling where small increases in VV_F contribute to large WD_E (0-15 km; 29-49 km). Figure 3.4 also depicts inverse WD_E and VV_F coupling where small increases in VV_F are complimented by large increases in WD_E between 21-28 km. Positive WD_E and VV_F coupling is indicated in Figure 3.4 where similar increases in VV_F create similar increases in WD_E. The relationship of WD_E and VV_F displayed by Figure 3.4 is

representative of all positive WD_E and VV_F coupling found in WRF upper troposphere forecasts (Tables 3.4, 3.5a, 3.6b).

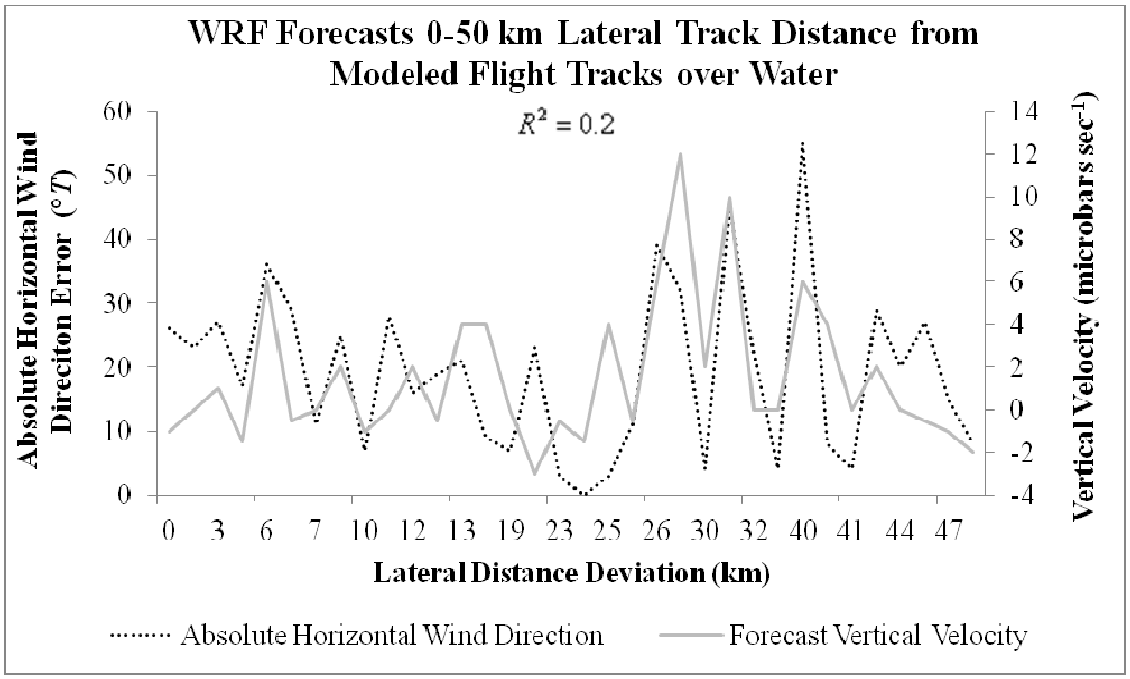

FIG. 3.4. Upper troposphere WRF horizontal wind direction forecast error (°*T*) and forecast vertical velocity (mb s^{-1}) within 0-50 kilometers (km) lateral distance deviation from MM5 and WRF modeled flight track over water ($R^2 = 0.2$).

WD_E and VV_F coupling exhibited in Figures 3.3 and 3.4 is a visual depiction of turbulent drag created by VV_F in WRF forecasts affecting WD_E. Depictions of WD_E and VV_F coupling suggest when forecast vertical movements are occurring forecast horizontal wind speed slows causing geostrophic flow to be disrupted resulting in horizontal flow to cross the isobars (to the left of the geostrophic wind direction in the northern hemisphere) resulting in $+WD_E$ calculated by modifying Equation 2.7b to

$$WD_E = WD_{Ob} - WD_F \qquad (3.1)$$

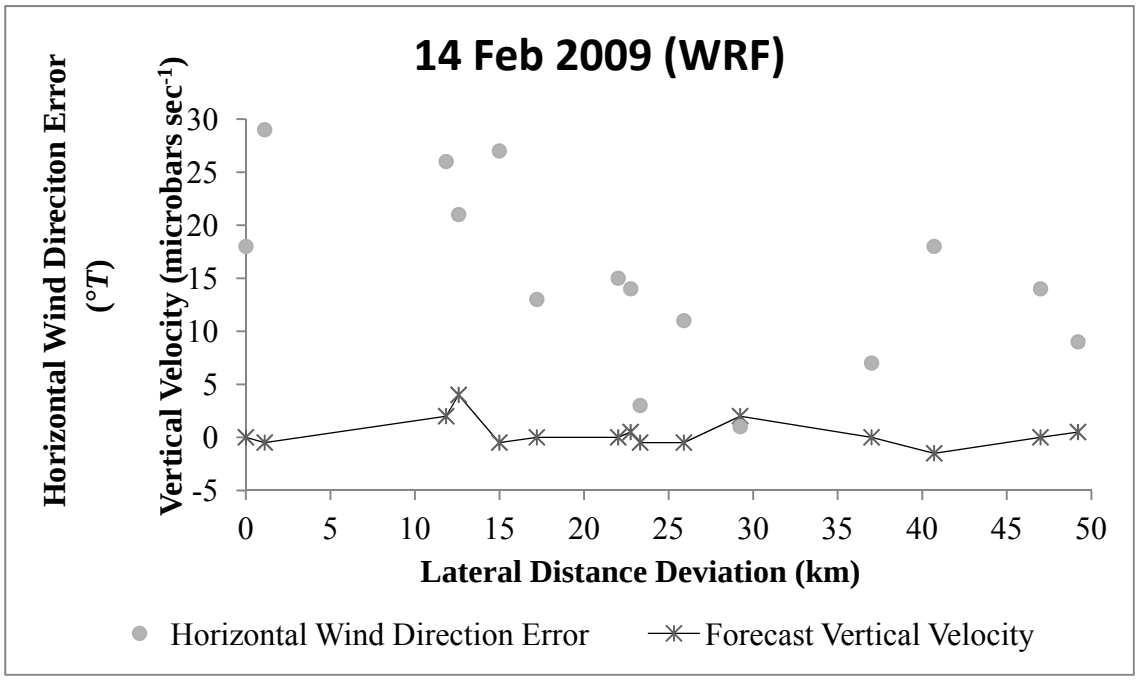

FIG. 3.5. Upper troposphere horizontal wind direction forecast error (°*T*) and forecast vertical velocity (mb s^{-1}) within 0-50 kilometers (km) lateral distance deviation from WRF modeled flight track en route between England and Romania.

Figure 3.5 indicates horizontal flow is crossing the isobars to the left ($+WD_E$) (x axis) of the geostrophic wind direction when VV_F occurs but is not related to the strength of VV_F. Figure 3.3 (0-14 km) demonstrates small VV_F can have large effects on WD_E and corresponds to Figure 3.4 (3-19 km) where large VV_F has small effects on WD_E. The remaining data indicates VV_F can have similar WD_E in WRF forecasts (Fig. 3.3, 22-29 km; Fig. 3.4, 21-42 km).

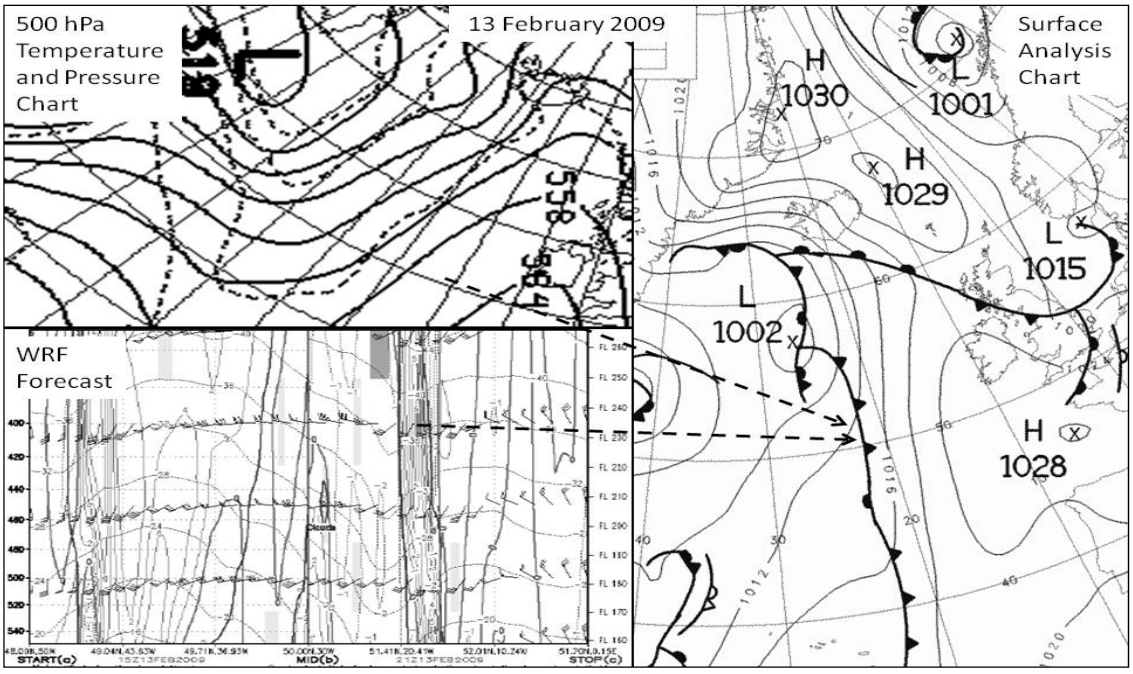

FIG. 3.6. Surface analysis (right) and 500 hectopascals (hPa) temperature and pressure (upper left) charts compared to MM5 multi-leg vertical cross section (lower left) forecast on 13 February 2009. Dashed lines indicate convective and frontal zone crossing during aircraft flight (Colorado State University 2012, United Kingdom Meteorological Office 2012).

A possible explanation for different behaviors of VV_F and WD_E may be attributed to strength of geostrophic flow in WRF upper troposphere forecasts. When geostrophic flow is predicted to be strong, VV_F may not have enough momentum to impart sufficient turbulent drag to slow the forecast geostrophic flow significantly resulting in a small WD_E (Fig. 3.4, 3-19 km; Fig 3.5. 29 km). When geostrophic flow is predicted to be weak, VV_F may create enough momentum to impart sufficient turbulent drag on forecast geostrophic flow causing large WD_E (Fig. 3.3, 0-14 km; Fig 3.5. 29 km). Where VV_F momentum imparts turbulent drag which is equivalent to geostrophic flow

WD_E and VV_F magnitude tend to be similar (Fig. 3.3, 22-29 km; Fig. 3.4, 21-42 km; Fig. 3.5, 22-26 km).

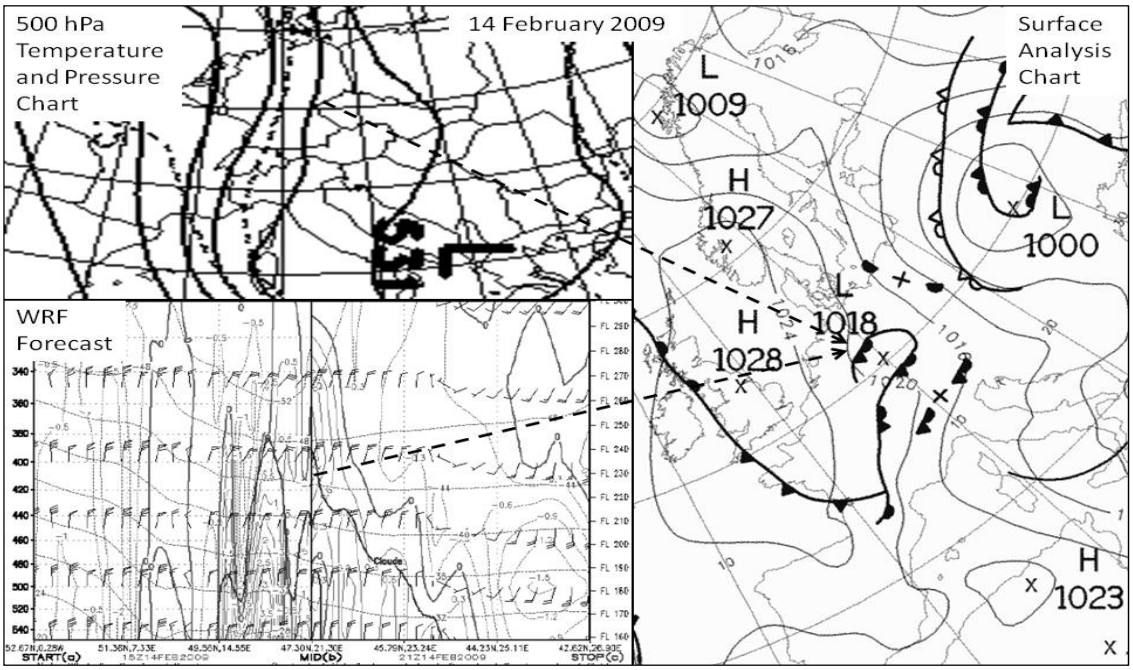

FIG. 3.7. Surface analysis (right) and 500 hectopascals (hPa) temperature and pressure (upper left) charts compared to MM5 multi-leg vertical cross section (lower left) forecast on 14 February 2009. Dashed lines indicate convective and frontal zone crossing during aircraft flight (Colorado State University 2012, United Kingdom Meteorological Office 2012).

A frontal zone was crossed during six of seven flights in which four frontal zone crossings can be linked to WD_E and VV_F coupling in WRF forecasts. One occurrence is exhibited in Figure 3.6 (dashed line) and depicts a frontal zone crossing over water (Table 3.6a; WRF 0-50 km water $R^2 = 0.2$; $CI \neq 0$) and detailed by VV_F in the WRF upper troposphere forecast and surface analysis. Isobars at the 500 hPa level are widely spaced indicating a weak pressure gradient across the front allowing VV_F to impart turbulent drag on geostrophic flow in the WRF model. Slowing of geostrophic flow

causes wind flow to cross the isobars toward the low pressure center to the north ($+WD_E$; Fig. 3.5).

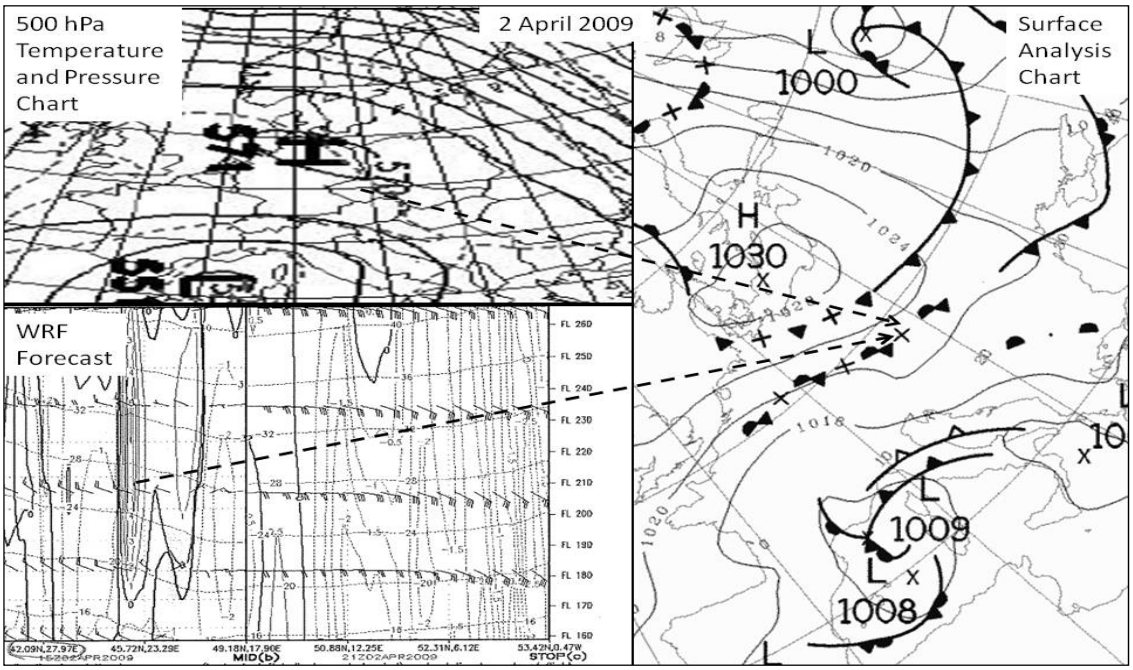

FIG. 3.8. Surface analysis (right) and 500 hectopascals (hPa) temperature and pressure (upper left) charts compared to MM5 multi-leg vertical cross section (lower left) forecast on 2 April 2009. Dashed lines indicate convective and frontal zone crossing during aircraft flight (Colorado State University 2012, United Kingdom Meteorological Office 2012).

Figures 3.7 and 3.8 also display frontal boundary crossings on two separate flights over the same surface elevations between 400-449 *m* above sea level (Table 3.5a; WRF 400-449 *m* $R^2 = 0.9$; $CI \neq 0$) where isobars at 500 hPa are widely spaced and VV_F is increased. The flight in Figure 3.9 also crosses a frontal boundary over non-vegetated surface type (Table 3.6b; WRF no vegetation $R^2 = 0.4$) where increased VV_F is observed with a weak pressure gradient at the 500 hPa level.

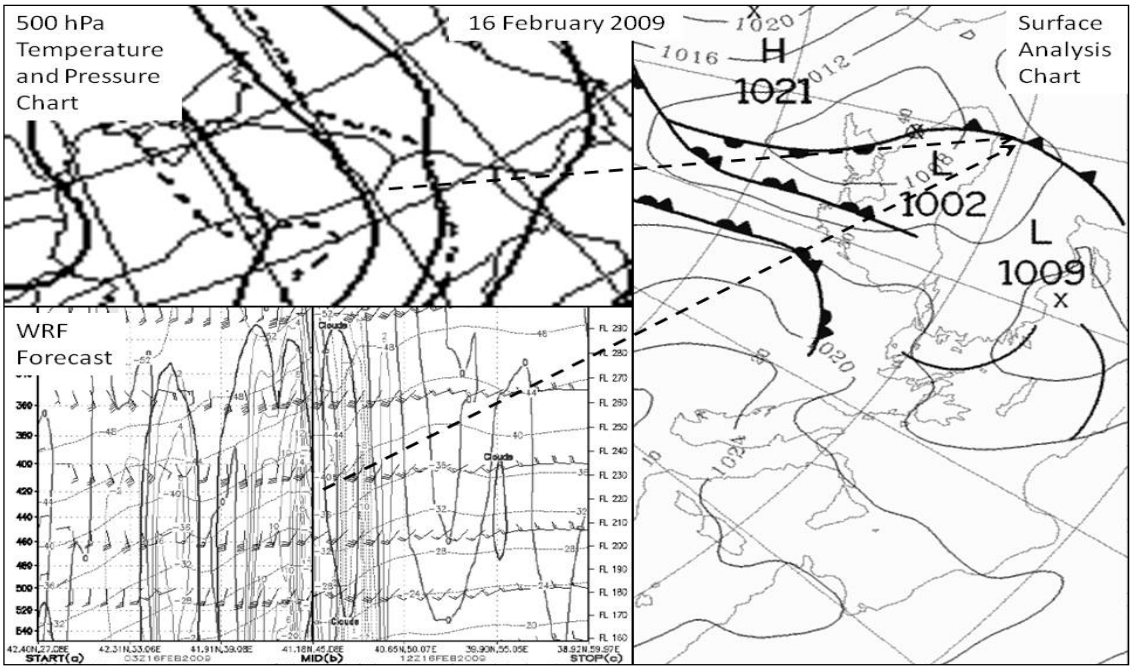

FIG. 3.9. Surface analysis (right) and 500 hectopascals (hPa) temperature and pressure (upper left) charts compared to MM5 multi-leg vertical cross section (lower left) forecast on 16 February 2009. Dashed lines indicate convective and frontal zone crossing during aircraft flight (Colorado State University 2012, United Kingdom Meteorological Office 2012).

The mechanism creating erroneous VV_F may reside in entrainment rates in the New Kain-Fritch cumulus parameterization schemes used in WRF upper troposphere forecasts (Kain and Fritsch 1990; Siebesma and Holtslag 1996; Derbyshire et al. 2004; Kain 2004; Jonker 2005; de Rooy and Siebesma 2008). The New Kain-Fritsch cumulus parameterization scheme was used in WRF upper troposphere forecasts which included changes to entrainment rates used by the Kain-Fristch cumulus parameterization scheme in MM5. The New Kain-Fritsch cumulus parameterization scheme imposes a minimum entrainment rate suppressing convection and if set incorrectly may allow too much moisture into areas of forecasted unstable dry air regions resulting in erroneous

convection across the frontal zone. The difference in entrainment settings between the New Kain-Fritsch (WRF) and the Kain-Fritsch (MM5) cumulus parameterization schemes may be why VV_F and WD_E coupling is exhibited in WRF forecasts only. Increased humidity predicted by WRF forecasts may also be erroneously releasing latent heat increasing temperature Δ across the frontal zone resulting in erroneous VV_F and turbulent drag on forecast horizontal wind velocity resulting in WD_E.

WRF horizontal wind direction forecasts may be used by air transportation flight planners where WD_E can increase operating costs. Flight planners choose flights based on the most favorable horizontal wind direction forecast minimizing head wind components (WD_F 0-70°*T* relative to aircraft TC °*T*) to reduce fuel use. If WRF horizontal wind direction forecasts are in error depicting a cross wind component (WD_F 70-100°*T* relative to aircraft TC °*T*), when an actual head wind component exists, more fuel is used escalating operating costs. For example, if operating costs are $5000 per flight hour a WD_E of 30°*T* at a horizontal wind velocity of 6.0 ms^{-1} can result in a $1250 increase in operating costs at a speed of 556 kph over 100 km. WD_E in WRF horizontal wind direction forecasts due to errors in storm and volcanic ash forecast tracks, for instance, can create aircraft holding delays increasing operating expenses by increased fuel use.

3.3 Horizontal Wind Velocity

3.3.1 MM5 and WRF Upper Troposphere Forecast Horizontal Wind Velocity RMSE Evaluation

RMSE was calculated analyzing the WV_E skill of MM5 and WRF in upper troposphere forecasts within 100 km lateral distance deviation from modeled flight tracks between 39-59°*N* (Table 3.7). MM5 (MM5 WV_E 0-50 km land RMSE=7.2 ms^{-1}; MM5 51-100 km land WV_E RMSE=5.8 ms^{-1}) exhibited moderate (WV_E RMSE=3.8-7.6 ms^{-1}) WV_E skill in the upper troposphere between 0-50 km and 51-100 km lateral distance deviation from modeled flight tracks over land. WRF upper troposphere forecasts (WRF 0-50 km land WV_E RMSE=6.6 ms^{-1}; WRF 51-100 km land WV_E RMSE=5.3 ms^{-1}) also exhibited moderate WV_E skill between 0-50 km and 51-100 km lateral distance deviation from modeled flight tracks over land (Table 3.7). Upper troposphere WRF (WRF 0-50 km water WV_E RMSE=5.2 ms^{-1}; WRF 51-100 km water WV_E RMSE=11.7 ms^{-1}) forecasts exhibited moderate and poor (WV_E RMSE>7.6 ms^{-1}) WV_E skill over water between 0-50 km and 51-100 km lateral distance deviation from modeled flight tracks. MM5 (MM5 0-50 km water WV_E RMSE=9.2 ms^{-1}) forecasts displayed moderate WV_E skill over water between 0-50 km lateral distance deviation from modeled flight tracks, similar to WRF forecasts.

TABLE 3.7. RMSE (ms^{-1}) and regression analysis results for horizontal wind velocity error (ms^{-1}) (WV_E) and forecast vertical velocity (mb s^{-1}) (VV_F) coupling for lateral distance deviation from MM5 and WRF modeled flight tracks.

Bold figures indicate: $R^2 \geq 0.1; CI \neq 0$ *Indicates CI=0		0-50 km		51-100 km	
		Land	**Water**	Land	Water
RMSE	MM5	7.2	9.2	5.8	16.7
	WRF	6.6	5.2	5.3	11.7
R^2	MM5	0.1	**-0.4**	0.2	0.0
	WRF	0.0	-0.1	-0.1	1.0
SE_R	MM5	6.7	6.9	4.9	4.3
	WRF	4.8	5.1	5.3	10.7
a	MM5	0.8	-3.0	1.5	1.2
	WRF	-0.2	-0.6	-1.1	2.2
b	MM5	1.0	4.8	2.2	16.8
	WRF	0.2	-0.3	0.0	-7.7
n	MM5	30	4	29	7
	WRF	61	40	43	13
CI=0.95					
MM5	VV_{FU}	-0.1*	**-4.6**	0.3*	-22.8*
	VV_{FL}	1.7	**-1.4**	2.8	25.2
WRF	VV_{FU}	-0.6*	-1.1*	-2.3*	-0.3*
	VV_{FL}	0.1	0.0	0.2	5.8

TABLE 3.8a. RMSE (ms^{-1}) and regression analysis results for upper troposphere horizontal wind velocity error (ms^{-1}) (WV_E) and forecast vertical velocity ($mb\ s^{-1}$) (VV_F) coupling over surface elevations < 499 meters (*m*) above sea level.

Bold figures indicate: $R^2 \geq 0.1; CI \neq 0$ *Indicates CI=0		**0-99 *m***	**100-199 *m***	200-299 *m*	300-399 *m*	**400-499 *m***
RMSE	MM5	10.0	7.2	6.0	4.2	4.1
	WRF	4.3	3.9	5.9	5.7	4.3
R^2	MM5	-0.3	**0.4**	0.0	0.2	0.4
	WRF	**-0.2**	0.2	0.0	0.0	**-0.6**
SE_R	MM5	6.6	5.3	6.5	3.5	3.5
	WRF	4.0	3.8	6.4	6.3	3.0
a	MM5	-2.1	2.3	0.6	0.7	0.8
	WRF	-1.1	3.3	0.1	0.1	-2.6
b	MM5	11.6	-0.9	0.5	1.8	-2.3
	WRF	-0.4	0.8	-0.1	-0.2	1.7
n	MM5	11	14	7	12	3
	WRF	23	12	13	11	11
CI=0.95						
MM5	VV_{FU}	-4.4*	**0.3**	-10.6*	-0.3*	-0.6*
	VV_{FL}	1.1	**4.2**	11.8	1.8	2.3
WRF	VV_{FU}	**-2.1**	-0.9*	-1.3*	-1.1*	**-4.4**
	VV_{FL}	**-0.2**	7.5	1.6	1.3	**-0.9**

TABLE 3.8b. RMSE (ms^{-1}) and regression analysis results for upper troposphere horizontal wind velocity error (ms^{-1}) (WV_E) and forecast vertical velocity (mb s^{-1}) (VV_F) coupling over surface elevations > 500 meters (*m*) above sea level.

Bold figures indicate: $R^2 \geq 0.1; CI \neq 0$ *Indicates CI=0		500-599 *m*	600-699 *m*	**700-999 *m***	1000-1299 *m*	1300 *m*<
RMSE	MM5	-	-	-	-	-
	WRF	5.3	4.0	5.5	-	5.5
R^2	MM5	-	-	-	-	-
	WRF	-0.3	-0.5	**-0.9**	-	0.0
SE_R	MM5	-	-	-	-	-
	WRF	3.7	3.3	2.3	-	5.9
a	MM5	-	-	-	-	-
	WRF	-4.5	-3.7	-1.1	-	0.1
b	MM5	-	-	-	-	-
	WRF	2.2	1.4	-4.8	-	-1.2
n	MM5	-	-	-	-	-
	WRF	6	5	8	-	11
CI=0.95						
MM5	VV_{FU}	-	-	-	-	-
	VV_{FL}					
WRF	VV_{FU}	-13.5*	-9.3*	**-1.9**	-	-0.9*
	VV_{FL}	4.4	1.8	**-0.3**		1.0

TABLE 3.9a. RMSE (ms^{-1}) and regression analysis results for upper troposphere horizontal wind velocity error (ms^{-1}) (WV_E) and forecast vertical velocity ($mb\ s^{-1}$) (VV_F) coupling over land, water, crops, and grass/scrub brush surface type.

Bold figures indicate: $R^2 \geq 0.1; CI \neq 0$ *Indicates CI=0		**Land**	**Water**	Grass/ scrub brush	Crops
RMSE	MM5	6.6	11.5	7.2	4.7
	WRF	5.1	7.5	4.9	5.0
R^2	MM5	**0.1**	**-0.4**	0.3	0.1
	WRF	0.0	0.0	0.0	-0.1
SE_R	MM5	5.8	7.7	6.6	4.7
	WRF	7.4	7.4	1.8	5.1
a	MM5	0.8	-3.6	1.4	1.0
	WRF	-0.3	-0.3	-0.1	-1.7
b	MM5	1.8	7.7	1.2	1.6
	WRF	-1.7	-1.7	-0.6	0.3
n	MM5	59	11	10	8
	WRF	104	53	26	49
CI=0.95					
MM5	VV_{FU}	**0.2**	**-5.4**	-0.2*	-1.0*
	VV_{FL}	**1.5**	**-1.9**	0.3	3.0
WRF	VV_{FU}	-1.0*	-1.0*	-0.5*	-3.4*
	VV_{FL}	0.5	0.5	0.3	0.0

TABLE 3.9b. RMSE (ms^{-1}) and regression analysis results for upper troposphere horizontal wind velocity error (ms^{-1}) (WV_E) and forecast vertical velocity ($mb\ s^{-1}$) (VV_F) coupling over forest, no vegetation, urban, and non-urban surface type.

Bold figures indicate: $R^2 \geq 0.1; CI \neq 0$ *Indicates CI=0		Forest	No Vegetation	**Urban**	**Non-Urban**
RMSE	MM5	7.1	-	7.2	6.3
	WRF	6.5	3.7	4.8	5.3
R^2	MM5	0.0	-	0.1	**0.2**
	WRF	-0.1	-0.1	-0.1	0.0
SE_R	MM5	6.2	-	6.7	5.6
	WRF	4.8	5.9	4.7	5.5
a	MM5	0.2	-	0.6	1.1
	WRF	-1.6	-0.6	-0.3	-0.6
b	MM5	3.2	-	1.5	1.9
	WRF	-1.8	1/3	0.6	-0.6
n	MM5	41	-	4	55
	WRF	11	18	69	35
CI=0.95					
MM5	VV_{FU}	-0.9*	-	-0.9*	**0.3**
	VV_{FL}	1.4		2.0	**2.0**
WRF	VV_{FU}	-3.8*	-1.9*	-0.6*	-1.8*
	VV_{FL}	0.7	0.7	0.1	0.5

MM5 (MM5 51-100 km water WV_E RMSE=16.7 ms^{-1}) upper troposphere forecasts mirrored WRF forecasts over water between 51-100 km lateral distance deviation from modeled flight tracks exhibiting poor WV_E skill.

WRF (WRF WV_E RMSE=3.9-5.9 ms^{-1}) forecasts exhibited moderate WV_E skill over surface elevations $\leq$ 499 *m* above sea level and no trend in performance with increasing or decreasing surface elevation above sea level (Table 3.8a). MM5 (MM5 WV_E RMSE=4.1-7.2 ms^{-1}) forecasts displayed moderate WV_E skill over surface elevations between 100-499 *m* above sea level indicating an increase in skill with increasing surface elevation above sea level. Between surface elevations of 0-99 *m* above sea level MM5 (MM5 0-99 *m* WV_E RMSE=10.0 ms^{-1}) upper troposphere forecasts exhibited poor WV_E skill. No RMSE assessment was available for MM5 forecasts over surface elevations > 499 *m* above sea level since MM5 was not used over these regions (Europe/Southwest Asia). WRF upper troposphere forecasts were utilized over surface elevations > 499 *m* above sea level (WRF WV_E RMSE=4.0-5.5 ms^{-1}) indicating moderate WV_E skill seen over surface elevation $\leq$ 499 *m* above sea level (Table 3.8b).

WRF (WRF land WV_E RMSE=5.1 ms^{-1}; WRF water WV_E RMSE=7.5 ms^{-1}) forecasts exhibited moderate WV_E skill in the upper troposphere over land and water, while MM5 (MM5 land WV_E RMSE=6.6 ms^{-1}; MM5 water WV_E RMSE=11.5 ms^{-1}) forecasts exhibited moderate WV_E skill over land and poor WV_E skill over water (Table 3.9a). WV_E skill was moderate for WRF (WRF grass/scrub brush WV_E RMSE=4.9 ms^{-1}) and MM5 (MM5 grass/scrub brush WV_E RMSE=7.2 ms^{-1}) forecasts over grass/scrub brush and crop surface type (MM5 crops WV_E RMSE=4.7 ms^{-1}; WRF

crops WV_E RMSE=5.0 ms^{-1}) (Table 3.9b). MM5 (MM5 WV_E RMSE=6.3-7.2 ms^{-1}) and WRF (WRF WV_E RMSE=4.8-6.5 ms^{-1}). Upper troposphere forecasts also exhibited moderate skill over forest, urban and non-urban surface types. MM5 forecasts were not used over non-vegetated areas so no RMSE was computed however WRF (WRF no vegetation WV_E RMSE=3.7 ms^{-1}) forecasts were utilized indicating good (RMSE<3.8 ms^{-1}) WV_E skill.

3.3.2 Lateral Distance Deviation from MM5 and WRF Modeled Flight Track

MM5 and WRF analysis of WV_E and VV_F coupling within 100 km lateral distance deviation from modeled flight tracks between 39-59°*N* were evaluated with findings in Table 3.7. MM5 upper troposphere forecasts initially suggested WV_E and VV_F coupling over land was rejected with CI=0, but did indicate moderate inverse WV_E and VV_F coupling (MM5 0-50 km water $R^2 = -0.4$; $CI \neq 0$) over water between 0-50 km lateral distance deviation from modeled flight tracks (Table 3.7). WRF upper troposphere forecasts originally suggested evidence of weak inverse WV_E and VV_F coupling over land between 0-50 km lateral distance deviation from modeled flight tracks with the WRF land $R^2 = -0.1$ but was rejected with a CI=0 (Table 3.7). Table 3.7 indicated rejection of WV_E and VV_F coupling between 51-100 km lateral distance deviation from modeled flight tracks over land and water by MM5 and WRF with all CI=0 (Table 3.7). These findings suggest WRF is not subject to WV_E and VV_F coupling as a result of lateral distance deviation from modeled flight tracks within 100

km while WV_E and VV_F coupling in MM5 appears to occur inversely over water between 0-50 km lateral distance deviation from modeled flight tracks.

3.3.3 Changes in Surface Elevation above Sea Level

MM5 and WRF upper troposphere forecast assessment indicated WV_E and VV_F coupling for specific surface elevations above sea level and detailed in Tables 3.8a and 3.8b. Examination of Table 3.8a indicates moderate WV_E and VV_F coupling is present in MM5 upper troposphere forecasts between surface elevations of 100-199 *m* above sea level depicted by the MM5 100-199 *m* $R^2 = 0.4$ and $\mathrm{CI} \neq 0$. WRF upper troposphere forecasts posted two instances where inverse WV_E and VV_F coupling was weakly observed over surface elevations between 0-99 *m* (WRF 0-99 *m* $R^2 = -0.2$; $\mathrm{CI} \neq 0$; *n*=23) and strongly over surface elevations between 400-499 *m* (WRF 400-499 *m* $R^2 = -0.6$; $\mathrm{CI} \neq 0$; *n*= 11) above sea level (Table 3.8a). MM5 upper troposphere forecasts were not used over surface elevations > 499 *m* above sea level but assessment of WRF forecasts over surface elevations > 499 *m* above sea level produced strong inverse WV_E and VV_F coupling between 700-999 *m* (WRF 700-999 *m* $R^2 = -0.9$; $\mathrm{CI} \neq 0$; *n*=8); however they may not be representative of the general population given the smaller sample size (Table 3.8b). Overall, MM5 and WRF upper troposphere forecasts exhibited WV_E and VV_F coupling with MM5 forecasts promoting a single positive WV_E and VV_F coupling association and WRF posting three inverse WV_E and

VV_F coupling relationships with R^2 values increasing (*n* decreasing) corresponding to increasing surface elevations above sea level.

3.3.4 Surface Type

MM5 and WRF upper troposphere forecasts were assessed in search of WV_E and VV_F coupling over different surface type and urban influences with findings displayed in Tables 3.9a and 3.9b. MM5 and WRF upper troposphere forecasts were examined where MM5 forecasts indicated weak WV_E and VV_F coupling over land (MM5 land $R^2 = 0.1$; $CI \neq 0$) and moderate inverse WV_E and VV_F coupling exhibited over water (MM5 water $R^2 = -0.4$; $CI \neq 0$) (Table 3.9a). Additionally MM5 upper troposphere forecasts indicated WV_E and VV_F coupling over areas of non-urban influence as displayed by a MM5 non-urban $R^2 = 0.2$ and $CI \neq 0$ (Table 3.9b). The remaining surface type categories (grass/scrub brush, crops, forest, or urban areas) rejected WV_E and VV_F coupling in MM5 upper troposphere forecasts, posting results of $R^2 = 0.0$ or CI=0. WV_E and VV_F coupling was rejected in WRF upper troposphere forecasts over all surface types and urban influences tested indicating an $R^2 = 0.0$ or a CI=0, suggesting WRF is not subject to WV_E and VV_F coupling over a specific surface type (Table 3.9b).

3.3.5 Discussion

Use of RMSE as an indicator of WV_E and VV_F coupling was rejected (R=0.0) due to similar RMSE when WV_E and VV_F coupling was observed (i.e. WRF 0-99 *m* RMSE=4.3 ms^{-1}; $R^2 = -0.2$; $CI \neq 0$) or rejected (i.e. WRF 200-299 *m* RMSE=3.9 ms^{-1}; $R^2 = 0.2$; CI=0) (Table 3.8b). MM5 upper troposphere forecast WV_E over land were plotted against increasing VV_F illustrating a positive WV_E and VV_F coupling signature (MM5 land $R^2 = 0.1$; $CI \neq 0$) (Fig. 3.10).

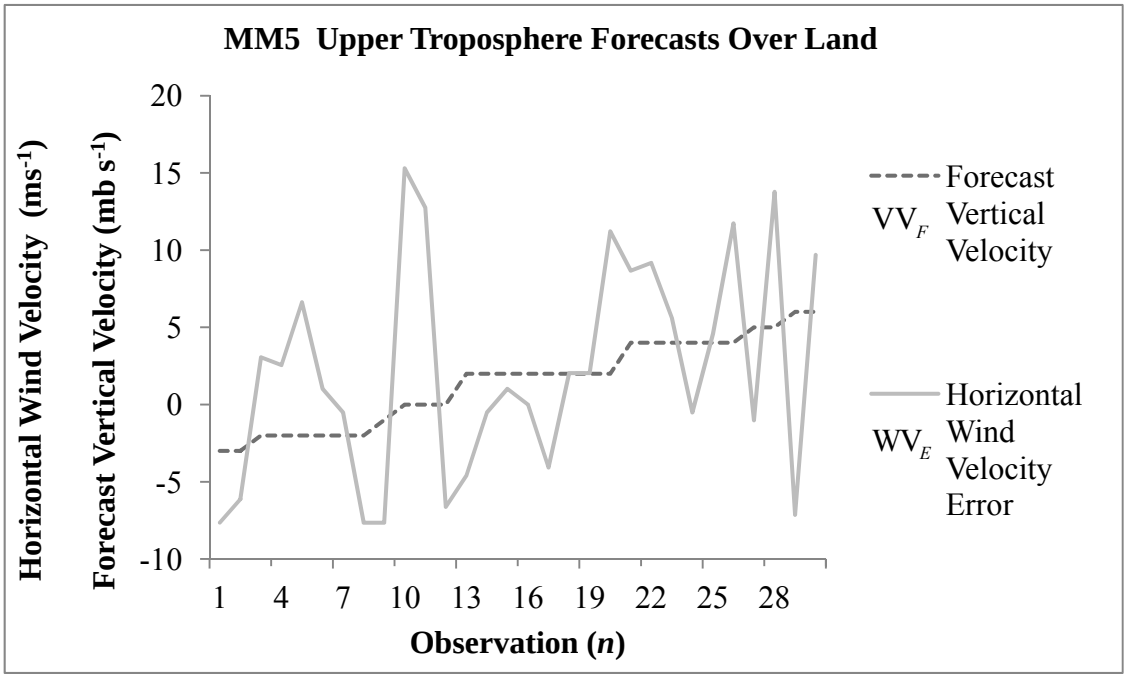

FIG. 3.10. Upper troposphere combined MM5 horizontal wind velocity error (WV_E) (ms^{-1}) and forecast vertical velocity (VV_F) (mb s^{-1}) over land < 100 kilometers (km) lateral distance deviation from modeled flight tracks between 39-59 degrees (°) north latitude (*N*) ($R^2 = 0.1$).

A positive signature (similar to Figure 3.10) was also found in all land-based surface type WV_E and VV_F plots where positive WV_E and VV_F coupling was identified. In Figure 3.11 WV_E data from MM5 upper troposphere forecasts over water (MM5 water $R^2 = -0.4$; CI $\neq 0$) were plotted by increasing VV_F and displayed a negative WV_E and VV_F coupling signature. The negative WV_E and VV_F coupling signature was present when WV_E remained positive during -VV_F (WV_E=2-23 ms^{-1}; *n*=1-11), exhibited positive and negative WV_E when $VV_F = 0.0$ mb s^{-1} ($WV_E = \pm 4.3$ ms^{-1}; *n*=12-25) and negative WV_E during +VV_F (WV_E = -1.5 to -16.8 ms^{-1}; *n*=26-29).

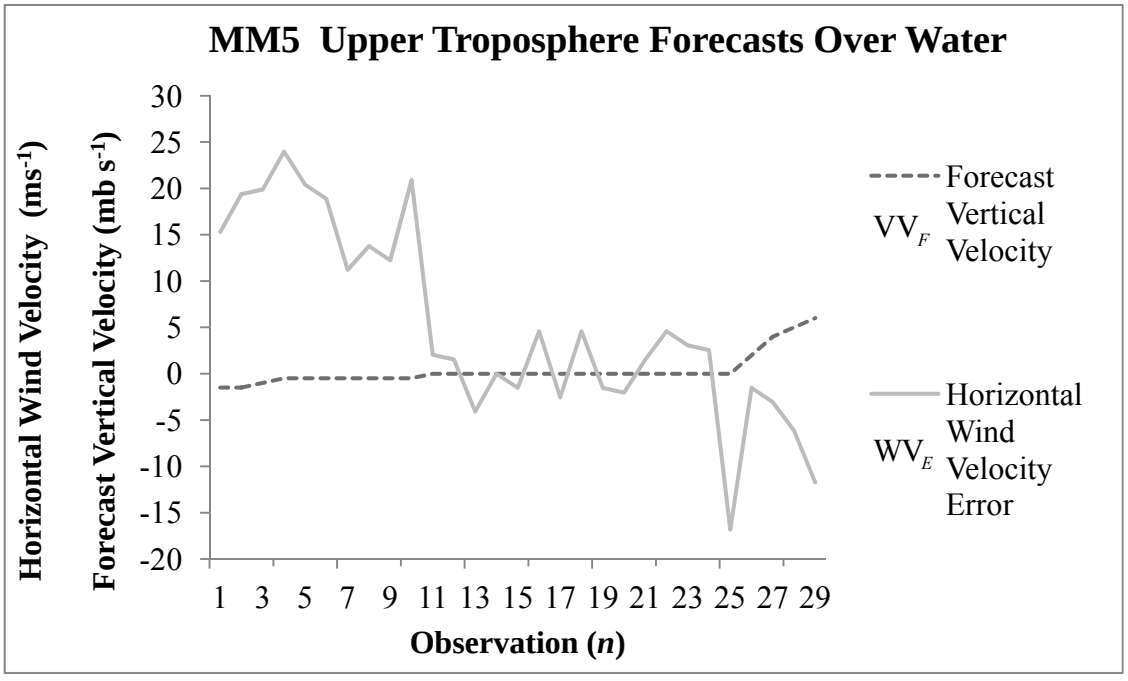

FIG. 3.11. Upper troposphere MM5 horizontal wind velocity error (WV_E) (ms^{-1}) and forecast vertical velocity (VV_F) (mb s^{-1}) comparison over water ($R^2 = -0.4$) between 39-59 degrees (°) north latitude (*N*).

Data were combined in Figure 3.12 reflecting inverse WV_E and VV_F coupling in WRF upper troposphere forecasts between surface elevations of 0-99 *m* and 400-499 *m* above sea level, exhibiting a similar signature illustrated in Figure 3.11.

WV_E in Figure 3.12 also remained positive during $-VV_F$ (WV_E=0.5-6.6 ms^{-1}; *n*=1-11), positively sloped when $VV_F = 0.0$ mb s^{-1} (WV_E = -5.6 to 3.6 ms^{-1}; *n*=12-24) and negative (WV_E = -2.0 to -8.7 ms^{-1}; *n*=25-37) during $+VV_F$. Amplitude of WV_E decreased when comparing *n*=1-11 and *n*=26-29 (Fig. 3.11) to *n*=1-11 and *n*=25-37 (Fig. 3.12) and *n*=12-24 in Figures 3.11 and 3.12. When $VV_F = 0.0$ mb s^{-1} (Fig. 3.11; Fig. 3.12; *n*=12-24) WV_E and VV_F coupling was no longer present similar to data sets where WV_E and VV_F coupling was rejected ($R^2 = 0.0$ or CI=0) in MM5 and WRF upper troposphere forecasts. Absence of WV_E and VV_F coupling is seen when surface elevation data between 100-399 *m* above sea level (Table 3.8a; $R^2 = 0.0$ or CI=0) are combined in Figure 3.13. No WV_E and VV_F coupling signatures were observed in Figure 3.13 exhibiting positive and negative WV_E during $-VV_F$ (WV_E= -7.6 to 6.6 ms^{-1}; *n*=25-37), sloped positively when $VV_F = 0.0$ mb s^{-1} (WV_E= -9.2 to 4.6 ms^{-1}; *n*=13-25) and positive and negative WV_E during $-VV_F$ (MM5 WV_E= -3.1 to 6.6 ms^{-1}; *n*=25-37).

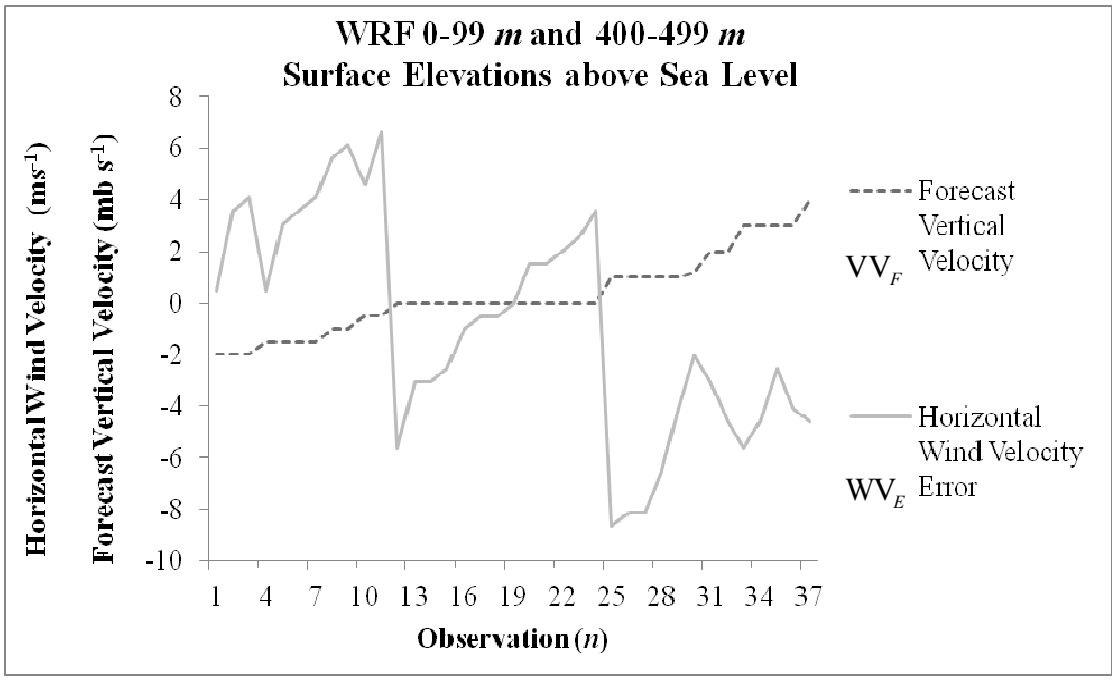

FIG. 3.12. Upper troposphere combined WRF horizontal wind velocity error (WV_E) (ms^{-1}) and forecast vertical velocity (VV_F) (mb s^{-1}) comparison between 0-99 meter (*m*) ($R^2 = -0.2$) and 400-499 *m* ($R^2 = -0.6$) surface elevation above sea level between 39-59 degrees (°) north latitude (*N*).

Since WV_E and VV_F coupling signatures occur in MM5 and WRF upper troposphere forecasts (Figures 3.10, 3.11 and 3.13) vertical movements interfering with horizontal momentum (*p*), as defined by the product of mass (*m*) and velocity (*v*), may be responsible for WV_E and VV_F coupling. Signatures in Figures 3.11 and 3.12 (*n*=1-11) indicate over prediction of horizontal momentum during forecasted downward vertical movements ($-VV_F$) causing a $+WV_E$ and inverse WV_E and VV_F coupling in MM5 and WRF forecasts. Upward forecasted vertical movements ($+VV_F$) in Figures 3.11 (*n*=26-29) and 3.12 (*n*=25-27) correspond to under prediction of horizontal momentum in MM5 and WRF forecasts creating a $-WV_E$.

A frontal/convective boundary crossing occurred on six of seven flights (MM5=2, WRF=4) in which each frontal zone can be linked to specific occurrences of identified WV_E and VV_F coupling suggesting frontal zones are an important source of WV_E and VV_F coupling in MM5 and WRF upper troposphere forecasts. Figures 3.14 and 3.15 depict (dashed line) frontal boundary crossing over water (Table 3.9a; MM5 water $R^2 = -0.4$; $CI \neq 0$; Fig. 3.10) and land (Table 3.9a; MM5 land $R^2 = 0.1$; $CI \neq 0$; Fig. 3.11) over surface elevations between 100-199 *m* above sea level (Table 3.8a; MM5 100-199 *m* $R^2 = 0.4$; $CI \neq 0$) and non-urban areas (Table 3.9b; MM5 non-urban $R^2 = 0.2$; $CI \neq 0$).

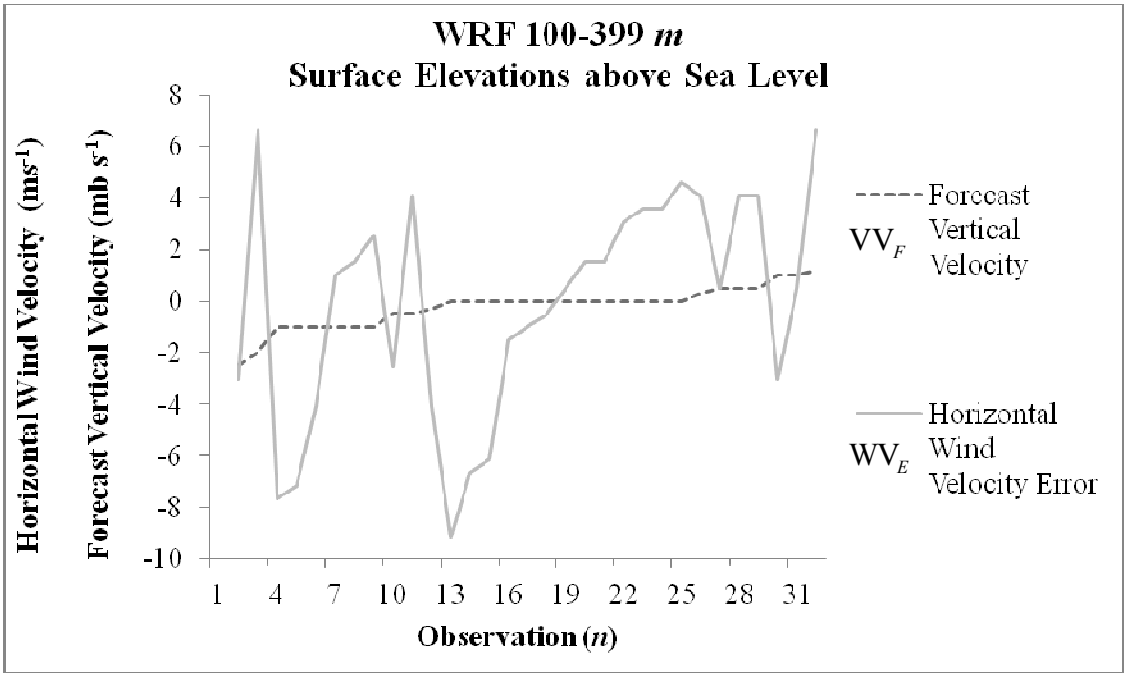

FIG. 3.13. WRF upper troposphere combined horizontal wind velocity error (WV_E) (ms^{-1}) and forecast vertical velocity (VV_F) (mb s^{-1}) comparison between 0-399 meters (*m*) surface elevation above sea level (CI=0) between 39-59 degrees (°) north latitude (*N*) ($R^2 = 0.1$).

These regions correspond to identified WV_E and VV_F coupling in MM5 forecasts. Figures 3.7 and 3.8 indicate frontal boundary and convection crossing over surface elevations between 400-499 *m* (WRF 400-499 *m* $R^2 = -0.6$; $CI \neq 0$) and 700-999 *m* (WRF 700-999 *m* $R^2 = -0.9$; $CI \neq 0$) above sea level where inverse WV_E and VV_F coupling has been identified in WRF forecasts (Table 3.8a; 3.8b; Fig. 3.12). Figure 3.9 also exhibits crossing a frontal and convection zone where WV_E and VV_F coupling is present over surface elevations between 0-99 *m* above sea level (Table 3.8a; WRF 0-99 *m* $R^2 = -0.2$; $CI \neq 0$).

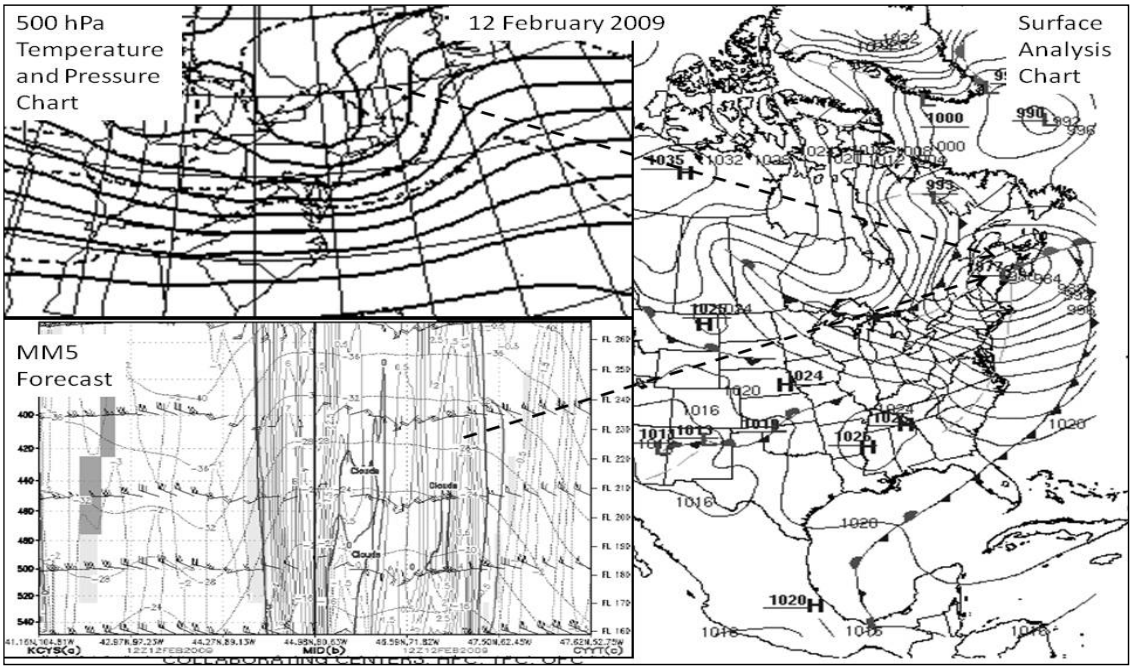

FIG. 3.14. Surface analysis (right) and 500 hectopascals (hPa) temperature and pressure (upper left) charts compared to MM5 multi-leg vertical cross section (lower left) forecast on 12 February 2009. Dashed lines indicate convective and frontal zone crossing during aircraft flight (Colorado State University 2012, United Kingdom Meteorological Office 2012).

Figure 3.6 indicates convection across a frontal boundary over water depicted by the WRF forecast in which WV_E and VV_F coupling was not established (Table 3.9a) suggesting a land based anomaly in WRF upper troposphere forecasts. WV_E and VV_F coupling appears to react differently in MM5 and WRF forecasts over land and water surface type during observed frontal or convective zone crossing. WV_E and VV_F coupling is a response by horizontal flow in the general circulation of MM5 (positive over land, inverse over water) and WRF (inverse over land) forecasts to VV_F across frontal or convection zones.

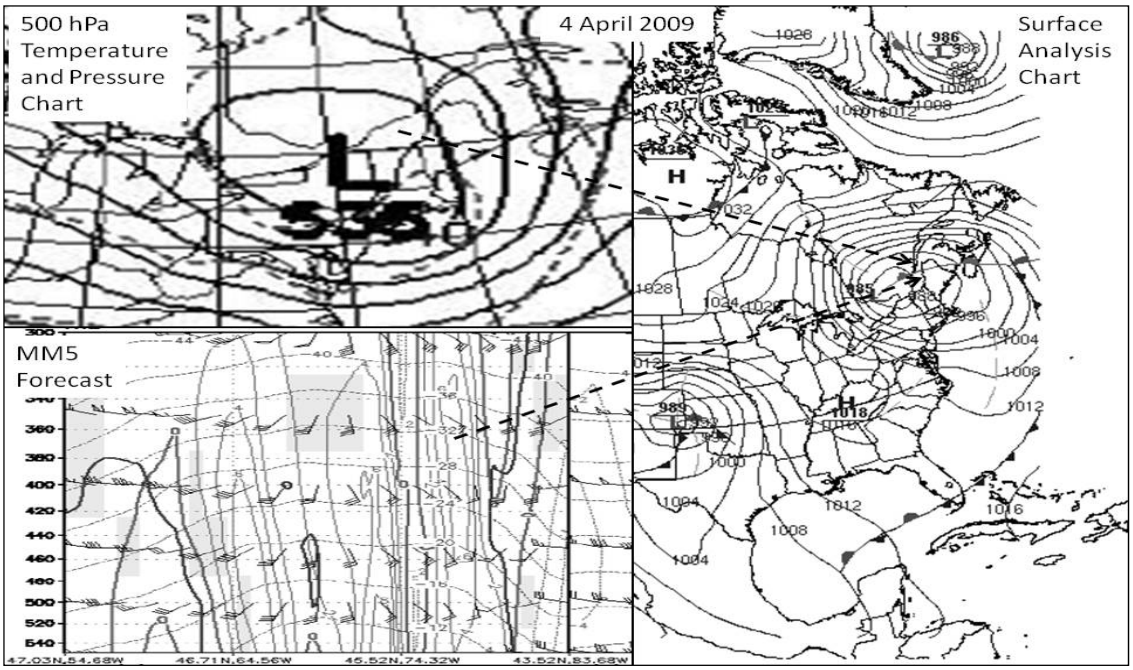

FIG. 3.15. Surface analysis (right) and 500 hectopascals (hPa) temperature and pressure (upper left) charts compared to MM5 multi-leg vertical cross section (lower left) forecast on 4 April 2009. Dashed lines indicate convective and frontal zone crossing during aircraft flight (Colorado State University 2012, United Kingdom Meteorological Office 2012).

The response may be due to the temperature Δ across frontal zones forecasted to be too strong causing erroneous $+VV_F$ followed by excessive $-VV_F$. WV_E and VV_F coupling over land in MM5 upper troposphere forecasts suggests frontal zones strength may be incorrectly predicted in the MM5 model and accelerate horizontal flow over land ($+WV_E = +VV_F$; Fig 3.10) and decelerate horizontal flow over water ($-WV_E = +VV_F$; Fig. 3.11). WV_E and VV_F coupling in WRF upper troposphere forecasts also suggests deceleration of horizontal flow in the WRF model during convective or frontal zone crossing.

Improvement of MM5 and WRF upper troposphere horizontal wind velocity forecasting should be considered when possible. Enhancements of horizontal wind velocity forecast skill in MM5 and WRF in the upper troposphere have the potential to reduce operating cost for air transportation and improve air traffic operations. For instance flight routes may be chosen during planning to use the most favorable horizontal wind velocity from a upper troposphere forecast attempting to reduce flight time and fuel used. An error in forecasted horizontal velocity of 6.0 ms^{-1} can increase operating costs by $335 at a speed of 556 kph for a 100 km trip. Additional costs may be incurred as a result of early weather arrival (i.e. thunderstorms or ash clouds) due to erroneous horizontal wind forecasts causing air traffic congestion introducing holding delays further increasing operating costs as a result of unplanned fuel use.

Chapter 4

Conclusions

4.1 General Conclusions

MM5 and WRF upper troposphere forecast T_E, WD_E, and WV_E were observed to be coupled to VV_F. Upper troposphere T_{Ob}, $\mathrm{WD}_{\mathrm{Ob}}$, and $\mathrm{WV}_{\mathrm{Ob}}$ were gathered using C-130 navigation system displays between 6000-7600 *m* above sea level between 39-59°*N*. Aircraft observations were gathered between North America and Southwest Asia during six successive transcontinental flights and one transoceanic crossing providing upper troposphere observations for analysis. C-130 navigation system displayed T_{Ob}, $\mathrm{WD}_{\mathrm{Ob}}$, and WV_E were found to be in reasonable agreement with T_{RC} (-3.0 to 2.0°*C*), $\mathrm{WD}_{\mathrm{RC}}$ (1.0-44.0°*T*), and $\mathrm{WV}_{\mathrm{RC}}$ (≤ 10.0 ms^{-1}) measurements. MM5 and WRF upper troposphere T_E, WD_E, and WV_E were tested against VV_F using regression analysis, and statistically significant findings were confirmed to a 95% confidence level.

MM5 and WRF upper troposphere T_E, WD_E, and WV_E coupling to VV_F reacted differently to lateral distance deviation within 100 km of model flight tracks. T_E and VV_F coupling in MM5 and WRF upper troposphere forecasts was indicated over land < 50 km lateral distance deviation from model flight tracks. This may indicate possible error in entrainment rates governed by the cumulus parameterization schemes. WD_E and VV_F coupling was found in WRF upper troposphere forecasts only, suggesting the vertical mass transport across frontal boundaries may be causing turbulent drag on weak

forecast geostrophic flow < 100 km lateral deviations from model flight tracks. WV_E and VV_F coupling was found in MM5 upper troposphere forecasts < 50 km lateral distance deviation from model flight tracks, and may be instigated by interruption of horizontal flow from vertical movements in the atmospheric column across convective and frontal boundaries in MM5. Upper troposphere forecast T_E, WD_E, and WV_E coupling to VV_F also favored different surface cover types and surface elevations above sea level within 100 km lateral distance deviation from modeled flight tracks.

T_E and VV_F in MM5 and WRF upper troposphere forecasts was exhibited over grass/scrub brush, crops, and urban surface type. A possible cause may be significant moisture due to evapotranspiration rates and soil saturation properties incorrectly parameterized in the Noah land surface model. Erroneous evapotranspiration rates may be a result of increases in plant populations while saturated soils might result from changes in urban drainage patterns. Increase in evapotranspiration and soil saturation may be creating excess humidity not captured by the Kain-Fritsch (MM5) and New Kain-Fritsch (WRF) cumulus parameterization schemes causing errors in entrainment rates. Erroneous entrainment rates may be influencing errors in temperature gradients across frontal boundaries introducing errors in latent heat release.

WD_E and VV_F coupling was observed to occur during convective and frontal zone crossing under weak pressure gradients aloft. Erroneous forecast vertical velocity across frontal zones appears to be causing turbulent drag during weak geostrophic flow in the WRF model. A possible source of erroneous vertical velocity may be due to minimum entrainment rate changes in the New Kain-Fritsch cumulus parameterization scheme

causing increased humidity resulting in increased latent heat release. Erroneous latent heat release will create an erroneous temperature differential across the front contributing to excessive VV_F. Therefore frontal boundaries indicate an important source of WD_E and VV_F coupling in WRF upper troposphere forecasts.

Finally, MM5 and WRF upper troposphere forecasts incorrectly predicting vertical velocity across convective areas and frontal zones may be resulting in an interference of horizontal momentum within the model's general circulation. Errors in forecast vertical movements across convective and frontal zones may be decelerating horizontal flow in WRF upper troposphere forecasts (inverse WV_E and VV_F coupling). Horizontal flow also appears to be accelerated over land in MM5 upper troposphere forecasts (positive WV_E and VV_F coupling) and decelerating over water (inverse WV_E and VV_F coupling). As seen with WD_E and VV_F coupling, convective areas and frontal zones forecasted by MM5 and WRF appear to be an important source of WV_E and VV_F coupling in upper troposphere forecasts. Alleviating T_E, WD_E and WV_E in MM5 and WRF upper troposphere forecasts will provide flight planners an opportunity to reduce operating costs by reducing fuel used. This study suggests a possible cumulative savings of $4085 in operating costs could be achieved by eliminating unnecessary deviations around erroneously predicted turbulence preventing unfavorable winds over a 100 km flight.

4.2 Recommendations to Further Studies

This study identified a relationship and explored potential causes between T_E, WD_E, and WV_E coupling to VV_F in MM5 and WRF upper troposphere forecasts. While no work is planned to improve MM5 by the scientific community, the primary focus will be on improvements to WRF. Following on from this study, work should include aircraft in situ measurements over areas where T_E, WD_E, and WV_E coupling to VV_F were identified and examined using reanalysis to determine divergence/convergence flow aloft. To better explore VV_F as a cause for T_E, WD_E, and WV_E the aircraft should be capable of recording atmospheric vertical velocity for comparison to WRF VV_F. Use of observed atmospheric vertical velocity will provide information about divergence and convergence, which would be important for providing further explanation into causes of T_E, WD_E, and WV_E seen in WRF upper troposphere forecast presented in this study.

Chapter 5

References

Ali, A.H., 2004: Application of Neural Principal Components to Climate Data. *J. Atmos. Oceanic Technol.*, **21**, 149-158.

Benjamin, S.G., B. Jamison, W. Moninger, S. Sahm, B. Schwartz, and T. Schlatter, 2010: Relative Short-range Forecast Impact from Aircraft, Profiler, Radiosonde, VAD, GPS-PW, METAR, and Mesonet Observations via the RUC Hourly Assimilation Cycle. *Mon. Wea. Rev.,* **138**, 1319-1343.

Bernardet, L., R., S. Koch, M. Pyle, E. Szoke, A. Loughe, J. Mahoney, L. Nance, M. Demirtas, T. Fowler, R. Gall, and H. Chuang, 2008: The Developmental Testbed Center and its Winter Forecasting Experiment. *Bull. Amer. Meteor. Soc.,* **89** 611-627.

Boisier, J.P., N. de Noblet-Ducoudre, A. Pitman, F. Cruz, C. Delire, B. van den Hurk, M. Molen, C. Muller, and A. Voldoire, 2012: Attributing the Impacts of Land-cover Changes in Temperate Regions on Surface Temperature and Heat Fluxes to Specific Causes: Results from the First LUCID Set of Simulations. *J. Geophys. Res.*, **117**, D12116, doi: 10.1029/2011JD017106.

Bromwich, D.H, J. Cassano, T. Klein, G. Heinemann, K. Hines, K. Steffen, and J. Box, 2001: Mesoscale Modeling of Katabatic Winds over Greenland with the Polar MM5. *Mon. Wea. Rev.,* **129**, 2290-2309.

Cardinali, C., and L. Isaksen, 2003: Use and Impact of Automated Aircraft Data in a Global 4DVAR Data Assimilation System. *Mon. Wea. Rev.* **131**, 1865-1877.

Cardinali, C., L. Rukhovets, and J. Tenenbaum, 2004: Jet Stream Analysis and Forecast Errors Using GADS Aircraft Observations in the DAO, ECMWF, and NCEP Models. *Mon. Wea. Rev.* **132**, 764-779.

Chandrasekar, A., C. Philbrick, B. Doddridge, R. Clark, and P. Georgopoulos, 2002: A Comparative Study of Prognostic MM5 Meteorological Modeling with Aircraft, Wind Profiler, Lidar, Tethered Balloon and Rass Data over Philadelphia during a 1999 Summer Episode. *Environ. Fluid Mech.,* **4**, 339-365.

Chen, F., and J. Dudhia, 2001a: Coupling an Advanced Land Surface–Hydrology Model with the Penn State–NCAR MM5 Modeling System. Part I: Model Implementation and Sensitivity. *Mon.Wea. Rev.,* **129**, 569–585.

Chen, F., and J. Dudhia, 2001b: Coupling an Advanced Land Surface–Hydrology Model with the Penn State–NCAR MM5 Modeling System. Part II: Preliminary Model Validation. *Mon. Wea. Rev.,* **129**, 587–604.

Cheng, W.Y., and W. Steenburgh, 2005: Evaluation of Surface Sensible Weather Forecasts by the WRF and the Eta Models over the Western United States. *Wea. Forecasting,* **20**, 812-821.

Cocke, S., H. Lee, G. Lim, and C. Lee, 2006: The NCAR CCM as a Numerical Weather Prediction Model. *Mon. Wea. Rev.,* **134**, 1954-1971.

Cole, R., and M. Jardin, 2000: Improving RUC-1 Wind Estimates by Incorporating Near-Real-time Aircraft Reports. *Wea. Forecasting,* **15**, 447-460.

Coniglio, M.C., K. Elmore, J. Kain, S. Weiss, M. Xue, and M. Weisman, 2010: Evaluation of WRF Model Output for Severe Weather Forecasting from the 2008

NOAA Hazardous Weather Testbed Spring Experiment. *Wea. Forecasting,* **25**, 408-427.

de Noblet-Ducoudré, N., J. Boisier, A. Pitman, G. Bonan, V. Brovkin, F. Cruz, C. Delire, V. Gayler, B. van den Hurk, P. Lawrence, M. van der Molen, C. Muller, C. Reick, B. Strengers, and A. Voldoire, 2012: Determining Robust Impacts of Land-use Induced Land-Cover Changes on Surface Climate over North America and Eurasia: Results from the first of LUCID Experiments. *J. Climate*, **25**, 3261–3281.

de Rooy, W. C., P. Siebesma, 2008: Simple Parameterization for Detrainment in Shallow Cumulus. *Mon. Wea. Rev.,* **136**, 560–576.

Derbyshire, S. H., I. Beau, P. Bechtold, J. Grandpeix, J. Piriou, J. Redelsperger, and P. Soares, 2004: Sensitivity of Moist Convection to Environmental Humidity. *Quart. J. Roy. Meteor. Soc.,* **130**, 3055–3079.

Evans, J., and R. Geerken, 2004: Discrimination between Climate and Human-induced Dryland Degradation, *J. Arid Environ*., **57**, 535–554, doi:10.1016/S0140-1963(03)00121-6.

Giorgi, F., 2006: Climate Change Hot-spots. *Geophys. Res. Lett*., **33**,

Fischer, G., F. Nachtergaele, S. Prieler, H.T. van Velthuizen, L. Verelst, and D. Wiberg, cited 2011: Global Agro-ecological Zones Assessment for Agriculture (GAEZ 2008). IIASA, Laxenburg, Austria and FAO, Rome, Italy. [Available online at http://www.iiasa.ac.at/Research/LUC/External-World-soil-database/HTML/Dominant_2000.html] L08707, doi:10.1029/2006GL025734.

Grell, G.A., J, Dudhia, D, Stauffer, 1994: A Description of the Fifth-generation Penn State/NCAR Mesoscale Model (MM5), NCAR Technical Note: NCAR/TN-398+STR, 128 pp.

Goodrich Sensor Systems, 2002a: *Sensor Systems Air Data Handbook*. Rosemount Aerospace, 20 pp.

Goodrich Sensor Systems, 2002b: *C-130 Product Guide*. Rosemount Aerospace, 39 pp.

Guo, Z., D. Bromwich, and J. Cassano, 2003: Evaluation of Polar MM5 Simulations of Antarctic Atmospheric Circulation. *Mon. Wea. Rev.,* **131**, 384-411.

Hines, K., and D. Bromwich, 2008: Development and Testing of Polar Weather Research and Forecasting (WRF) Model. Part I: Greenland Ice Sheet Meteorology. *Mon. Wea. Rev.,* **136**, 1971-1989.

Hogue, T.S., L. Bastidas, H. Gupta, S. Sorooshian, K. Mitchell, and W. Emmerich, 2005: Evaluation of Transferability of the Noah Land Surface Model in Semiarid Environments. *J. Hydrol.,* **6**, 68-84.

Jolliffe, I.T., 2007: Uncertainty and Inference for Verification Measures. *Wea. Forecasting,* **22**, 637-650.

Jonker, S., 2005: Evaluation Study of the Kain–Fritsch Convection Scheme. KNMI Tech. Rep. TR275, KNMI, 69 pp.

Kain, J. S., 2004: The Kain–Fritsch Convective Parameterization: An Update. *J. Appl. Meteor.,* **43**, 170–181.

Kain, J. S, and J. Fritsch, 1990: A One-dimensional Entraining/Detraining Plume Model and its Application in Convective Parameterization. *J. Atmos. Sci.,* **47**, 2784–2802.

Khelif, D., S. Burns, and C. Friehe, 1999: Improved Wind Measurements on Research Aircraft. *J. Atmos. Oceanic Technol.,* **16**, 860-875.

Knutti, R., R. Furrer, C. Tebaldi, J. Cermak, and G. Meehl, 2010: Challenges in Combining Projections from Multiple Climate Models. *J. Climate,* **23**, 2739-2758.

LeMone, M.A., M. Tewari, and F. Chen, 2008: Evaluation of the Noah Land Surface Model Using Data from a Fair-weather IHOP 2002 Day with Heterogeneous Surface Fluxes. *Mon. Wea. Rev.,* **136**, 4915–4941.

Lin, J., D. Brunner, C. Gerbig, J. Cermak, and G. Meehl, 2011: Studying Atmospheric Transport through Lagrangian Models. *EOS,* **92**, 177-184.

Manning, K.W., and C. Davis, 1997: Verification and Sensitivity Experiments for the WISP94 MM5 Forecasts. *Wea. Forecasting,* **12**, 719-735.

Mass, C., 2006: The Uncoordinated Giant: Why U.S. Weather Research and Prediction Are Not Achieving Their Potential. *Bull. Amer. Meteor. Soc.,* **87**, 573-584.

Moninger, W., R. Mamrosh, and P. Pauley, 2003: Automated Meteorological Reports from Commercial Aircraft. *Bull. Amer. Meteor. Soc.,* **84**, 203-216.

Montreal Weather Center, cited 2012: Archives. [Available online at http://meteocentre.com/archive/archive.php?lang=en]

Myoung, B., Y. Choi, S. Choi, and S. Park, 2012: Impact of Vegetation on Land-Atmosphere Coupling Strength and its Implication for Desertification Mitigation over East Asia. *J. Geophys. Res.*, **117**, D12113, doi: 10.1029/2011JD017143.

National Weather Service, cited 2012: National Snow Analysis. [Available online at http://www.nohrsc.noaa.gov/nsa/index.html?region=National&year=2009&month=4&day=4&units=e]

Pattanayak, S., and U. Mohanty, 2008: A Comparative Study on Performance of MM5 and WRF Models in Simulation of Tropical Cyclones over Indian Seas. *Curr. Sci.,* **95**, 923-936.

Pitman, A. J., N. de Noblet-Ducoudré, F. Cruz, E. Davin, G. Bonan, V. Brovkin, M. Claussen, C. Delire, L. Ganzeveld, V. Gayler, B. van den Hurk, P. Lawerence, C. Muller, C. Reick, S. Seneviratne, B. Strengers and A. Voldoire, 2009: Uncertainties in Climate Responses to Past Land Cover Change: First Results from the LUCID Intercomparison Study., *Geophys. Res. Lett*., **36**, L14814, doi:10.1029/2009GL039076.

Riggs, H. C., 1985: *Developments in Water Science: Streamflow Characteristics*. Elsevier, 249 pp.

Sauter, B., and T. Henmi, 2004: Average Forecast Errors Using MM5 and WRF. *Army Research Laboratory*. www.arl.army.mil/arlreports/2004/ARL-MR-597.pdf.

Seidel, D., S. Bomin, M. Pettey, and A. Reale, 2011: Global Radiosonde Balloon Drift Statistics. *J. Geophys. Res.,* **116**, D07102, doi:10.1029/2010JD014891.

Sheffield, J., and E. Wood, 2008: Projected Changes in Drought Occurrence under Future Global Warming from Multi-Model, Multi-Scenario, IPCC AR4 simulations. *Clim. Dyn.*, **31**, 79–105, doi:10.1007/s00382-007-0340-z.

Siebesma, A. P., and A. Holtslag, 1996: Model Impacts of Entrainment and Detrainment Rates in Shallow Cumulus Convection. *J. Atmos. Sci.,* **53**, 2354–2364.

Skamarock, W., J. Klemp, J Dudhia, D. Gill, D. Barker, M. Duda, X. Huang, W. Wang, J. Powers, 2008: A Description of the Advanced Research WRF version 3. NCAR Tech Note NCAR/TN-475+STR, 125 pp.

Soich, K., and B. Rappenglueck, 2012: Upper Troposphere MM5 and WRF Temperature Error and Vertical Velocity Coupling. *J. Appl. Meteor*, in revision.

Stohl, A., A. Prata, S. Eckhardt, A. Durant, S. Henne, N. Kristiansen, A. Minikin, U. Schumann, P. Seibert, K. Stebel, H. Thomas, T. Thorsteinsson, K. Tørseth, and B. Weinzierl, 2011: Determination of Time and Height Resolved Volcanic Ash Emissions for Quantitative Ash Dispersion Modeling: The 2010 Eyjafjallajökull eruption. *Atmos. Chem. Phys.,* **11**, 4333-4351.

Stull, R. B., 2000: *Meteorology for Scientists and Engineers*. Brooks/Cole, 502 pp.

Telfeyan, R., D. Rozema, and J. Wesely, 2005: The Interactive Grid Analysis and Display System (IGrADS) for the Armed Forces. *21st International Conf. on Interactive Information and Processing Systems (IIPS) for Meteorology, Oceanography, and Hydrology, San Diego, CA, Amer. Meteor. Soc.*, Paper 15.1.

U.S. Air Force, 2006: *C-130 Operations Procedures*. Department of the Air Force, 300 pp.

United Kingdom Meteorological Office cited 2012: Weather Center. [Available online at http://www.wetterzentrale.de/topkarten/tkfaxbraar.htm]

University of Wyoming, cited 2012: Upper Air Sounding Database. [Available online at http://weather.uwyo.edu/upperair/sounding.html]

van den Kroonenberg, A., T. Martin, M. Buschmann, J. Bange, and P. Vörsmann, 2008: Measuring the Wind Vector Using the Autonomous Mini Aerial Vehicle M2AV. *J. Atmos. Oceanic Technol.,* **25**, 1969-1982.

Wei, H. Y. Xia, K. Mitchell, and M. Ek, 2012: Improvement of the Noah Land Surface Model for Warm Season Process: Evaluation of Water and Energy Flux Simulation. *Hydrol. Process.,* doi:10.1002/hyp.9214.

Wilson, A. B., D. Bromwich, and K. Hines, 2011: Evaluation of Polar WRF Forecasts on the Arctic System Reanalysis Domain: Surface and Upper Air Analysis. *J. Geophys. Res.,* **116**, D11112, doi:10.1029/2010JD015013.

Wilson, A. B., D. Bromwich, and K. Hines, 2012: Evaluation of Polar WRF Forecasts on the Arctic System Reanalysis Domain. 2. Atmospheric Hydrologic Cycle. *J. Geophys. Res.*, **17**, D04107, doi: 10.1029/2011JD016765.

Wroblewski, D.E, O. Coté, J. Hacker, and R. Dobosy, 2010: Velocity and Temperature Structure Functions in the Upper Troposphere and Lower Stratosphere from High-Resolution Aircraft Measurements. *J. Atmos. Sci.,* **67**, 1157-1170.

Yang, B., Y. Qian, G. Lin, R. Leung, and Y. Zhang, 2012: Some Issues in Uncertainty Quantification and Parameter Tuning: A Case Study of Convective Parameterization Scheme in the WRF Regional Climate Model. *Atmos. Chem. Phys.*, **12**, 2409-2427, doi: 10.5194/acp-12-2409-1012.

Zhang, Y., V. Dulière, P. Mote, and E. Salathé, 2009: Evaluation of WRF and HadRM Mesoscale Climate Simulations over the U.S. Pacific Northwest. *J. Climate,* **22**, 5511-5526.

Zhu, Y., Z. Toth, R. Wobus, D. Richardson, and K. Mylne, 2002: The Economic Value of Ensemble-based Weather Forecasts. *Bull. Amer. Meteor. Soc.,* **83**, 73-83.

Zill, D. G., J. Dewar, 2010: *Algebra and Trigonometry*. Jones & Bartlett, 750 pp.